

UNIVERSITY OF THESSALY

DEPARTMENT OF MECHANICAL ENGINEERING

LABORATORY OF MECHANICS AND STRENGTH OF MATERIALS

Post-Graduate Diploma

**Structural capacity of HSS tubular members under axial
compression and combined loading- Comparison with
current provisions**

Aglaia-Eugenia Pournara

Advisor: Spyros A. Karamanos

Submitted to the Department of Mechanical Engineering

in Partial Fulfillment of the Requirements

for the Degree of Post-Graduate Diploma

University of Thessaly, 2011



**ΠΑΝΕΠΙΣΤΗΜΙΟ ΘΕΣΣΑΛΙΑΣ
ΒΙΒΛΙΟΘΗΚΗ & ΚΕΝΤΡΟ ΠΛΗΡΟΦΟΡΗΣΗΣ
ΕΙΔΙΚΗ ΣΥΛΛΟΓΗ «ΓΚΡΙΖΑ ΒΙΒΛΙΟΓΡΑΦΙΑ»**

Αριθ. Εισ.: 9412/1
Ημερ. Εισ.: 24-03-2011
Δωρεά: Συγγραφέα
Ταξιθετικός Κωδικός: Δ
620.1123
ΠΟΥ

Table of Contents

Introduction	5
1. Literature Research.....	5
1.2. Review of experimental and numerical works on high strength steel tubular beam-columns.....	6
1.2.1. Material characteristics of High Strength Steel	6
1.2.2. Ductility of HSS elements and sections.....	7
1.2.3. Local and global buckling of high strength steel.....	7
1.2.4. Available design standard & recommendation provisions on tubular beam-columns in comparison with available experimental studies.....	8
1.2.4.1. Compression members of high strength steel- Numerical and experimental work.....	10
1.2.5. Classification of cross section for CHS made of HSS.....	11
2. Initial imperfections.....	13
3. Material Modeling	15
4. Model Geometry.....	17
4.1. Out-of straightness	17
4.2. Out-of-roundness in combination with out-of-straightness	19
4.3. Initial wrinkling	19
5. Stability curves.....	21
5.1. Out-of-straightness.....	21
5.1.1. Buckling response	21
5.1.2. Stability curves.....	25
5.2. Combination of out-of-roundness and out-of straightness.....	33
5.3. Initial wrinkling	36
6. Interaction diagrams.....	40
6.1. Out-of straightness imperfection	41
6.2. Combined out-of-straightness and out-of-roundness.....	54
6.3. Initial wrinkling	56

7. Conclusions	61
References	62
ANNEX A-Benchmark problems.....	65
A.1. Cross sectional ovalization instability of elastic tubes under bending-Problem#1.....	65
A.2 Elastic Tube under pure axial compression (parametric analysis)-Problem#2	73
A.3. Inelastic strip ovalization and inelastic tube failure under bending in comparison- Problem#3.....	81
ANNEX B- Current provisions.....	86
B.1. Recommended practice for Planning, Designing and Constructing Fixed Offshore Platforms- Load and Resistance Factor design [American Petroleum Institute-API, 1993]	86
B.1.1 Axial Compression	86
B.1.1.1 Column Buckling	86
B.1.1.2 Local Buckling	87
B.1.2. Bending.....	88
B.1.3 Combined Axial Compression and Bending.....	89
B.2. Eurocode3: Design of steel structures.....	90
B.2.1. Buckling strength in axial compression for tubular sections.....	90
B.2.1.1 Buckling strength in axial compression Class 1, 2 & 3 [EN-1993-1-1, 2005]	90
B.2.1.2 Buckling Strength Class4.....	92
B.2.1.2.1 Local buckling stress design.....	93
B.2.1.2.2 ANNEX D	95
B.2.2 Bending.....	98
B.2.2.1 Bending Class 1, 2 & 3 [EN-1993-1-1, 2005]	98
B.2.2.2 Bending Class 4	98
B.2.3 Combined loads	99
B.2.3.1 Class 1, 2 & 3.....	99
B.2.3.2 Class 4	99
B.3 Structural stability of hollow sections [CIDECT1992]	100
B.3.1 Tubular Members in axial compression for class 1, 2 & 3	100

B.3.2 Tubular members in bending for class 1, 2 &3	101
B.3.3 Members in combined compression and bending class 1, 2 & 3	102
B.3.4 Members in axial compression, bending and combined loads- class 4 [ECCS 1988]	103
B.3.4.1 Buckling Stress σ_u	103
B.3.4.2 Pure axial compressive load for class4	104
B.3.4.3 Pure bending of the cylinder for class4	105
B.3.4.4 Combined loading for class 4.....	105
B.4 AISC-Load and Resistance Factor Design Specification for Steel Hollow Structural Sections [AISC 2000]	106
B.4.1. Design Requirements.....	106
B.4.2 Tubular Compression Members	107
B.4.3. Beams and other Flexural Members	107
B.4.4 Members under Combined Forces	108
ANNEX C-Simulation of CSM experiments.....	111
C.1 HSS tubular members with initial out-of straightness under combined loadings.....	111
C.2 Initially wrinkled steel tubular member under axial compression.....	121

Introduction

The present study aims at investigating the structural response of high strength steel imperfect tubular beam columns ($\sigma_y=590\text{MPa}$) under axial compression and combined loading. Buckling curves and interaction diagrams are calculated through finite element analysis for various cross sections and different cases of imperfections. The finite element results are compared with the proposed curves and equations by the current standards such as Eurocode [EN-1993-1-1, 2005], [EN-1993-1-6, 2007], API [API-RP2A, 1993], AISC [AISC-LRFD, 2000] & CIDECT [CIDECT, 1992]. In these provisions, regular steel is assumed so that cross section classification and slenderness limits are penalized and structural strengths proposed might be rather conservative. In hence, there is limited information for cross sections of high strength steel (over 460 MPa) and the current work aims at contributing at the enhancement of the current guidelines considering stability curves and interaction diagrams for high strength steel imperfect tubes.

For the above purposes a parametric finite element analysis has been conducted simulating of tubular models. Additionally, a case study is presented where tests on high strength steel tubular beam columns under combined loading are simulated in terms of the experimental work to be performed by Centro Sviluppo Materiali institute (CSM).

http://www.c-s-m.it/layout_html_standard/english/home.html

1. Literature Research

Steel tubes, in structural applications, not only need sufficient strength, but also sufficient deformation capacity to allow for redistribution of stresses and loads. Such redistribution is important because in structural applications such as tubular members, the stresses are not only the result of the design loads, but often are also caused by loads that are usually not taken into account in the design. In elongated steel (regular or high strength) cylinders, the usual forces encountered are combinations of bending moment and axial force (tensile or compressive). Under this combined loading situation, the tubular member may buckle when stressed or strained above a certain level. This instability is crucial for the structural integrity of the cylinder, resulting in failure and collapse. This may be in the form of global buckling (Euler-type instability) when significant axial load is applied or local buckling due to bending and/or axial compression, at the compressive side of the cylinder wall.

As far as axial compression (column buckling) is concerned during the design process, the diameter to wall thickness ratio (D/t) is chosen in order to obtain optimal stiffness and strength. The limiting factor is local buckling and the limitations in load carrying capacity and deformation capacity that comes with local buckling. The higher the D/t ratio is chosen, the lower the strain at which local buckling will occur and the lower the deformation capacity is.

Another factor that affects local buckling occurrence is the presence of initial imperfections produced during the manufacturing process, As a result the buckling strength is reduced and the buckling response of members subjected to axial compressive loads is influenced by the amplitude and the type of initial imperfection.

The use of Circular Hollow Section (CHS) has recently had a significant development both for their excellent structural and architectural properties. High strength steel CHS members, especially, have become commercial about 3 decades ago and their use is still very limited in the construction industry although growing demand for high strength but lightweight fabrications is widely recognized. More specifically, the use of high strength steel could provide high cost efficiency as column and beam cross sectional dimensions used to satisfy the constructional safety standards are now decreased, on behalf of the higher structural strength that HSS offers.

Consequently, the structural behavior of high strength steel members with initial imperfections should be under investigation in order to define the advantages or disadvantages arising in order to be used in structural/industrial applications in relation to the widespread use of regular steel.

In this present study the initial imperfections investigated for HSS tubular members are initial crookedness, out-of-roundness and initial wrinkling.

1.2. Review of experimental and numerical works on high strength steel tubular beam-columns

A review of previous experimental or analytical work on regular and high strength steel members is presented in the following sections under monotonic structural loading. Material testing and full scale tests have been conducted by previous experimental researches in order to clarify the behavior of the high strength steel in material and structural bases.

1.2.1. Material characteristics of High Strength Steel

In the construction sector, steel with yield strength from 460 up to 690 MPa is considered HSS. The high-strength steels have specific chemical compositions which depend primarily on rolling and tempering techniques, element thickness and producers, developing a stress-strain behavior considerably different from that of mild steel, exhibiting considerably lower material ductility. HSS steels vary from other steels in that they are not produced to meet a specific chemical composition, but rather to specific mechanical properties.

High strength steel is used in cars, trucks, cranes, bridges, roller coasters and other structures that are designed to handle large amounts of stress or need a good strength-to-weight ratio. Nevertheless, the stress-strain behavior of HSS ($\sigma - \epsilon$) is considerably different from that of mild steel, exhibiting considerably lower material ductility.

In this present study the tubular members investigated are extruded cold formed seamless with a nominal yield stress of 590 MPa.

1.2.2. Ductility of HSS elements and sections

Several studies have verified the difficulty of using plastic analysis for high strength steel elements due to the reduced ductility parameters of the material [Sivakumaran & Bing (1998)]. The ratio between the tensile strength (f_u) and the yield strength (f_y) is lower than that of mild steel; the ratio between the strain at ultimate load level (ϵ_u), and the strain at yielding (ϵ_y) is considerably lower than that of mild steel found. More specifically, as proved by stub column tests on W-shaped sections reported in Sivakumaran and Bing (1998), the ratio ϵ_u/ϵ_y is found equal to 107 for mild steel (300W) but 17 for high strength steel (700Q). However these studies were carried out on W sections and are not directly extensible to circular sections. Moreover, as reported by Rasmussen and Hancock (1995), strain at rupture ϵ_{rp} of HSS ranges from 10% to 15%, strain at ultimate load level ϵ_u is about 10%, found by coupon tests extracted from box and I beams of high strength steel (690MPa).

1.2.3. Local and global buckling of high strength steel

There are numerous studies on the effect of buckling on structures of HSS including H-sections and I-sections [Bernt Johansson & Collin (2008)]. In general those studies show that HSS performs better than ordinary steel or at least not worse [Sivakumaran & Bing (1998)], [Rasmussen and Hancock (1995)] and [Beg & Hladnik (1996)]. This means that the normal design rules can be used as a conservative approach. The reason for the better behaviour of HSS is a smaller influence of imperfections, especially considering the residual stresses [Sivakumaran & Bing (1998)], [Rasmussen and Hancock (1995)], [Beg & Hladnik (1996)] and [H. Jiao, X.L. Zhao (2003)].

Studies and tests on long box and I-section columns fabricated from HSS have shown that the buckling behaviour of these sections is better than that described in Eurocode [Rasmussen and Hancock (1995)]. In fact the Eurocode 3 design curves are conservative compared with the tests and with American specifications. This is because the slenderness reduction factor due to flexural buckling (χ) in the Eurocode is more penalizing than in American standards AISC [American Institute of Steel Construction (2005)] specification for example.

Therefore a more rational way to account for the increased relative resistance would be to give a gradual increase of the buckling curves by modifying the imperfection parameter as reported by Bernt Johansson & Collin as far as high strength steel is concerned.

Nevertheless, a direct use of these results is not suggested for other kind of section such as CHS because it is necessary to carry out analytic, numerical and experimental tests on these sections.

1.2.4. Available design standard & recommendation provisions on tubular beam-columns in comparison with available experimental studies

In 1959 the German standard DIN 4114 introduced a special column curve for tubes and used another curve for all the other column types. The later work of the ECCS (European Convention for Constructional Steelwork) included a testing programme on column strength has included 1067 main buckling tests on various types of members (I, H, T, round and square hollow sections) and the corresponding stub and tension tests (as reported in ECCS Publication No 22 Manual on Stability of Steel Structures, 1976-Section 3.1.1.9 and Section 3.1.2) resulted in recommended design application and code adoption in several countries. This research has been described by D. Sfintesco (1970), Beer and Schultz (1970) and J. Jacquet (1970). The cross-sectional dimensions of the test pieces were limited in this programme by the force and height of the testing machines. Moreover in order to complete the information needed for establishing the ECCS column curves, the range of heavier sections with greater thicknesses had been covered by N. Tebedge et al [Tebedge et al. (1971)], [Tebedge et al. (1972)] and gave the opportunity of a comparison between the ECCS and the Lehigh University testing procedures (1960).

The following figures compare the statistically evaluated column tests with theoretical column curves. Figure 1.1.4.1 shows the test results for rolled tubes, Figure 1.1.4.2 for welded tubes, hot-finished. For the comparison curve "a", the design curve for tubes, is evaluated with the statistically determined yield point of the tubes tested, and is in good agreement with the test results. Also, the comparison shows clearly the lower load carrying capacity of welded tubes in the range of small slenderness ratios.

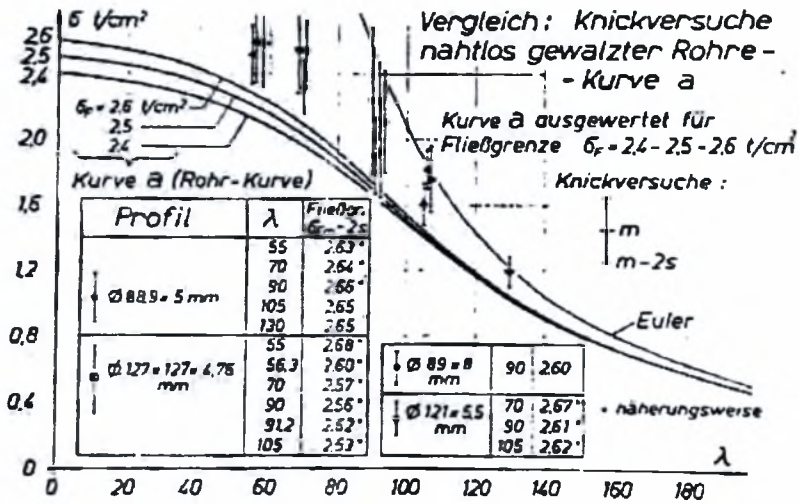


Figure 1.1.4.1 ECCS test results for rolled tubes.

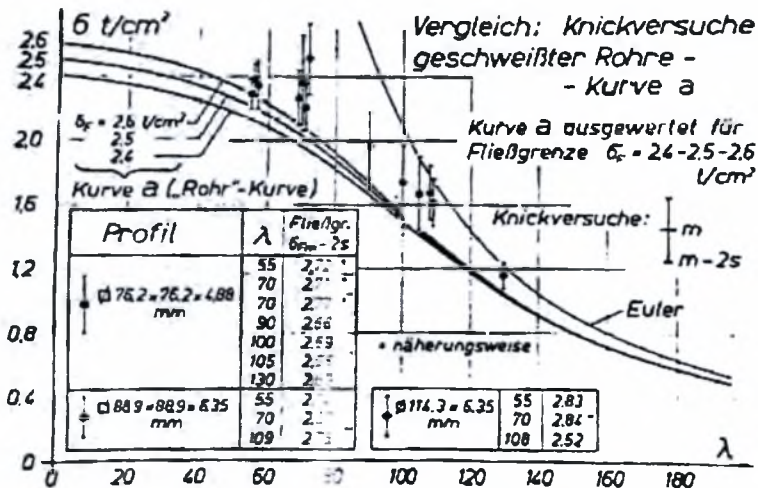


Figure 1.1.4.2 ECCS test for welded tubes, hot-finished

Furthermore, maximum loading values under axial compression, bending and combined loadings such as proposed slenderness and deformation limits are presented in the available current standards (such as Eurocode, CIDECT, AISC and API) developed based on the information obtained by experimental research through the last decades described above which are thoroughly described in the ANNEX B. The current standards remain valid not only, under specific values of initial imperfections but steel grades (up to 460 MPa), as well. Subsequently, the cross section classification is penalized and the strength values proposed can be considerably conservative for high strength steel members. More specifically, the API-

LRFD standard considers an upper yield stress limit up to 414 MPa, EN-1993-1-1 and CIDECT 460MPa. Additionally, imperfection limit values are defined for the stability curves proposed by the current standards. Especially, the limit of initial crookedness of tubular members ranges among the current standards; Eurocode and CIDECT consider an out-of-straightness limit of $L/300$ for cold formed CHS sections but the reduction factor imposed in the buckling load calculations α includes a range of additional imperfections such as out-of-roundness, variation of thickness and residual stresses. Moreover AISC proposes a crookedness limit of $L/1500$ and API a limit of $L/1000$. Furthermore API induces a bound value of out-of-roundness imperfection up to 3% when external pressure is considered.

1.2.4.1. Compression members of high strength steel- Numerical and experimental work

Design rules for columns of high yield strength steel (S460 at that time) have been included in the Eurocode to allow designers to take advantage, not only of their obvious enhanced load-bearing capacity due to increased material strength, but of additional strength conferred on columns due to lessening of detrimental effect of residual stresses.

As the one of the more favourable cross-sectional shapes for a column is of a circular tube, Beer and Schulz [Beer & Schulz (1972)] have computed the column curve for such cross-section assuming no residual stresses and a diameter to wall thickness ratio of 40. This column curve has been given the designation "a₀" and represents an approximate upper bound to the strength of tubular columns having an initial crookedness (out-of-straightness) of $1/1000$ of the column length.

Experimental results for the buckling of hot-finished welded, round and square tubes have been obtained at the University of Liège [Massonet & Janss]. The steel had a yield stress in excess of 700 MPa. The tubular columns were tested at six values of non dimensional slenderness and the results are shown plotted in Figure . Each point represents the mean strength from eight tests less twice the standard deviation except at non dimensional slenderness equal to 1.7 where only three tests were performed. Twelve tests have been performed at a non-dimensional slenderness ratio of 1.1. The single point shown on Figure represents the mean of the twelve results less twice the standard deviation divided by the mean yield stress less twice the standard deviation. Experimental failure stresses in Figure 1.2.4.1.1 are dimensionalised not with respect of guaranteed minimum yield stress but with

the mean yield stress which is lessened by twice the standard deviation in order to conform with the Eurocode column curve for hot-finished welded tubes.

Additionally, Figure 1.2.4.1.1 shows that most of the experimental results are between curves “a” and “a0”. It is possible that manufacturing processes of high yield strength tubes will be improved to allow such section to be designed not only according to curve “a0” that refers to steels grades up to 460Mpa, but new curves that correspond to values beyond the current limits of the current standards.

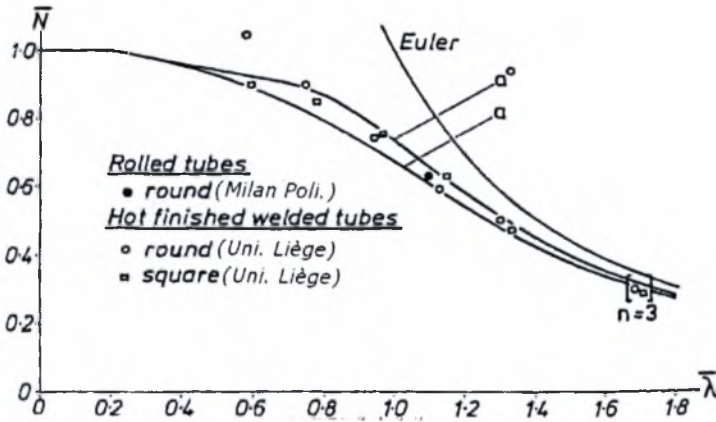


Figure 1.2.4.1.1 Experimental results for the buckling of hot-finished welded, round and square tubes made of high strength steel.

Furthermore, a series of tests on rolled, heat-treated circular tubes of steel having a mean yield stress of 654 MPa has been carried out by Milan Polytechnic [Ballio, Finzi, Urbano & Zandonini (1975)].

1.2.5. Classification of cross section for CHS made of HSS

The classification of cross sections is closely related to the ductility of the material, the ductility of the element section and the local buckling phenomena. An important problem of HSS section, owing to the high yield strength, consists of respecting the classification limits imposed by Eurocode 3-1-1. The classification of cross sections is function of the factor

$$\varepsilon = \sqrt{\frac{235}{f_y}}$$

so that HSS is penalised. In addition the classification is function of D/t that is often high with use of HSS sections. Beg and Hladnik [Beg & Hladnik (1996)] have shown by series of bending tests on I beam sections with nominal yield strength of 800 MPa that the

slenderness limits in EC3-1-1 are probably too conservative both for mild steel up to grade S460 and for HSS, in particular for circular hollow section. There are significant differences in slenderness limits recommended in various codes for circular hollow sections (CHS) under bending as shown by Elchalakani [Elchalakani, Zhao, Grzebieta "Bending tests to determine slenderness limits for cold-formed circular hollow sections", Journal of Constructional Steel Research, Volume 58, Number 11, November 2002, pp. 1407-1430 et al (2002)].

Other research by Al-Shawi [F.A.N Al-Shawi (2001)] aimed at studying the behaviour and the rotational capacity of very high strength steel CHS members in the plastic range in order to investigate the behaviour of circular hollow sections beyond the stage of development of the plastic moment of resistance. In the standards, the possibility to develop plastic moment M_p is fitted in the classification of cross sections. But in this way it does not take into account the secondary P- Δ effect which takes place in the plane of the cross section of the tube. This effect will reduce the plastic section (ovalization) modulus due to the deformation in the form of flattening of the cross section. It is therefore necessary that experiments and tests are to be performed with regard to these issues, mainly investigating the behaviour of circular sections in HSS.

2. Initial imperfections

As far as steel members are concerned, geometric imperfections are generally developed during fabrication process. The imperfections are measured using non destructive inspection equipments and ultrasonic techniques. The measurements are evaluated according to limit imperfection values recommended by the available standards prior to any structural application. The members with geometrical imperfections beyond the limit values asserted are not acceptable for structural or industrial use.

Previous research has shown that the existence of geometrical initial imperfections can be significantly detrimental for the capacity of the column members under structural loads. The current standards cover several imperfection types that are generally included by compression or bending factors that reduce the maximum compressive or bending strengths. The present study aims at investigating the structural response of high strength steel beam-column tubular members of various diameter-to-thickness ratios and various types of imposed initial imperfections under axial compression and combined forces. The results are compared with the curves proposed by current available provisions and standards which consider general imperfections and regular strength steel.

The initial imperfections investigated in the present study are frequently encountered during the fabrication of steel tubular products:

- initial crookedness (out-of-straightness deflection),
- out-of-roundness
- wrinkling of the pipe wall

Schematic illustration of the imposed initial imperfections is presented in the following Figures 2.1, 2.2 and 2.3

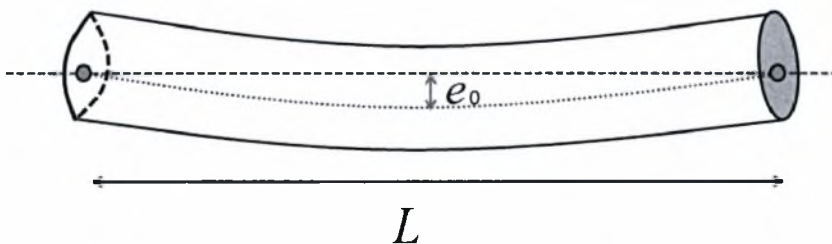


Figure 2.1 Out-of-straightness

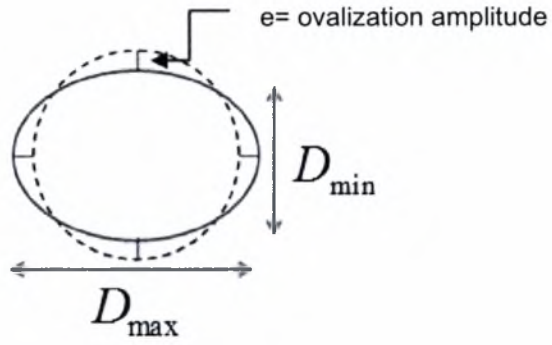


Figure 2.2 Cross sectional out-of-roundness

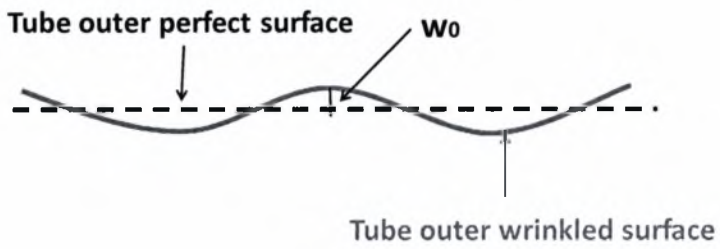


Figure 2.3 Wrinkling

3. Material Modeling

The plasticity model used in the present finite element analysis is rate-independent following a linear isotropic hardening rule. The plasticity model is generally composed of three elements: the yield criterion, the flow rule and the hardening rule. The yield criterion is a function that determines the yield surface so that when the equivalent stress is within the yield surface, the material response is elastic. On the other hand, when the equivalent stress is on the yield surface, plastic strain occurs. The flow rule determines the direction of the plastic strain increment when yielding starts.

The yield criterion is defined as:

$$F = \frac{1}{2} s \cdot s - \frac{k^2 (\bar{\epsilon}^p)}{3} = 0 \quad (3.1)$$

Where s is the deviatoric stress, $\bar{\epsilon}^p$ is the equivalent plastic strain and k is the yield stress determined based on the stress-strain of the material response curve from a uniaxial tensile test.

For the present study, the material data is derived from a bi-linear elastic-plastic nominal material curve with a constant plastic hardening of $E_{pl}=E/500$ as shown in Figure 3.1, where E is the elastic Young's modulus. The case of $E_{pl}=E/1000$ is also investigated for some cases. The yield stress is 590 MPa and the material data imported to ABAQUS are defined as follows:

For the elastic region, the material data imported are :

- $E=210000\text{MPa}$
- $\nu=0.3$

where E is the elastic Young's modulus and ν is the Poisson ratio.

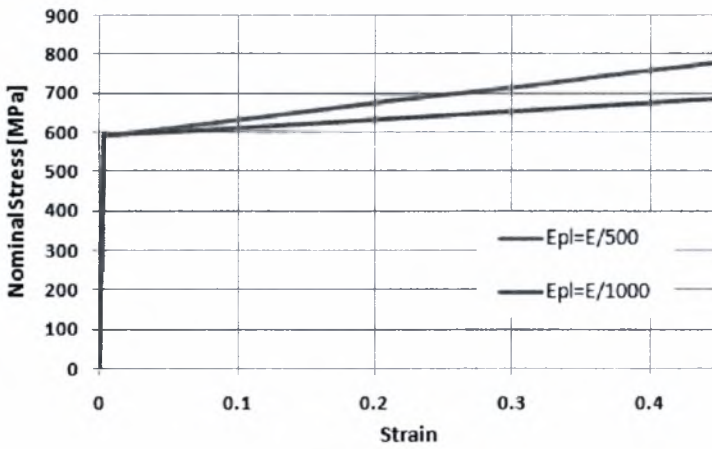


Figure 3.1 Inelastic high strength steel material curve

For the plastic region of the material the values of the nominal stress-strain curve were used, since they were converted to true stress and logarithmic plastic strain values, respectively as follows:

$$\sigma_t = \sigma_{nom} (1 + \epsilon_{nom}) \quad \epsilon_{pl} = \ln(1 + \epsilon_{nom}) - \frac{\sigma_t}{E} \quad (3.2)$$

where σ_{nom} , ϵ_{nom} , σ_t , ϵ_{pl} are the nominal stress, nominal strain, the true stress and the logarithmic plastic strain. The stress-strain values inserted are depicted in the table below.

Table 3.1 True stress-strain values

σ_t (MPa)	ϵ_{pl}
591.6576	0
615.9714	0.023414
666.0226	0.068652
717.9584	0.111896
827.6246	0.193229
944.8776	0.268376
1037.775	0.32119
1135.048	0.371422

4. Model Geometry

The numerical analysis of the tubular models of various considers nonlinear geometry through a large-strain description of the deformable continuum, as well as inelastic material behavior, accounted for through a J_2 flow (von Mises) large-strain plasticity model, with isotropic hardening. The nonlinear load-deflection or moment rotation equilibrium paths are traced for various length values and cross sections, using a Riks continuation algorithm.

Four-node reduced-integration shell elements (type S4R) are employed for the tube modeling. The element type was chosen through an extended parametric study in order to optimize the computational time and eliminate the results sensitivity, reported in ANNEX A.

Tubular members of five different diameter-to-thickness ratios and lengths from 500mm to 16 m, were developed in order to be subjected in various monotonic loadings. The geometric characteristics of the tubulars are defined below:

- D=193.7mm t=6mm, D/t=32.28
- D=193.7mm t=10mm, D/t=19.37
- D=355mm t=8mm, D/t=44.375
- D=355mm t=12mm, D/t=29.58
- D=355mm t=16mm, D/t=22.18

It is observed that the cross section of D=193.7mm and t=10mm is the thickest and the D=355mm t=8mm is the thinnest of the above.

4.1. Out-of straightness

The out-of-straightness imperfection was applied as a stress free parabolic smooth crookedness with the maximum deflection ($e_{\max}=e_0$) of the longitudinal axes placed at the mid span of the tube length (as shown in Figure 4.1.1). The value of the maximum deflection chosen was a proportion of the total length of the pipe (L/300, L/500 &L/1000). The finite element model and loading condition under axial compression is shown in Figure 4.1.2.

The model is simply supported with capped ends (RP1 and RP2) which are both free to rotate at the in-plane direction as shown in Figure 4.1.2. Reference nodes (RP1 and RP2), each one kinematically coupled with the corresponding end section shell nodes, are located at the centroids of the end sections. RP1 is a hinge while RP2 allows to motion in the

longitudinal direction of the tube, so that RP2 can be considered as a roller. Compression load is applied at RP2 in the longitudinal direction of the finite element model. The same boundary conditions were applied for all the tubular models of various lengths, loading conditions and types of initial imperfections.

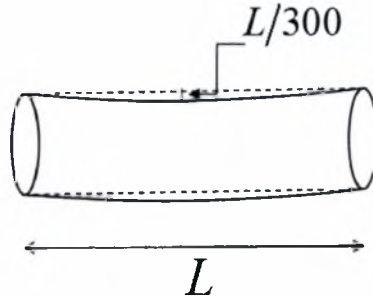


Figure 4.1.1 Schematic illustration of the out-of-straightness imperfection



Figure 4.1.2 The finite element model loading under axial compression and boundary conditions

4.2. Out-of-roundness in combination with out-of-straightness

The out-of-roundness imperfection is defined as a stress free initial ovalization of the pipe circumference that remains constant through the entire tube length, as shown in Figure 2.2. The ovalization amplitude is chosen up to $\alpha=3\%$ corresponding to the maximum limit set by the API standard [API RP2A, 1993], and $\alpha =10\%$ significantly higher than the maximum value proposed in order to investigate the numerical results sensitivity in the presence of various imperfection amplitudes. The out-of-roundness imperfection is defined as:

$$\alpha = \frac{D_{\max} - D_{\min}}{D_{\text{nom}}} 100\% \quad (4.2)$$

where

$$\begin{aligned} D_{\max} &= D_m + 2e \\ D_{\min} &= D_m - 2e \end{aligned}$$

And D_m is the mean diameter of the perfect circular cross section

In this case, out-of-roundness ($\alpha=10\%$) and out-of straightness ($L/300$ and $L/1000$) are both superimposed in the models as initial imperfections so that and the results could be compared with the ones referring, merely to the case of out-of-straightness imperfection. The material, mesh configuration and boundary conditions implemented in the models are mentioned in previous Chapters.

4.3. Initial wrinkling

In order to perform the finite element analysis for a wrinkled tubular model, a systematic methodology was followed. Initially, an eigen value analysis of a perfect elastic tubular member was conducted in order to gain the eigen mode. The eigen mode is characterized by the development of non-axisymmetric wrinkles of gradually increased amplitude from the capped ends to the mid span. The maximum amplitude is intentionally developed in the middle of the tube length. The displacements of the eigen mode were multiplied with a factor equivalent to specific maximum wrinkle-to-thickness ratios (0.25, 0.5). The buckling shape was superimposed to the initial perfect geometry of the model tube and non-linear finite element analysis was conducted in sequence in order to estimate the buckling response and the structural behavior under combined loading of the wrinkled tubular member.

A schematic representation of the imposed wrinkling is shown in the following figure. The amplitudes chosen are of various proportions of wall thickness (i.e. $w_0/t=0.25$ and 0.5).

The material, mesh configuration and boundary conditions used in the models are mentioned in previous Chapters.



Figure 4.3.1 Simulation of the wrinkled model with $w_0/t=0.5$ under axial compression

5. Stability curves

Initial imperfections (out-of straightness, out-of roundness, wrinkling) were imposed to the tubular models of various length values and cross sections and then monotonic axial compressive load was subjected. The critical buckling load was estimated for different tubular geometries, length values, and the types of imperfection mentioned above in order to develop buckling curves in terms of member slenderness of high strength steel tubular models. The finite element results are compared with the buckling curves proposed by current standards EN1993-1-1 [EN-1993-1-1, 2005], AISC [AISC-LRFD, 2000], CIDECT [CIDECT, 1998] and API-LRFD [API 2ARP, 1993] which are reported in ANNEX B. It is noted that the maximum crookedness limit permitted by the European standards is an amplitude of $e_0=L/300$ including the influence of residual stresses on the pipe wall. The limit proposed by AISC for out-of-straightness imperfection is $e_0=L/1000$.

5.1. Out-of-straightness

5.1.1. Buckling response

In order to estimate the stability curves for high strength steel tubular members, the buckling behavior was investigated in terms of the member slenderness and the amplitude of the initial crookedness e_0 . Load displacement curves were developed under axial compression for the HSS (TS590) imperfect ($e_0=L/300$) tubular member with $D=355\text{mm}$, $t=8\text{mm}$ as shown in Figure 5.1.1.1.

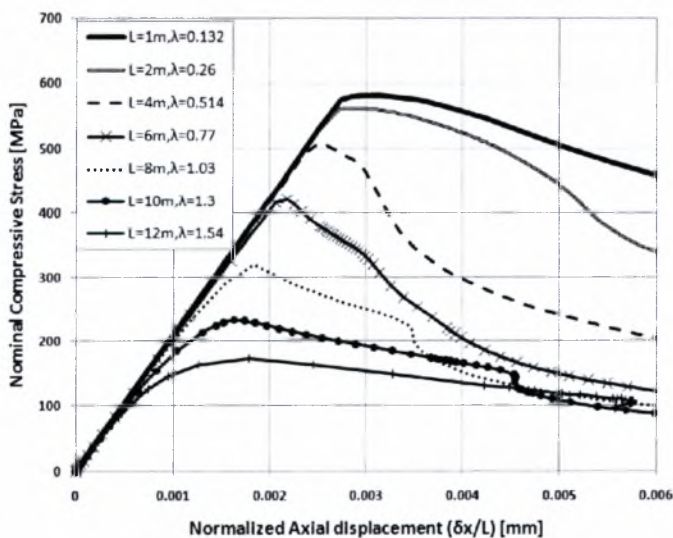


Figure 5.1.1.1 Comparison of load displacement paths for HSS tubular members with $D=355\text{mm}$, $t=8\text{mm}$ ($D/t=44$) and different values of member slenderness.

It is obvious that for a short relatively thin tube, buckling occurs progressively while plastic deformation is growing larger in the plastic region and the post buckling curve appears to be rather smooth. For intermediate values of member slenderness the transition from the elastic to the elastic-plastic region appears to be sharp and buckling occurs suddenly before the maximum capacity load is achieved. Additionally, it is shown that the buckling capacity load is significantly reduced when slender tubes are considered above the value of member slenderness $\lambda=0.5$.

The deformation of the pipe wall for low and intermediate value of member slenderness is shown in Figures 5.1.1.3 and 5.1.1.4, respectively. More specifically, for short cylinders with $D/t=44.375$ (class 4), local buckling occurs far from the peak axial load and buckles are developed in a non-symmetric form perpendicular to the longitudinal direction of the tube at the tube mid span, while for intermediate values of member slenderness the non axis-symmetric buckles are developed in a symmetric form corresponding to the axis coinciding with the longitudinal direction of the tube.

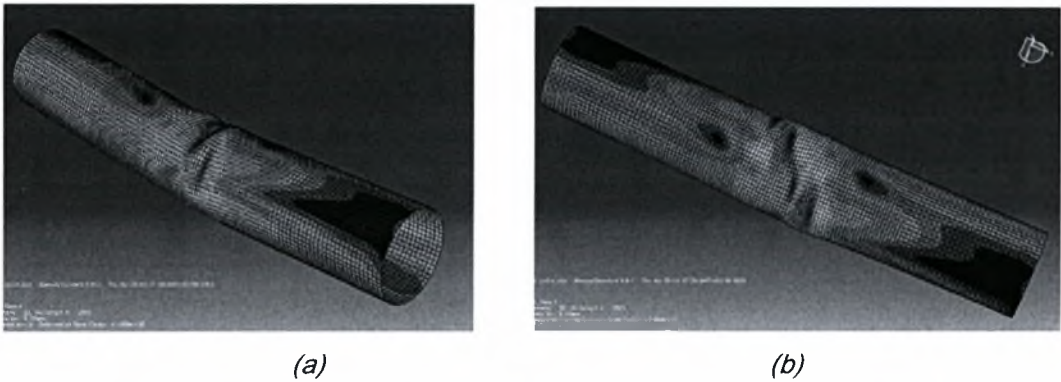


Figure 5.1.1.3 (a) Failure mode due to shell buckling and (b) the final non-axisymmetric buckle development for the model with $D/t=44.375$ and $L=2m$ ($\lambda = 0.26$)

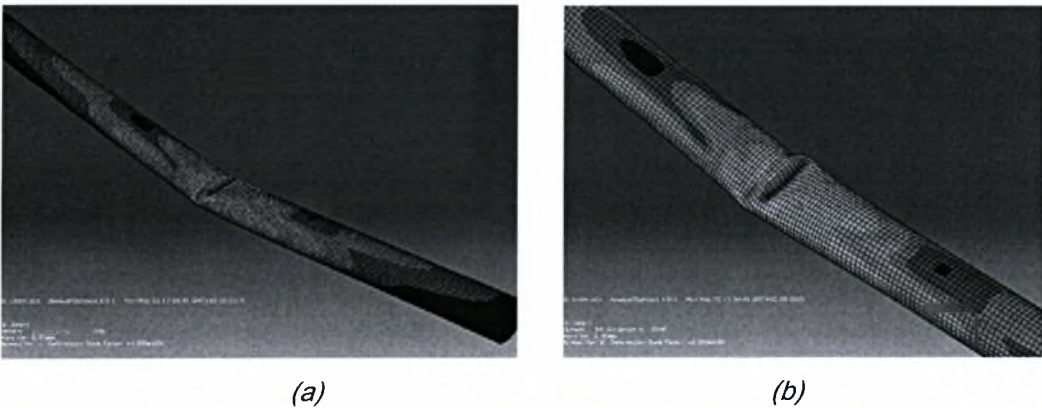


Figure 5.1.1.4 (a) Failure mode due to a combination of global and local buckling and (b) non-axisymmetric buckle development for the model with $D/t=44.375$ and $L=6m$ ($\lambda=0.77$)

Similarly, load-displacement paths and the buckle development on imperfect ($e_0=L/300$) HSS tubes with $D=355\text{mm}$, $t=12\text{mm}$ under axial compression are developed as shown in Figures 5.1.1.5 and 5.1.1.6, respectively.

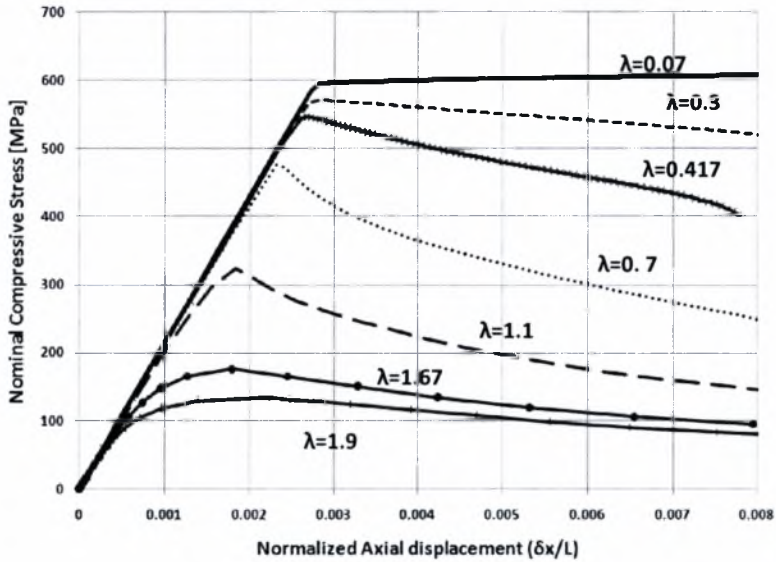
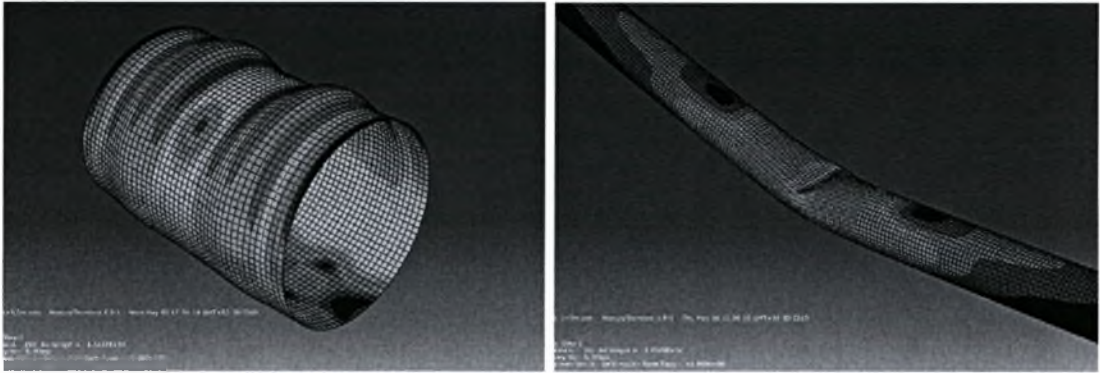


Figure 5.1.1.5 Comparison of load-displacement curves for tubular members with $D=355\text{mm}$, $t=12\text{mm}$ ($e_0=L/300$) for different values of member slenderness

The above Figure indicates that the buckling capacity load is significantly reduced as member slenderness is increased ($\lambda>0.5$). For short tubular members, buckling occurs while plastic deformation is gradually increased under plastic regime and the post buckling curve appears to be rather smooth. For intermediate values of member slenderness there is a sudden abrupt change in the slope of the load displacement curve. At this point, local buckling occurs before the maximum capacity load is achieved.



(a)

(b)

Figure 5.1.1.6 The failure mode of the tube model with $D/t=29.58$ (a) due to shell buckling for the model $L=0.5m$ ($\lambda=0.07$) and (b) global buckling of the tube with $L=5m$ ($\lambda=0.7$)

The deformation of the pipe wall for low and intermediate value of member slenderness is shown in Figures 5.1.1.6. It is shown that for short cylinders with $D/t=29.58$ (class 4), buckles are developed in a non-symmetric form perpendicular to the longitudinal direction of the tube close to the capped ends due to the influence of the boundary conditions. For intermediate values of member slenderness a single buckle is developed towards the inner part of the cross section perpendicular to the longitudinal direction.

In order to define the buckling strength sensitivity in the presence of initial imperfections and the corresponding post buckling behavior, load displacement curves of a model tube of $D=355\text{mm}$, $t=12\text{mm}$ and $L=3\text{m}$ with $e_0=L/300$ and $e_0=L/500$ are compared as shown in Figure 5.1.1.7. It is illustrated that the buckling strength considering $e_0=L/500$ is not significantly reduced (2%) compared with the case of $e_0=L/300$. Nevertheless the failure mode of a short cylinder (500mm) is different from the one observed for $e_0=L/300$, as shown in Figure 5.1.1.8. Herein, the buckles are developed around the circumference in an axis-symmetric form close to the boundary conditions. This is observed because, for short tubes, the $e_0=L/500$ imposed imperfection is considered rather small and does not induce significant flaw in the mid span compared to the significant influence of the boundary conditions, so the failure mode is developed similar to a perfect cylinder "elephant foot" failure at both capped ends.

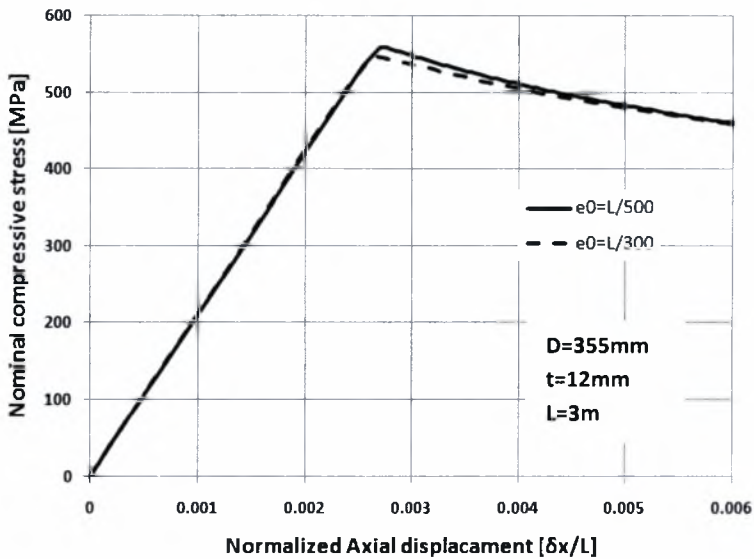


Figure 5.1.1.7 Comparison of load-displacement curves for HSS tubular members with $D=355\text{mm}$, $t=12\text{mm}$ and $L=3\text{m}$ for $e_0=L/300$ and $e_0=L/500$



Figure 5.1.1.8 Failure mode for the model with $D=355\text{mm}$, $t=12\text{mm}$ and $L=0.5\text{m}$ ($\lambda=0.07$) with $e_0=L/500$

5.1.2. Stability curves

Stability curves are developed through finite element analysis for a rather thick tube with a $D/t=29.58$ ($D=355\text{mm}$ and $t=12\text{mm}$) considering out-of-straightness with amplitudes of $e_0=L/300$, $e_0=L/500$. The maximum compressive strength obtained from the load-displacement curves for each length value (σ_{Rd}) through the finite element analysis is normalized with the nominal yield stress. The stability curves referring to $L/300$, $L/500$ and $L/1000$ are shown in Figures 5.1.2.1 in comparison.

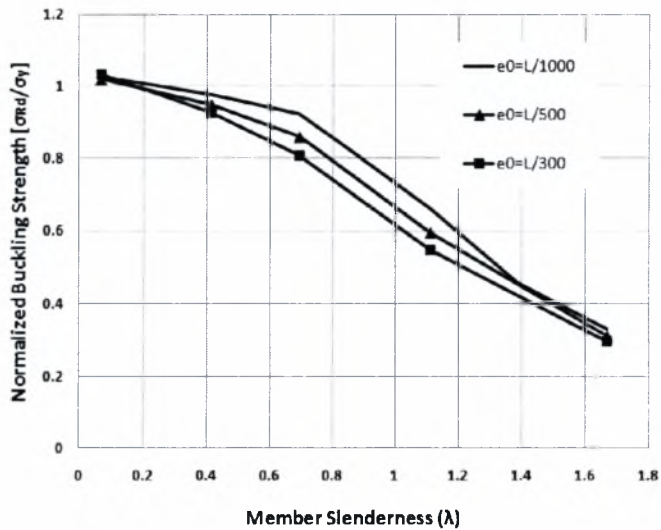
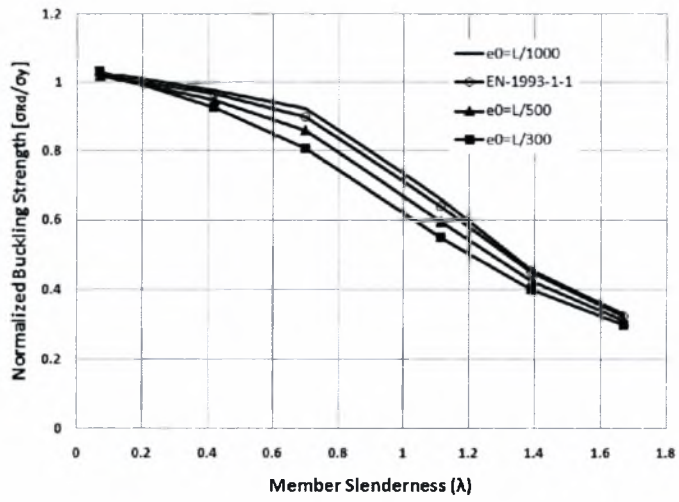
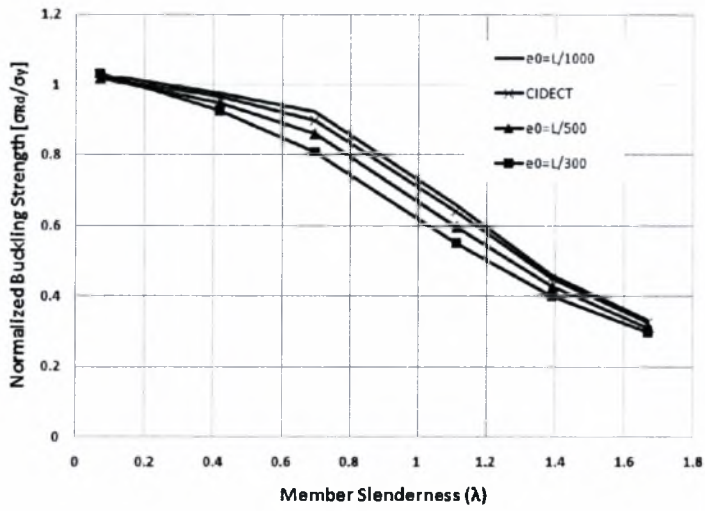


Figure 5.1.2.1 Comparison of stability curves for the cross section $D=355\text{mm}$ and $t=12\text{mm}$ with out-of-straightness (e_0) $L/300$, $L/500$ and $L/1000$

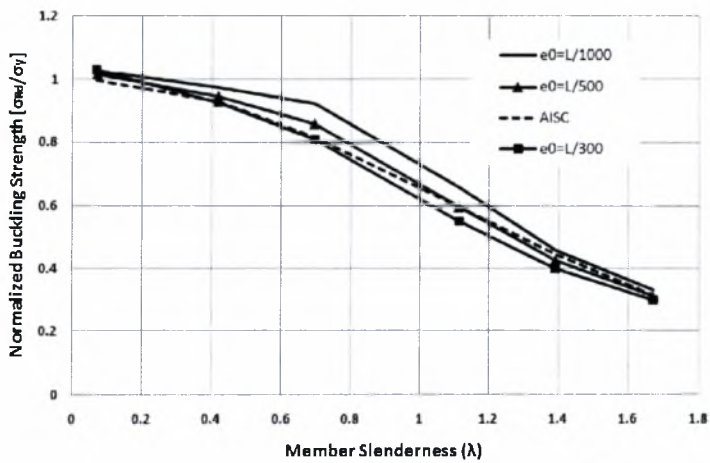
As shown in Figure 5.1.2.1, the critical buckling stresses obtained from the finite element analysis considering $L/300$ or $L/500$ is lower than $L/1000$. The most significant geometric deflection is imposed to the model tube when $e_0=L/300$ is considered. In this case, higher curvature and deformation are initially subjected on the model and the buckling strength is lessened significantly in comparison with the case of $L/1000$. Additionally, the finite element results are compared with the buckling curves proposed by current standards EN1993-1-1 [EN-1993-1-1, 2005], AISC [AISC-LRFD, 2000], CIDECT [CIDECT, 1998] and API-LRFD [API 2ARP, 1993], as shown in Figures 5.1.2.2. In order to form the proposed buckling curves, the buckling strengths are calculated in terms of member slenderness for the specific cross section classified as class 3 by the European standards and not slender by the American provisions. Additionally, it is proved that CIDECT propose similar buckling equations with the EN-1993-1-1 as far as compression strength for class 1, 2 and 3 cross sections are concerned.



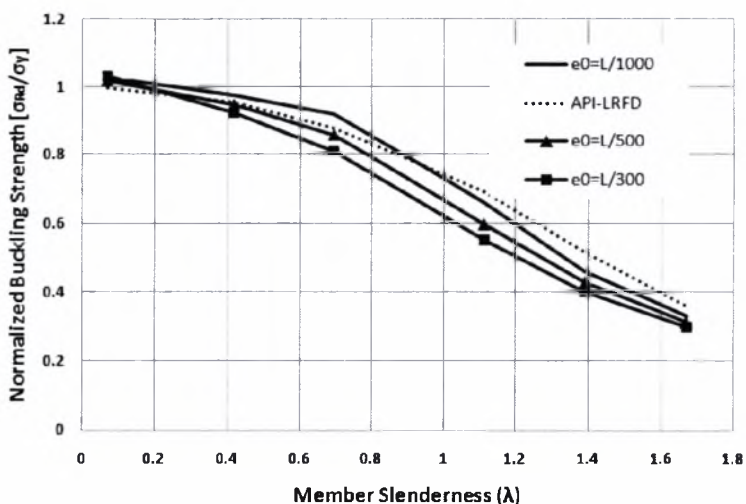
(a)



(b)



(c)



(d)

Figure 5.1.2.2 FEA results for $D=355\text{mm}$, $t=12\text{mm}$ and $e_0=L/300$, $L/500$ and $L/1000$ in comparison with (a) EN1993-1-1, (b) CIDECT, (c) AISC and (d) API- LRFD.

As shown in Figure 5.1.2.2a, the European buckling curves (EN-1993-1-1 and CIDECT), appear to be conservative for intermediate values of member slenderness compared to the cases of $e_0=L/300$ and $L/500$. On the contrary, the European curves are in good correlation with the one developed for the case of $e_0=L/1000$ even rather conservative because the proposed equations included in EN standard actually refer to out-of-straightness lower than $L/300$. Figure 5.1.2.2c indicates that the buckling curve proposed in AISC provision is penalizing enough in relation to the results obtained in the case of $L/1000$. Conversely, is in perfect correlation with the model of $L/500$ for member slenderness values equal to $\lambda>1.2$ and with the model of $L/300$ for $\lambda<0.7$. As shown in Figure 5.1.2.2d, for member slenderness values equal to $\lambda>1$, the buckling strength is overestimated by provision API for the three cases of out-of-straightness, but there is a good correlation-even penalizing-with the case of $e_0=L/1000$.

Furthermore, stability curve was developed through finite element analysis for the thick tube with a $D/t=19.37$ ($D=193.7\text{mm}$ and $t=10\text{mm}$) with $e_0=L/300$. The specific cross section is classified as class 1 according to European standards. The stability curve is compared with the current provisions is illustrated in Figure 5.1.2.3. It is shown that AISC provides the most correlative stability curve for the specific HSS cross section with $e_0=L/300$. On the contrary, EN-1993-1-1 and CIDECT appear to be gradually conservative for $\lambda<1.5$ while API remains conservative for member slenderness values up to $\lambda=2$. Above the

slenderness value of $\lambda=2$ the curves become identical, because tubular members which belong in this slenderness range are considered as slender members so elastic buckling is prevailing.

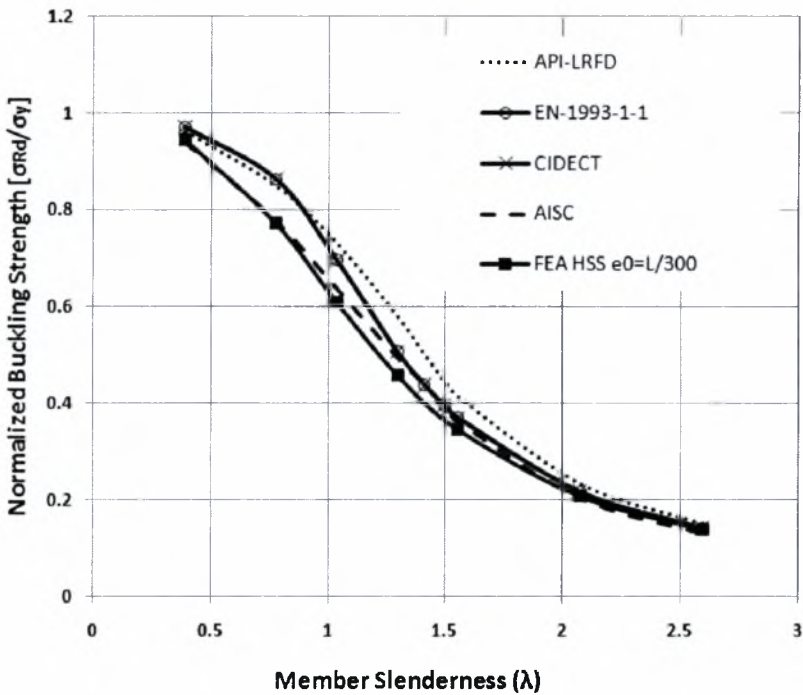


Figure 5.1.2.3 FEA results for $D=193.7\text{mm}$, $t=10\text{mm}$ and $e_0=L/300$ in comparison with EN1993-1-1, CIDECT, AISC-LRFD and API standards.

Similarly, stability curve was developed through finite element analysis for a relatively thin HSS tube with a $D/t=32.28$ ($D=193.7\text{mm}$ and $t=6\text{mm}$) and $e_0=L/300$. The specific cross section is classified as class 3 according to European standards. The stability curve and the comparison with the current provisions are illustrated in Figure 5.1.2.4. It is shown that the current provisions overestimate the buckling strength values for $0.2 < \lambda < 2$. More specifically, AISC provision predicts a buckling strength 11% greater than the finite element results for $\lambda=1.3$. Similarly, the maximum difference between EN-1993-1-1 or CIDECT curves with the FEA curves is figured at the point with $\lambda=1$ where the buckling strength proposed appears to be 15% greater than the value derived from the finite element analysis. API standard overestimates the buckling values for $0.2 < \lambda < 2.5$ and with a maximum proportion up to 40% for $\lambda=1.2$.

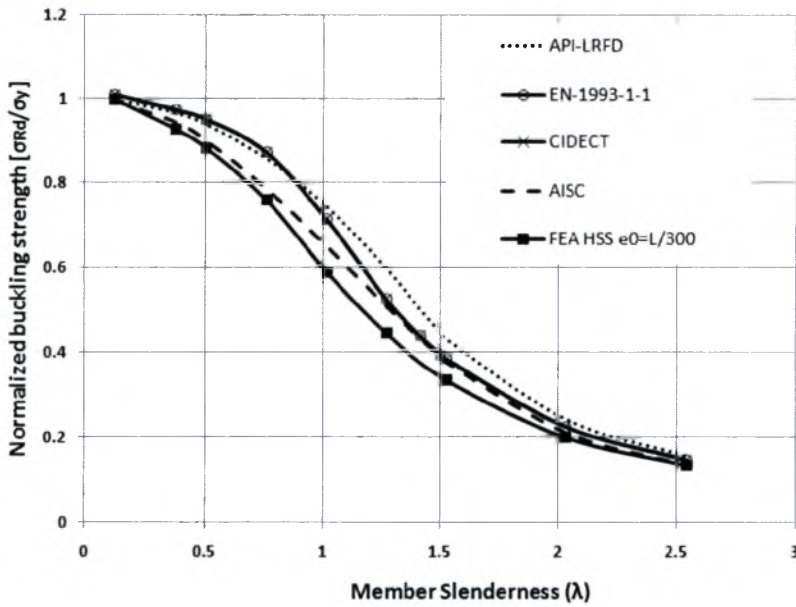


Figure 5.1.2.4 FEA results for $D=193.7\text{mm}$, $t=6\text{mm}$ and $e_0=L/300$ in comparison with EN-1993-1-1, CIDECT, AISC-LRFD and API standards.

Stability curve was defined through finite element analysis for the thin tube with a $D/t=44.375$ ($D=355\text{mm}$ and $t=8\text{mm}$) and $e_0=L/300$. The specific cross section can be considered as class 4 according to European standards and identified as slender by American provisions, so, in order to define the stability curve, a different procedure for calculating the buckling load for thin cross sections should be followed especially for European standards reported in the present study in ANNEX B. The stability curve in comparison with the current provisions is illustrated in Figure 5.1.2.5. It is shown that the most correlative curve is the AISC proposed curve. The curves proposed by European standards present an overestimating difference for $0.2 < \lambda < 2$ proposing 16% greater buckling strength for $0.6 < \lambda > 1$. API remains overestimating with a maximum difference of 30% for $0.9 < \lambda < 1.4$.

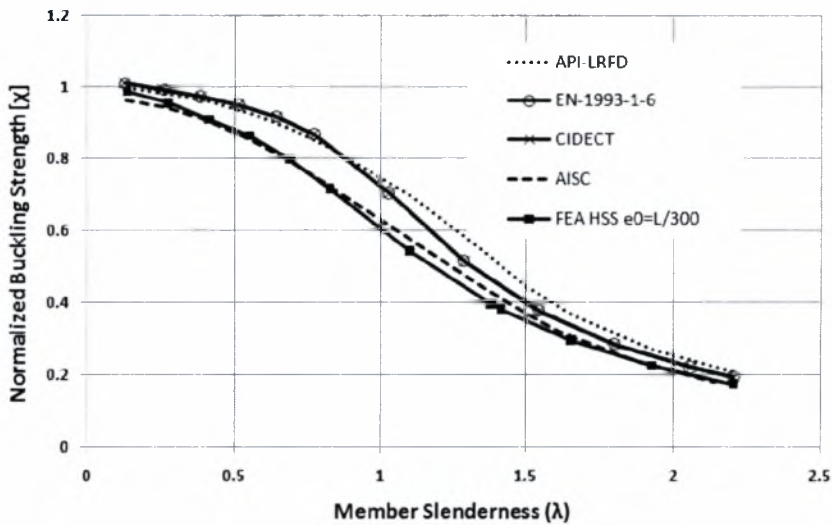


Figure 5.1.2.5 FEA results for $D=355$, $t=8\text{mm}$ and $e_0=L/300$ in comparison with EN1993-1-6, CIDECT, AISC- LRFD and API standards

Furthermore, stability curve was defined through finite element analysis for a relatively thick tube with a $D/t=22.18$ ($D=355\text{mm}$ and $t=16\text{mm}$) and out-of-straightness of $L/300$. The stability curve in comparison with the current provisions is illustrated in Figures 5.1.2.6. It is shown that the most correlative curve is the AISC proposed curve. The curves proposed by European standards present an overestimating difference gradually increased from $\lambda=0.2$ to $\lambda=0.75$ and decreased from $\lambda=0.75$ until $\lambda=2$ where all curves become identical. Similarly, API proposes overestimating values of buckling strengths with a maximum of 20% for $1 < \lambda < 1.25$.

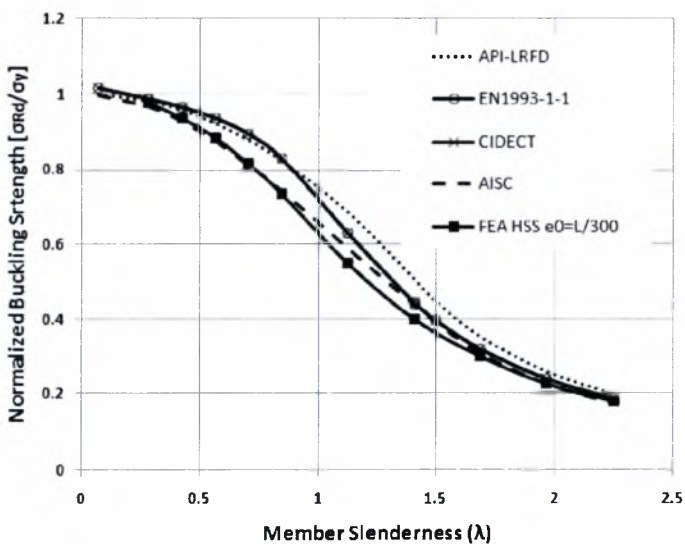


Figure 5.1.2.6 FEA results for $D=355$, $t=16\text{mm}$ and $e_0=L/300$ in comparison with EN1993-1-1, CIDECT, AISC-LRFD and API standards

Consequently, it is repeatedly shown that for the CHS cross sections of high strength steel, investigated in the present study (thick or thin), AISC-LRFD provision is the most correlative to the finite element results considering $e_0=L/300$, as far as stability curves are concerned.

Further finite element analysis was conducted for the thin walled tube with $D=355\text{mm}$, $t=8\text{mm}$ ($D/t=44.375$) and $e_0=L/300$ considering different material plastic modulus but similar yield stress. More specifically, the plastic hardening modulus chosen is constant and equal to $E_{pl}=E/1000$ is higher than the previous analysis ($E_{pl}=E/500$). Comparison of stability curves developed for both plastic modulus values is shown below in Figure 5.1.2.7. For specific member slenderness (especially for higher values $\lambda > 1$), when higher plastic hardening modulus is considered, higher buckling strength (increased by 15%) is observed. It is demonstrated that the buckling strength of a CHS member with $\lambda > 1$ is affected by the plastic behavior of the material. Comparison with the proposed stability curves for both material hardening values is shown in Figure 5.1.2.8.

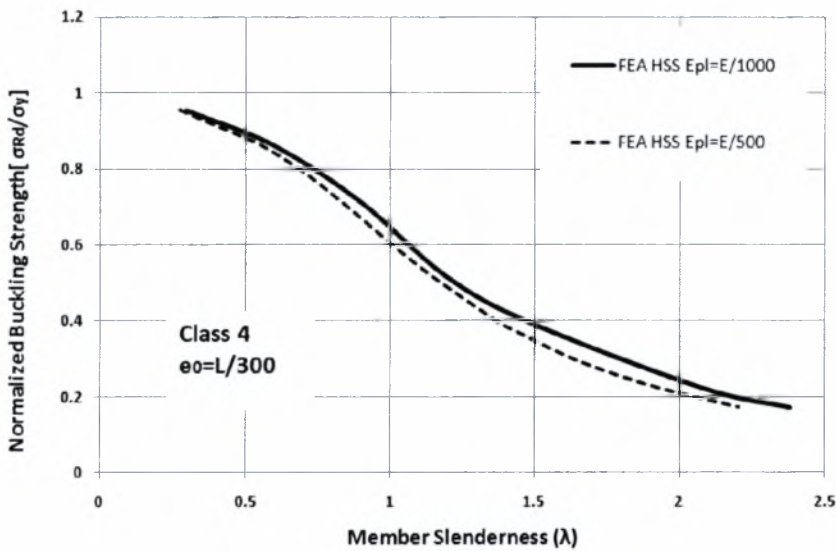


Figure 5.1.2.7 Comparison for $D=355\text{mm}$, $t=8\text{mm}$ with $e_0=L/300$ and plastic hardening of $E/500$ and $E/1000$

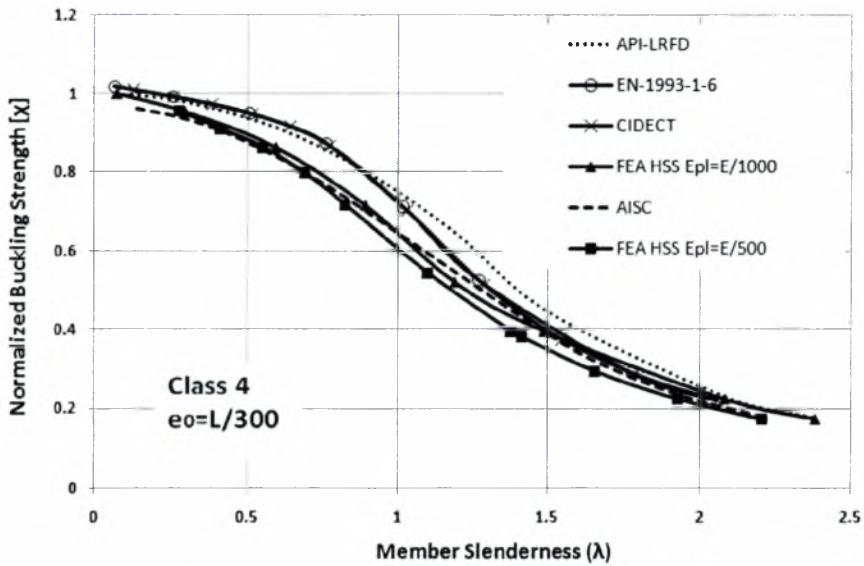


Figure 5.1.2.8 FEA results for $D=355$, $t=8\text{mm}$ and $e_0=L/300$ with plastic hardening $E/500$ and $E/1000$ in comparison with EN1993-1-1, CIDECT, AISC-LRFD, and API standards

Figure 5.1.2.9 shows that AISC stability curve is almost identical with the one developed for the case of $E_{pl}=E/1000$. Furthermore, EN-1993-1-1, CIDECT and API are considered overestimating for both plastic material hardening moduli investigated for the specific cross section (class 4).

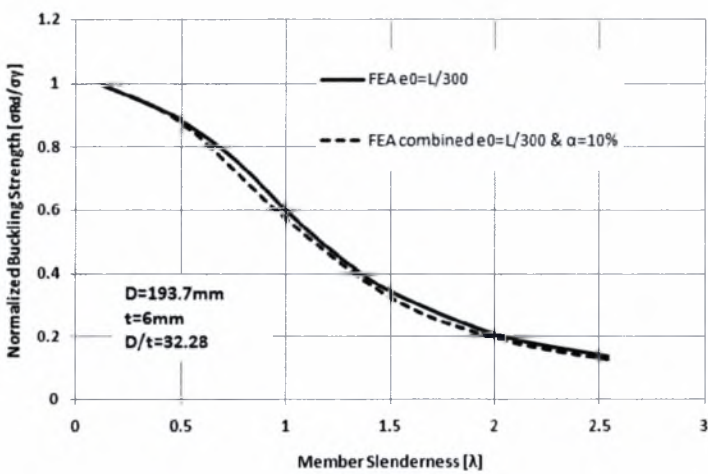
5.2. Combination of out-of-roundness and out-of straightness

The finite element models were designed with an initial longitudinal crookdness of $e_0=L/300$ at the mid span and an initial cross section ovalization of $\alpha=10\%$. The ovalization amplitude is defined as follows:

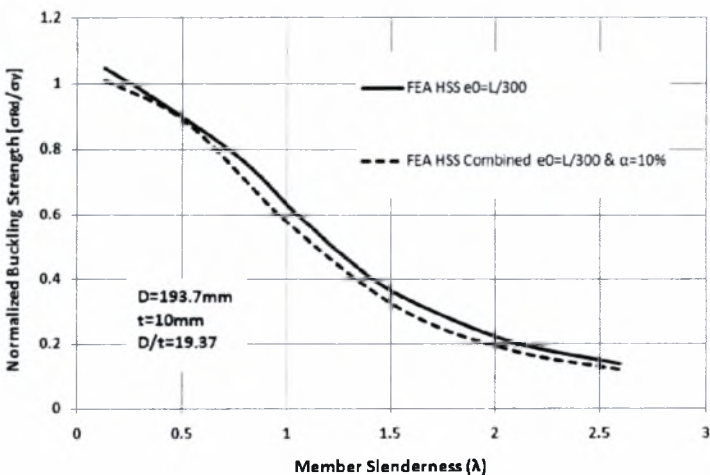
$$\alpha = \frac{D_{\max} - D_{\min}}{D_{\text{nom}}} 100\% \quad (5.2.1)$$

Stability curves were identified through finite element analysis for all the cases of cross sections mentioned in Chapter 4. A combination of $e_0= L/300$ and out-of-roundness $\alpha=10\%$ was imposed on the tubular models. The secondary axes of the elliptical cross section, where $D_{\max}= D_{\text{nom}} - 2e$ (Figure 2.2), is parallel to the direction deflection vector with amplitude of $e_0=L/300$ so that the two types of imperfections can be superimposed. Although, the ovalization amplitude can be considered rather high and the value is above the maximum limits proposed by the current provisions, it is chosen in order to illustrate clearly the influence

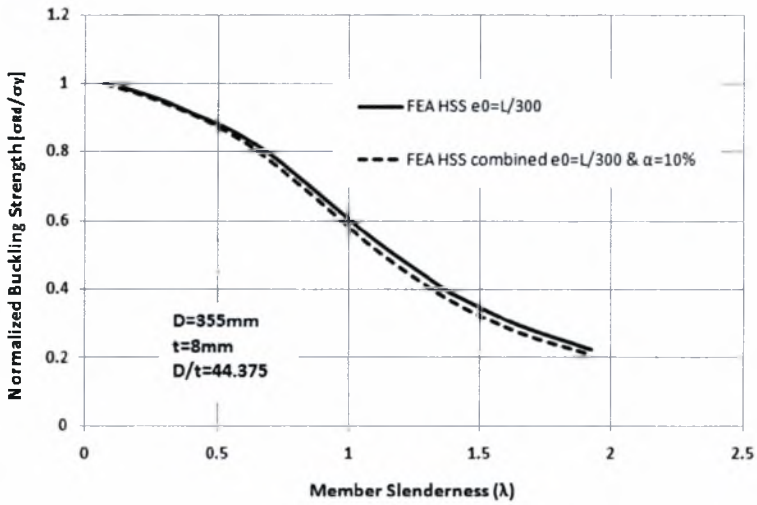
of the out-of-roundness in the buckling strength of the tubular members. As shown in Figures 5.2.1, the finite element stability curves considering out-of-straightness $e_0=L/300$ and the curves referring to the combination of $e_0=L/300$ and $a=10\%$ do not present significant differences, regardless of the high amplitude of α . So, it is proven that out of roundness does not affect significantly the buckling structural strength of the tube. Nevertheless, in the case of $D=355\text{mm}$ $t=16\text{mm}$ ($D/t=22.19$) the critical buckling load is slightly affected by the additional out-of-roundness imperfection for intermediate and high values of member slenderness and the buckling strength is decreased by 5% for intermediate values of member slenderness.



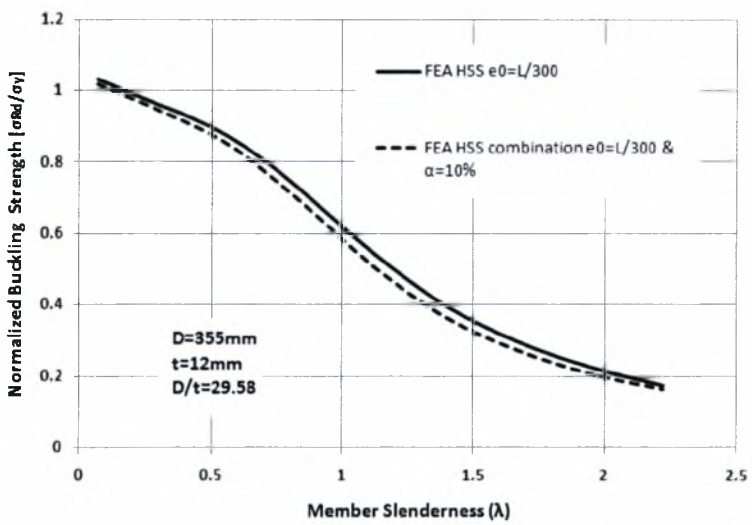
(a)



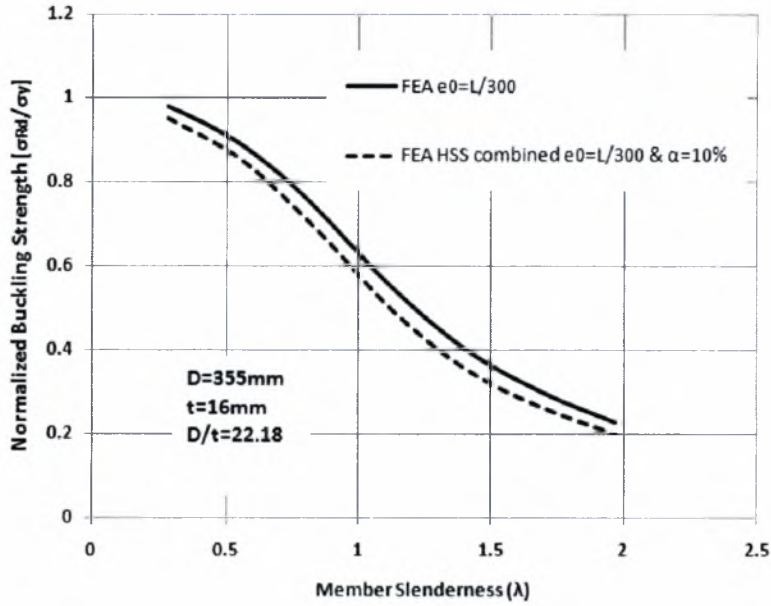
(b)



(c)



(d)



(e)

Figure 5.2.1 Stability curves for (a) $D=193.7\text{mm}$ $t=6\text{mm}$, (b) $D=193.7\text{mm}$ $t=10\text{mm}$, (c) $D=355\text{mm}$ $t=8\text{mm}$, (d) $D=355\text{mm}$ $t=12\text{mm}$ and (e) $D=355\text{mm}$ $t=16\text{mm}$ considering $e_0=L/300$ & $\alpha=10\%$ in comparison with the case of $e_0=L/300$

5.3. Initial wrinkling

Initial wrinkling with a maximum amplitude of $w_0=0.5t$ was imposed, as described in Chapter 4.3, to the tubular members with $D=323.9\text{mm}$ and $t=10\text{mm}$ of various length amplitudes. Axial compression was subjected to the wrinkled models and load- displacement curves were developed in order to define the buckling response of the imperfect models as shown in Figure 5.3.1. The stability curve is compared with the one proposed by the European and American standards (ANNEX B for class 3 cross section) as shown in Figure 5.3.2. The maximum buckling values presented in the diagrams were normalized with the yield stress equal to $\sigma_y=590\text{ MPa}$. Furthermore, the deformed geometries and the buckle development of the imperfect tubular models are identified under excessive deformation of the pipe wall, as shown in Figures 5.3.3. It is noted that the wrinkle amplitude ($w_0=0.5t$) imposed in the present analysis exceeds the tolerance limits for initial geometric imperfection and such tubular specimens should not be used for industrial applications. Nevertheless, the

specific case of imperfection is investigated in theoretical basis and it was chosen in order to clarify the detrimental effect of the presence of wrinkling on the tube wall.

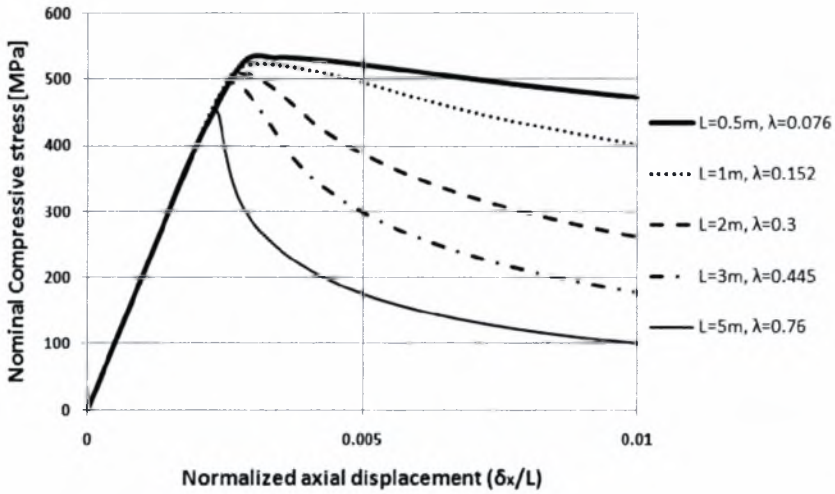


Figure 5.3.1 Load displacement curves for the cross section with $D=323.9\text{mm}$, $t=10\text{mm}$ and $w_0=0.5t$ under axial compression

Similar to the aforementioned cases of imperfect tubes, it is shown that for short wrinkled cylinders, buckling is produced smoothly under elastic-plastic regime and the post buckling curve is descending progressively. On the contrary, for medium or long tubular models the unstable postbuckling behaviour is abruptly initiated even at the elastic region developing a sharp significant change of the curve slope as the elastic buckling is prevailing.

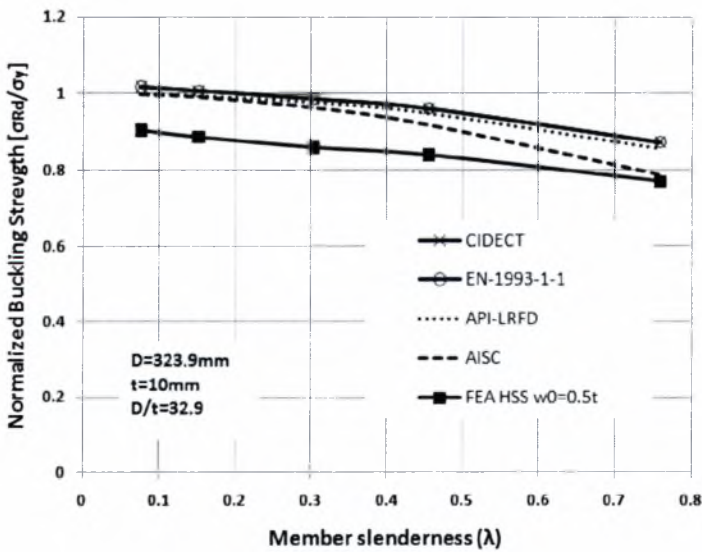


Figure 5.3.2 FEA results for $D=323.9\text{mm}$, $t=10\text{mm}$ with $w_0=0.5t$ in comparison with EN1993-1-1, CIDECT, AISC-LRFD and API standards

The comparison with the current provisions indicates that the buckling strength of the tubular models referring to the cross section with $D=323.9\text{mm}$ and $t=10\text{mm}$ considering the presence of initial wrinkling of an amplitude of $0.5t$ appears to be lower than the ones calculated in the current provisions. Furthermore, for intermediate values of member slenderness $0.3 > \lambda > 0.8$, Eurocode, CIDECT and API are considered more conservative than AISC-LRFD

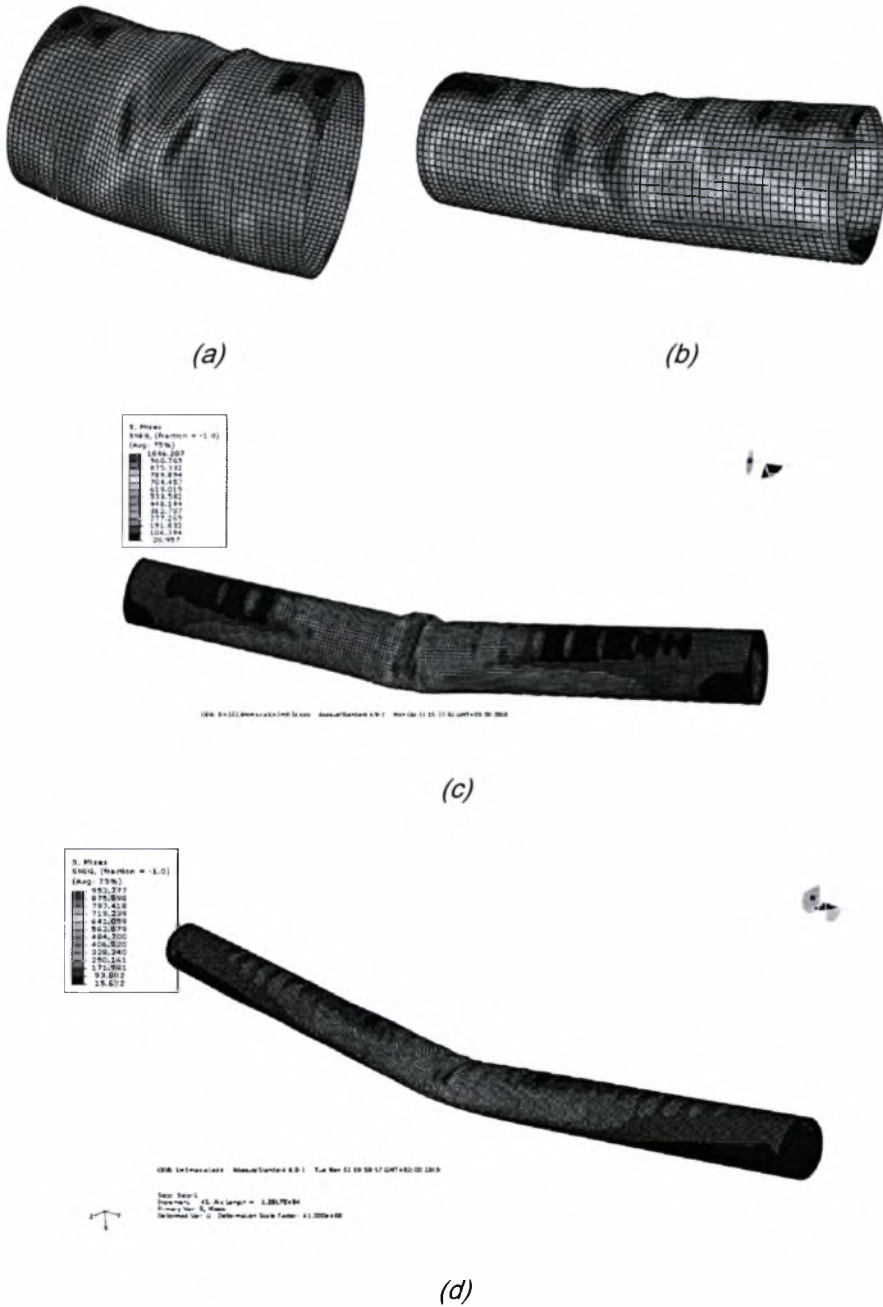


Figure 5.3.3 Deformed model geometry and buckle development of the cross section $D=323.9\text{mm}$, $t=10\text{mm}$ and $w_0=0.5t$ under axial compression for (a) $L=0.5\text{m}$ ($\lambda=0.076$), (b) $L=1\text{m}$ ($\lambda=0.152$), (c) $L=3\text{m}$ ($\lambda=0.456$) and (d) $L=5\text{m}$ ($\lambda=0.76$)

Unsimilar to the out-of-straightness imperfection, for the entire range of values of member slenderness investigated in this section, initial pipe wall wrinkling results in non-axisymmetric buckling development around the circumference in a symmetric form related to the longitudinal axis of the tubular member.

6. Interaction diagrams

Interaction diagrams are presented in this study, developed for imperfect tubular members 3 and 8m long with diameter-to-thickness ratios $D/t=29.58$ ($D=355\text{mm}$ and $t=12\text{mm}$) and $D/t=44.37$ ($D=355\text{mm}$ and $t=8\text{mm}$). The cases of initial imperfections imposed are out-of-straightness $e_0=L/300$, $e_0=L/1000$, a combination of out-of-straightness $L/300$ and out-of-roundness $\alpha=3\%$. The amplitude of the out-of-roundness imposed, corresponds to the boundary limit proposed by API standard. The length values of the tubular members were chosen so that relatively short and long columns are considered in order to compare the results between different values of member slenderness. Furthermore, interaction curves are defined for a 3m long tubular member with a cross section of $D=323.9\text{mm}$ and $t=10\text{mm}$ with initial non axi-symmetric wrinkling along the tube length. The material of the tubular members designed for the development of interaction diagrams is identical to the one used for the definition of stability curves with a yield stress of $\sigma_y=590\text{ MPa}$ as mentioned in Chapter 3. The geometry, the boundary conditions, the meshing of the tube models are the same described in Chapter 4.

In order to form the interaction curve, a specific loading sequence is followed: At first, the tube model is subjected to monotonic axial compression until global buckling occurs and the maximum load is reached (N_a). Then the model is subjected to axial compression up to 0.25, 0.5 and 0.75 N_a at the two capped ends and then subjected to lateral moment up to a high level of global deflection and local deformation. Finally, the interaction diagrams formed numerically, represent the maximum bending strength in terms of the initially subjected axial compression.

The axial load (N) and the maximum bending moment (M) obtained by numerical analysis are normalized with the N_0 and M_0 , respectively, which are defined as follows:

$$N_0 = \pi D_m t \sigma_y \text{ and}$$

$$M_0 = D_m^2 t \sigma_y$$

where

D_m : the mean tube diameter

t : the wall thickness

σ_y : the yield stress

6.1. Out-of-straightness imperfection

A schematic illustration of the model with out-of-straightness and the combined loading subjected in order to define the interaction diagrams is shown in Figure 6.1 where the axial compressive load, the bending moment and the initial deflection are represented as P , M and e_0 respectively.

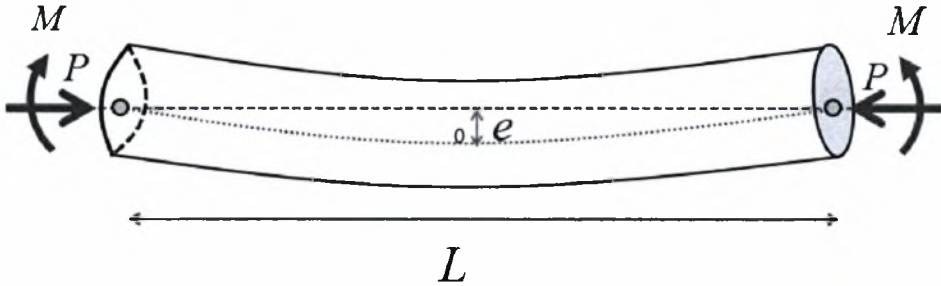


Figure 6.1.1 The model configuration and loading sequence

Interaction diagrams referring to the cross sections $D=355\text{mm}$, $t=12\text{mm}$ ($D/t=29.58$) and $D=355\text{mm}$, $t=8\text{mm}$ ($D/t=44.375$) are computed. The tubular models, 3 and 8m long, designed with out-of-straightness amplitude of $e_0=L/300$ and $e_0=L/1000$, were subjected to combined axial compression and lateral bending moment, both applied at the tubular member ends as shown in Figure 6.1.1.

Comparison of the interaction diagrams is illustrated in Figure 6.1.2, where different amplitudes of initial out-of-straightness are imposed for the short tube (3m long) with $D=355\text{mm}$ and $t=12\text{mm}$. As expected, under pure axial compression the buckling strength considering $L/300$ is lower than the strength in the case of $L/1000$. Nevertheless, as expected, the amplitude of the initial imperfection does not affect the bending capacity under pure bending condition. Moreover, the buckling strength for the larger value of initial out-of-straightness ($L/300$) is not-significantly reduced concerning the specific tube length compared with the case of $L/1000$.

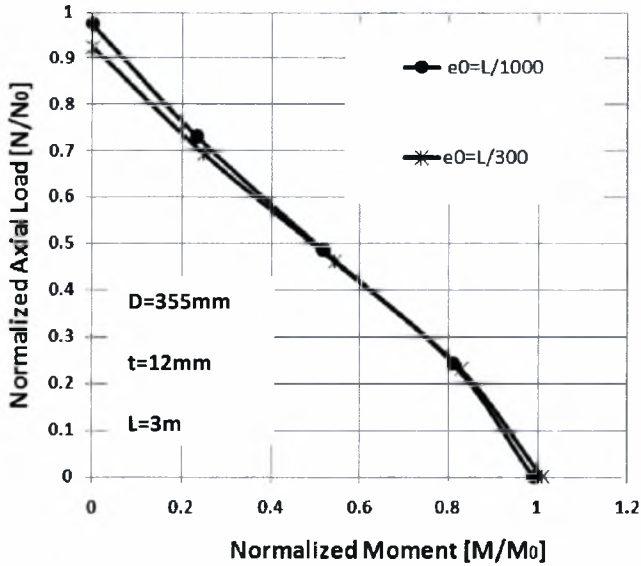


Figure 6.1.2 Comparison of interaction curves of the tube with $D=355\text{mm}$, $t=12\text{mm}$ and $L=3\text{m}$ with $e_0=L/1000$ and $e_0=L/300$

Furthermore, comparison of interaction curves is illustrated in Figure 6.1.3, where different amplitudes of initial out-of-straightness are imposed on the long tube (8m long) with $D=355\text{mm}$ and $t=12\text{mm}$. As shown in Figure 6.1.3, under pure axial compression the buckling strength considering $e_0=L/300$ is lower than the strength in the case of $e_0=L/1000$, as expected. More specifically, the buckling strength under pure axial compression is equal to $0.65N_0$ (for class 3, N_0 coincides with the compressive strength N_{Rd} of the cross section, [EN-1993-1-1,2005]) in the case of $e_0=L/1000$ but $0.55N_0$ (or N_{Rd}) for the case of $e_0=L/300$, concerning the specific tube. On the other hand, the amplitude of the initial imperfection does not affect the bending capacity under pure bending condition.

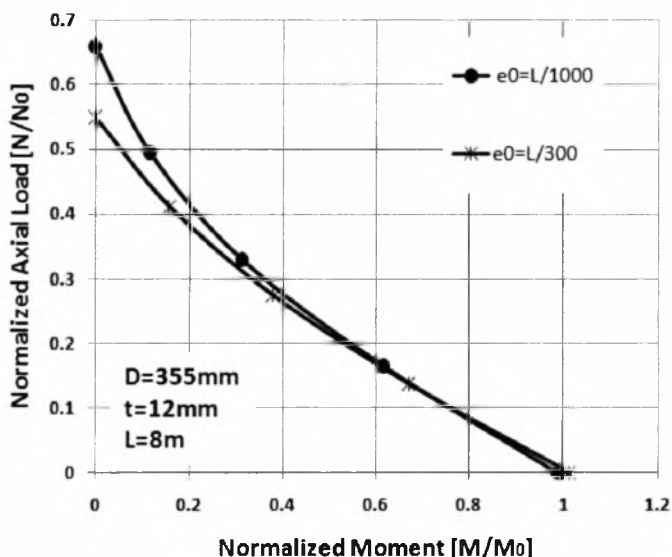


Figure 6.1.3 Comparison of interaction curves of the tube with $D=355\text{mm}$, $t=12\text{mm}$ and $L=8\text{m}$ with $e_0=L/1000$ and $e_0=L/300$

Comparison of the interaction diagrams is illustrated in Figure 6.1.4 for the short and the long imperfect tube with cross section $D=355\text{mm}$ and $t=12\text{mm}$ and initial out-of-straightness $e_0=L/300$. In Figure 6.1.4 the compression and bending values are normalized with $N_0 = \pi D_m t \sigma_y$ and $M_0 = D_m^2 t \sigma_y$. It is indicated that long tubular members exhibit lower buckling strength under pure compression than short ones, while bending strength is not affected by the slenderness of the tubular member under pure bending.

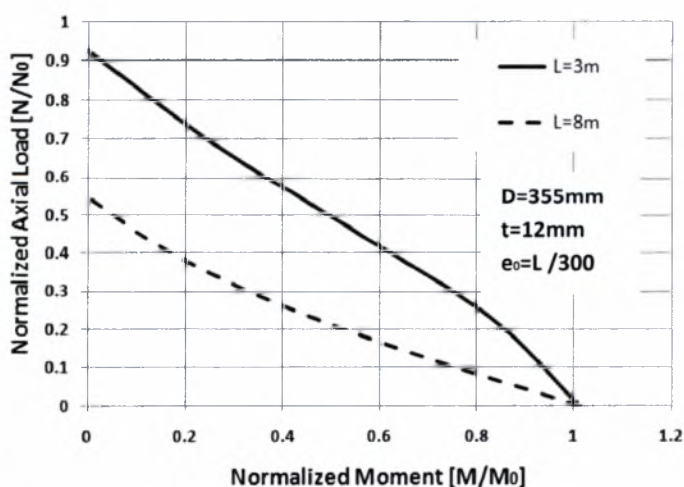


Figure 6.1.4 Comparison of interaction curves for cross section $D=355\text{mm}$, $t=12\text{mm}$ and $e_0=L/300$ with different length values

Furthermore, moment-rotation curves were developed for the short and long tubular members with $D=355\text{mm}$, $t=12\text{mm}$ in the case of $e_0=L/300$ as shown in Figures 6.1.5 and 6.1.6. The curves are traced for different amplitudes of initially subjected axial compression of amplitudes of $0.25N_a$, 0.5 and $0.75N_a$.

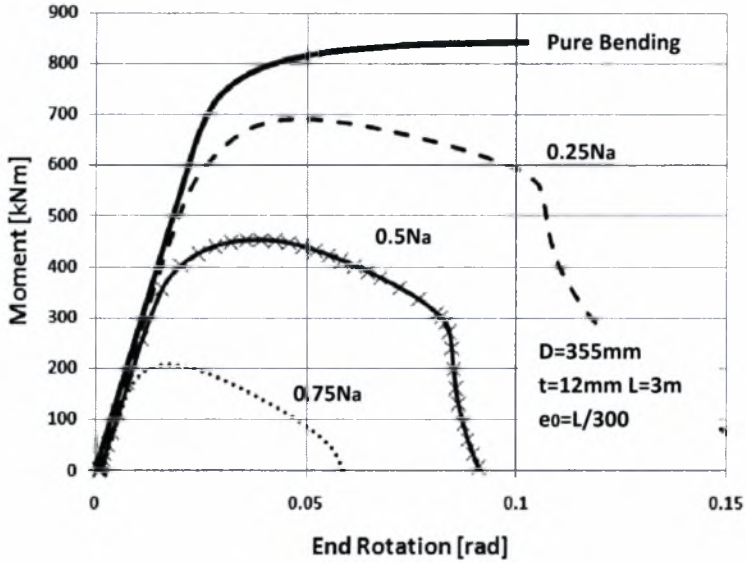


Figure 6.1.5 Comparison of moment-rotation curves of the tube with $D=355\text{mm}$, $t=12\text{mm}$ and $L=3\text{m}$ with $e_0=L/300$ for different values of axial compressive load.

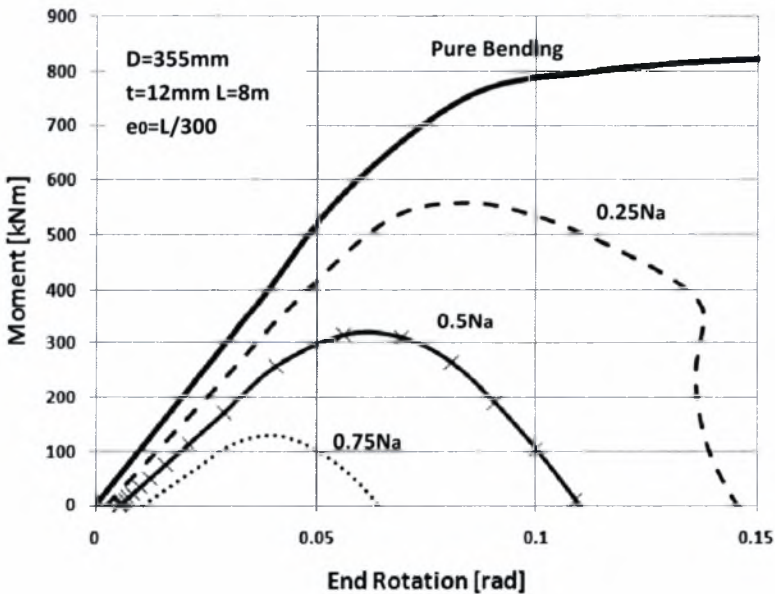


Figure 6.1.6 Comparison of moment-rotation curves of the tube with $D=355\text{mm}$, $t=12\text{mm}$ and $L=8\text{m}$ with $e_0=L/300$ for different values of axial compressive load.

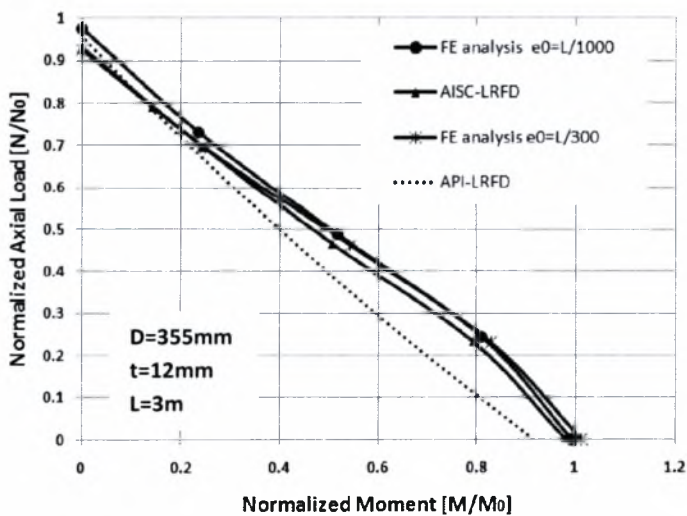
As shown in the above Figures, for both length values, the moment capacity reduces significantly as the value of the axial load increases, due to the increased level of the induced stress and strain field imposed when higher level of axial compression is subjected.

The deformed imperfect tubular member ($D=355\text{mm}$, $t=12\text{mm}$, $L=3\text{m}$ and $e_0=L/1000$) is shown in Figure 6.1.7 under combined loading when axial load of amplitude of $0.25N_a$ is subjected. A “single foot” buckle has been developed towards the inner part of the tube when bending load is applied, while global buckling deflection has already occurred under bending.

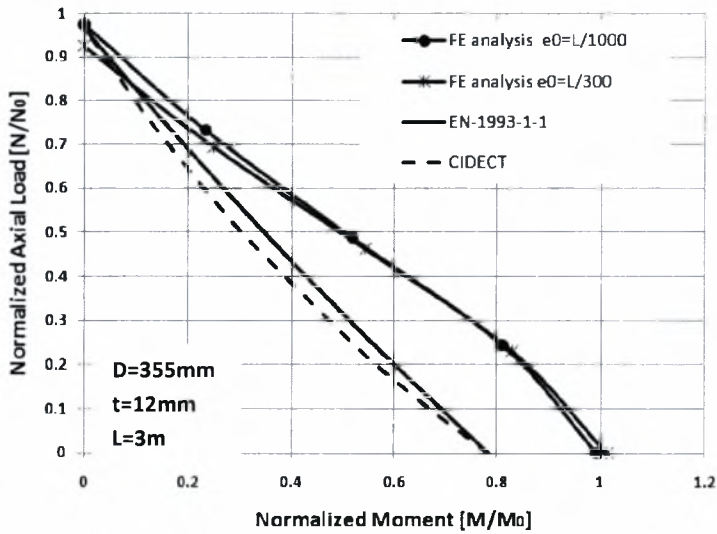


Figure 6.1.7 Deformed tubular member with $D=355\text{mm}$, $t=12\text{mm}$, $L=3\text{m}$ and $e_0=L/1000$ under combined loading with $0.25N_a$

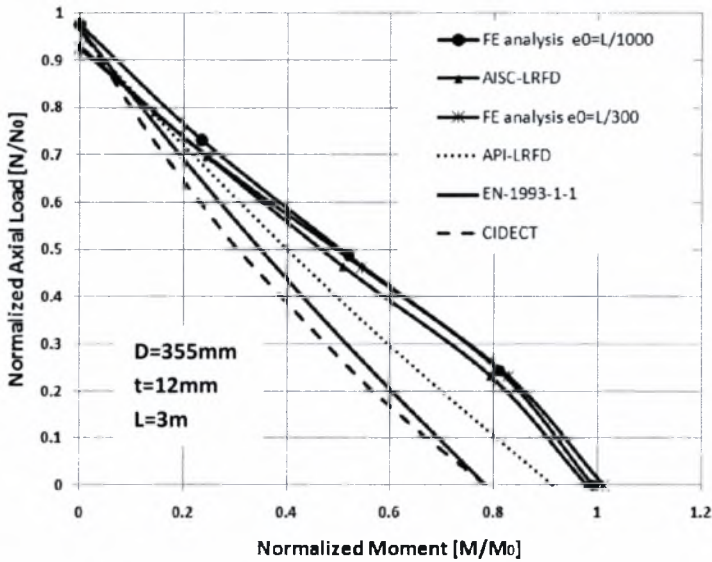
The interaction curves for the tubular member with cross section $D=355\text{mm}$ and $t=12$ and $L=3\text{m}$ and 8m are compared with the ones proposed by current standards and recommendations as shown in the following Figures 6.1.8 and 6.1.9. The initial imperfections considered are out-of-straightness with amplitudes of $e_0=L/300$ and $e_0=L/1000$.



(a)



(b)



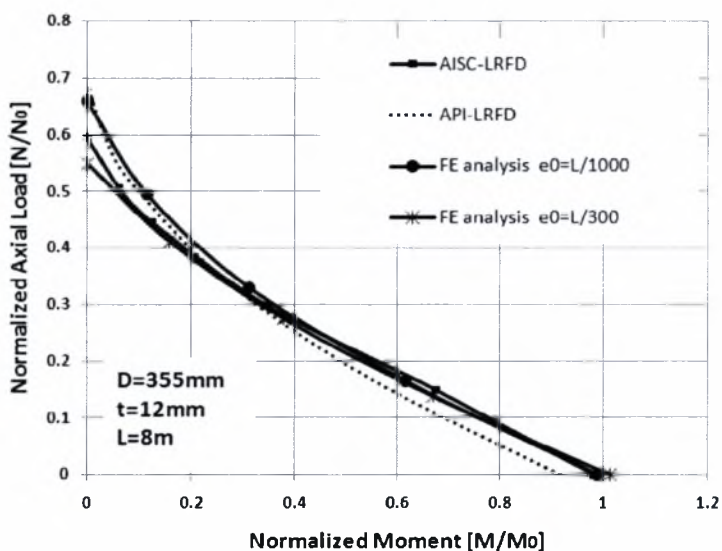
(c)

Figures 6.1.8 Comparison of interaction curves of the tube with $D=355\text{mm}$, $t=12\text{mm}$ and $L=3\text{m}$ with $e_0=L/1000$ and $e_0=L/300$ between a) API and AISC-LRFD, b) EN-1993-1-1 and CIDECT and c) all of the above standards

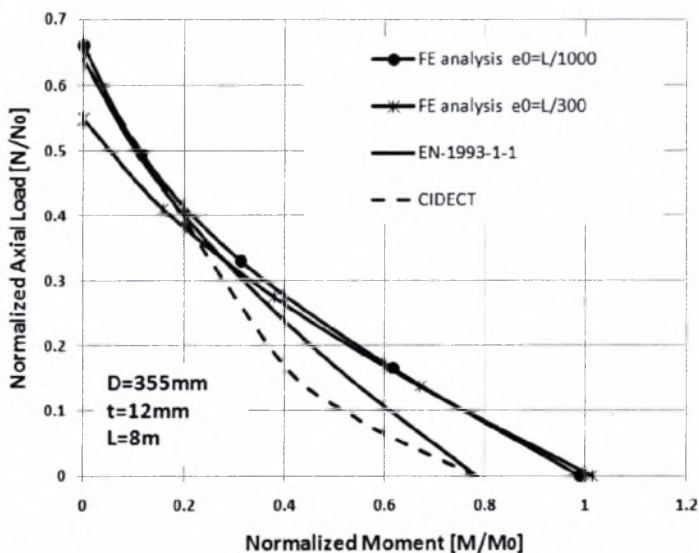
As shown in Figure 6.1.8, the design values for compression and bending moment are penalized in the case of high strength steel tubular members with $L=3\text{m}$ and class 3 cross section. Although, the axial compressive strength under pure compression is well predicted by the European and American standards, for compressive loads $N < 0.7N_0$ the bending strength proposed by API appears to be 10% lower than the results obtained in both cases of out-of-straightness imperfection. Similarly, EN-1993-1-1 and CIDECT underestimate the bending

strength under pure bending by 20%. On the contrary, AISC-LRFD curve is in good correlation with the both cases of out-of-straightness case especially for axial compressive load $N > 0.7N_0$

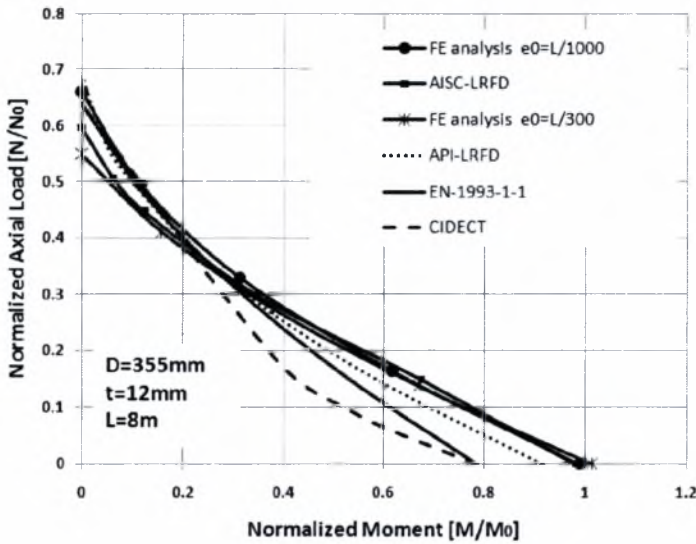
Figure 6.1.9 shows the finite element interaction curves for the cross section $D=355\text{mm}$ and $t=12\text{mm}$ and $L=8$ for $e_0=L/300$ and $e_0=L/1000$ in comparison with the proposed ones. It is shown that the bending design strengths are significantly penalized by the EN-1993-1-1 and CIDECT provisions (20%) while API and AISC underestimate the axial compressive design strengths by 10-15%.



(a)



(b)



(c)

Figure 6.1.9 Comparison of interaction curves of the tube with $D=355\text{mm}$, $t=12\text{mm}$, $L=8\text{m}$ and $e_0=L/1000$ and $L/300$ with a) API and AISC-LRFD, b) EN-1993-1-1 and CIDECT and c) all of the above standards

In Figure 6.1.9, it is indicated that for the tubular member with $L=8\text{m}$ and cross section of $D=355\text{mm}$ and $t=12\text{mm}$, the axial compressive strength obtained, considering both amplitudes of out-of-straightness ($L/1000$ and $L/300$) appear to be underestimated by the European standards. More specifically, EN-1993-1-1 is in good agreement with the case of $L/1000$ for $N < 0.3N_0$ the bending strength is underestimated for 20% especially under pure bending condition. Moreover, CIDECT curve is penalizing (up to 20% considering pure bending) considering all combined loading cases and both cases of initial crookedness. Conversely, the American standards are well correlated with the finite element results, especially AISC is in perfect correlation with the case of $e_0=L/1000$.

Comparison of the interaction diagrams is illustrated in Figure 6.1.10 for the short and the long imperfect tube with cross section $D=355\text{mm}$ and $t=8\text{mm}$ and initial out-of-straightness $e_0=L/300$. The compression and bending values are normalized with $N_0 = \pi D_m t \sigma_y$ and $M_0 = D_m^2 t \sigma_y$. It is illustrated, as expected, that long tubular members exhibit lower buckling strength under pure compression than short ones, while pure bending condition is not affected by the value of member slenderness.

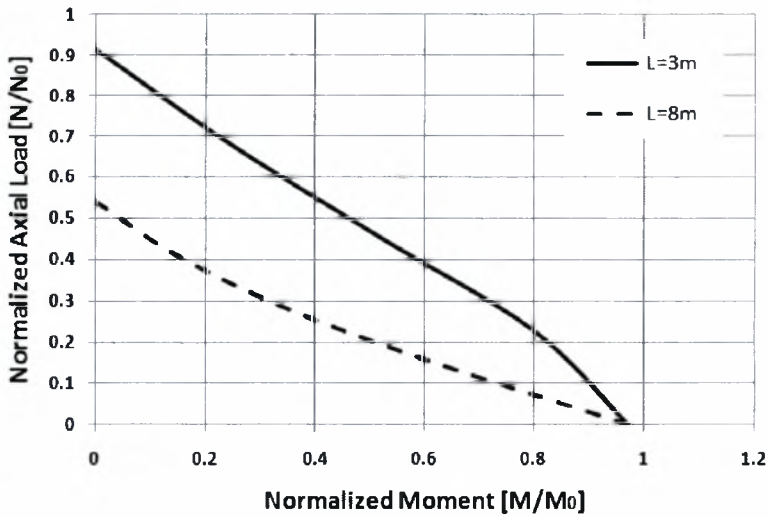


Figure 6.1.10 Comparison of interaction curves for cross section $D=355\text{mm}$, $t=8\text{mm}$ and $e_0=L/300$ with different length values

Furthermore, moment-rotation curves were identified as shown in Figure 6.1.11 for the short tubular member ($L=3\text{m}$) with $D=355\text{mm}$, $t=8\text{mm}$ in the case of $e_0=L/300$. The curves are formed under different amplitudes of initially subjected axial compression of amplitudes of 0.25, 0.5 and 0.75 N_a , held constant while bending is applied.

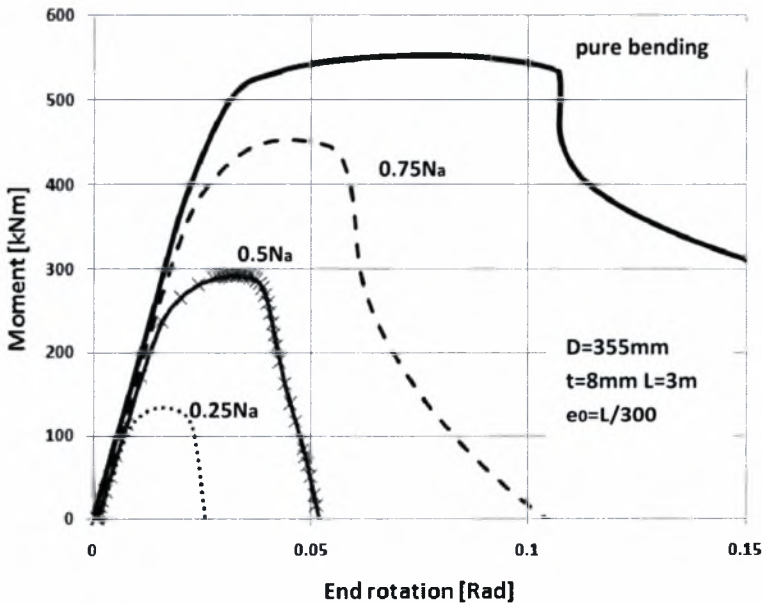


Figure 6.1.11 Comparison of moment-rotation curves of the tube with $D=355\text{mm}$, $t=8\text{mm}$ and $L=3\text{m}$ with $e_0=L/300$ for different values of axial compressive load

The deformed imperfect tubular member ($D=355\text{mm}$, $t=8\text{mm}$, $L=3\text{m}$ and $e_0=L/300$) under combined loading is shown in Figures 6.1.12. The deformed geometries presented are produced far beyond the maximum bending load, when local buckles have been developed at

the mid span of the tube length where the maximum deflection of the longitudinal axis ($e_0=L/300$) is initially located. As shown in these Figures, a local buckle is developed in a similar manner under combined loading with no symmetrical form with respect to the longitudinal axis. On the other hand, in the case of pure bending, the buckle develops a single “foot” buckle towards the inward part of the tube cross section at the mid span of the tube length and perpendicular to the longitudinal axis.

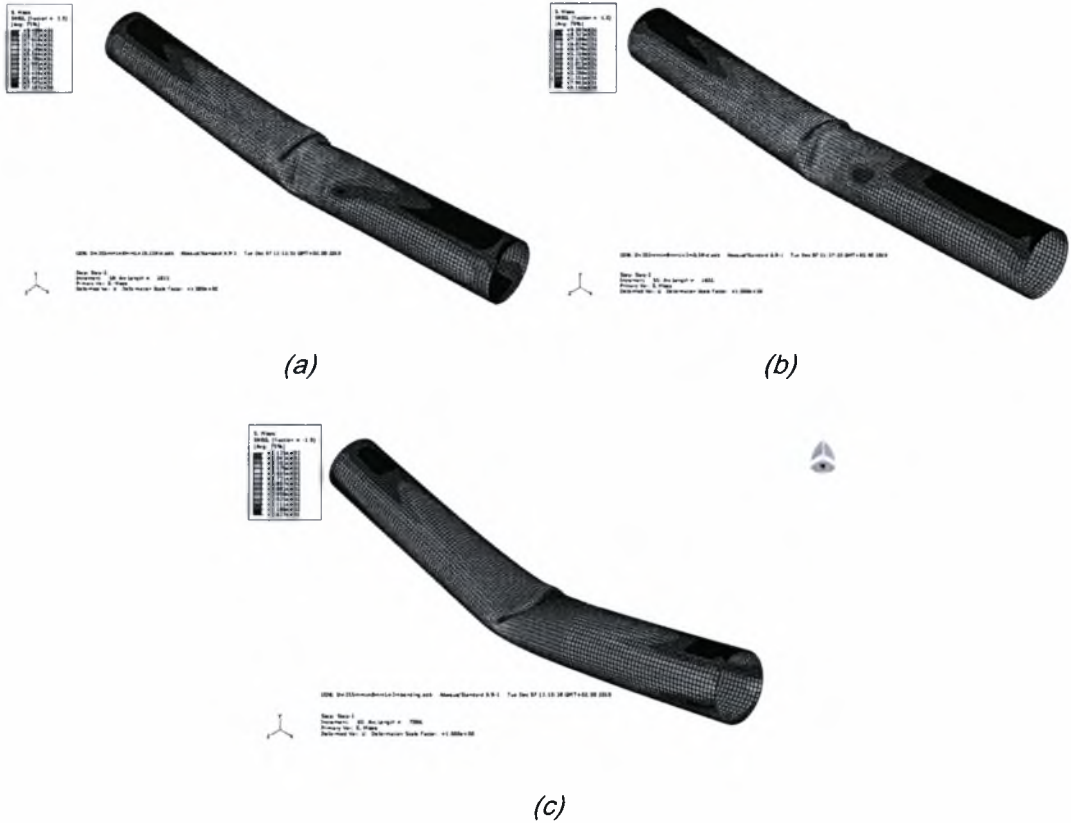
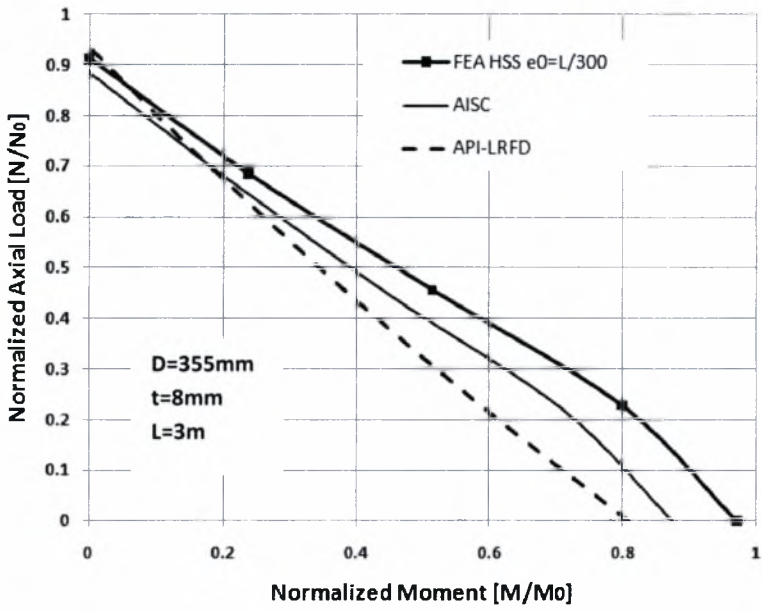
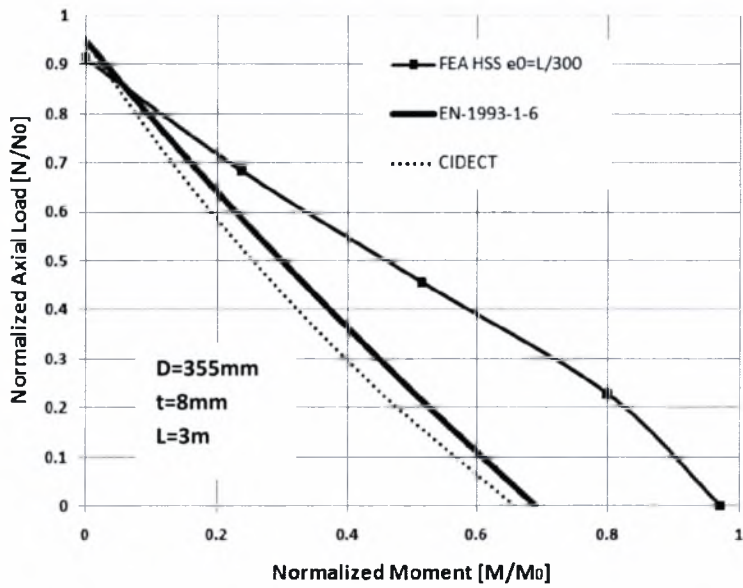


Figure 6.1.12 Deformed model geometry of the tubular member with $D=355\text{mm}$, $t=8\text{mm}$ and $L=3\text{m}$ ($e_0=L/300$) under (a) combined axial compression equal to $0.25N_a$ and bending, (b) combined axial compression equal to $0.5N_a$ and bending and (c) pure bending

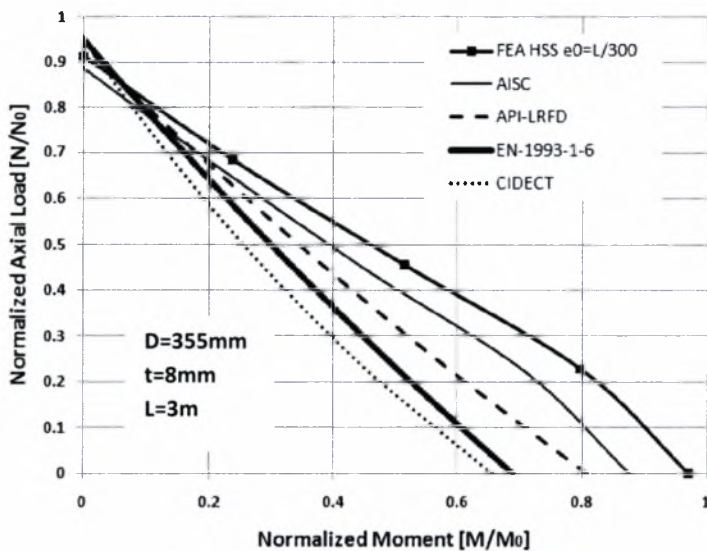
The finite element results for the tubular member with $D=355\text{mm}$, $t=8\text{mm}$ which is classified as class 4 according to European standards (mentioned in Chapter 5) are compared with the curves proposed by the current provisions and recommendations for $L=3\text{m}$ and 8m as shown in Figure 6.1.13 and 6.1.14, respectively. The initial imperfection considered is the out-of straightness with an amplitude of $e_0=L/300$ for both length values.



(a)



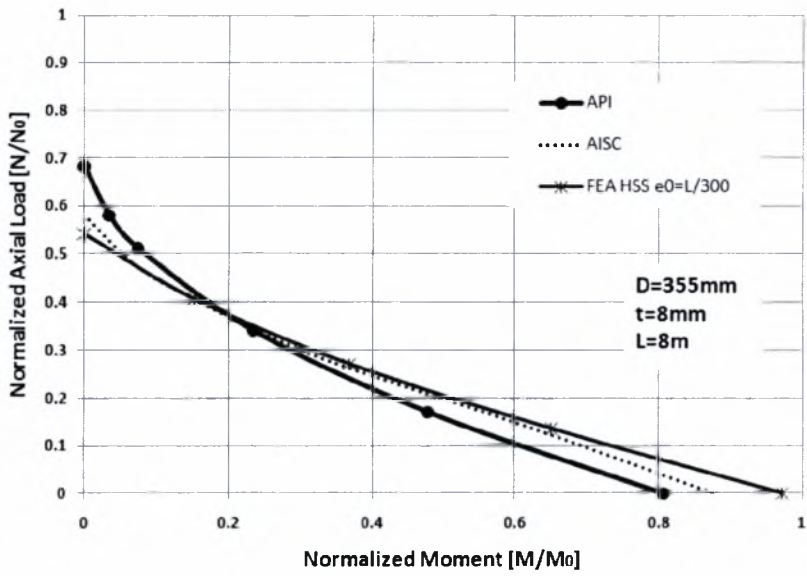
(b)



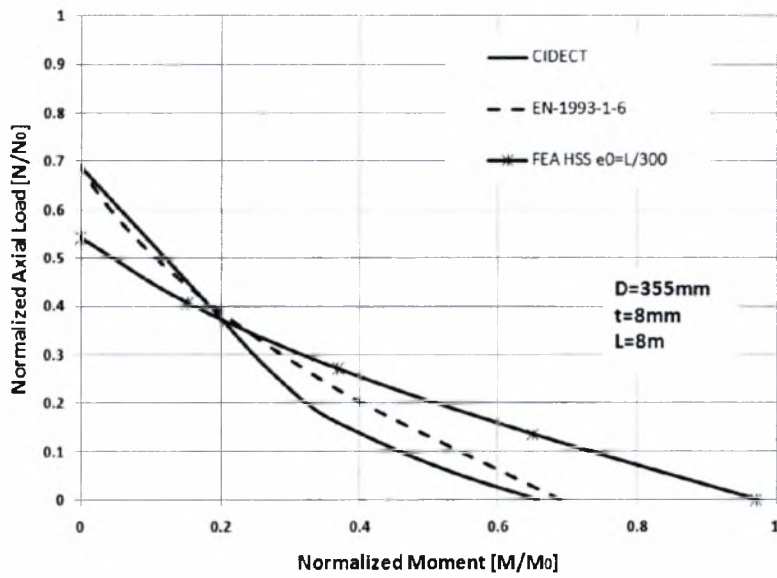
(c)

Figure 6.1.13 Comparison of interaction curves of the tube with $D=355\text{mm}$, $t=8\text{mm}$ and $L=3\text{m}$ in the case of $e_0=L/300$ between a) API and AISC-LRFD, b) EN-1993-1-1 and CIDECT and c) all of the above standards

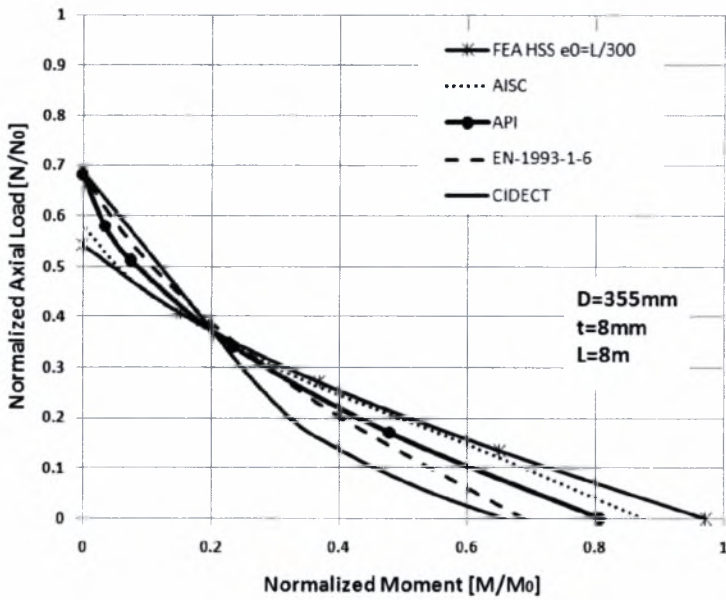
As illustrated in Figure 6.1.13 that unsimilar to class 3 cross sections, American standards highly underestimate the bending strength of tubular member ($L=3\text{m}$) under combined loading as far as class 4 cross sections are concerned. In fact, for specific value of axial compressive load, the bending strength predicted by API standard is 20% lower than the one estimated through the finite element analysis, while the bending strength proposed by AISC is in average 10% lower than the finite element values, especially when pure bending is concerned. Moreover European codes appear to be even more penalizing than American standards as far as the strength under combined loading is concerned. More specifically, for axial compressive load $N>0.7N_0$ the bending strength is significantly underestimated up to 30% compared to the finite element results. For the long tubular member of $L=8\text{m}$ (Figures 6.1.14), API predictions are overestimating by 20% under pure compression, and penalizing by 20% when pure bending is concerned. Similarly, for $N<0.4N_0$, the values proposed by European standards are conservative by 30% with respect to the FEA results, but for $N>0.4N_0$ appear to be overestimating up to 20% under pure compression. Finally, AISC standard is the curve which correlates better with the one obtained by finite element analysis.



(a)



(b)



(c)

Figure 6.1.14 Comparison of interaction curves of the tube with $D=355\text{mm}$, $t=8\text{mm}$ and $L=8\text{m}$ in the case of $e_0=L/300$ between a) API and AISC-LRFD, b) EN-1993-1-1 and CIDECT and c) all of the above standards

6.2. Combined out-of-straightness and out-of-roundness

The same loading sequence was followed in order to develop the interaction diagram for the tubular member with $D=355\text{mm}$, $t=8\text{mm}$, $L=3\text{m}$ and a combination of initial imperfections. The initial imperfection of amplitude of $L/300$ was imposed at the mid span of the tube length and the out-of-roundness amplitude ($a=3\%$) was imposed at the circumference along the longitudinal axes as described in Chapter 4.2. The value of out-of-roundness (3%) imposed in the model, corresponds to the maximum limit of out-of-roundness imperfection determined by API provisions. Comparison of the interaction curves developed for a 3 m long tube with $D=355\text{mm}$, $t=8\text{mm}$ for two different types of initial imperfection; out-of-straightness ($e_0=L/300$) and the combination of out-of-straightness ($e_0=L/300$) and out-of-roundness ($\alpha=3\%$) is shown in Figure 6.2.1. The out-of roundness is defined as: $\alpha = \frac{D_{\max} - D_{\min}}{D_{\text{nom}}} 100\%$. In Figure 6.2.1 the compression and bending values are normalized

with $N_0 = \pi D_m t \sigma_y$ and $M_0 = D_m^2 t \sigma_y$.

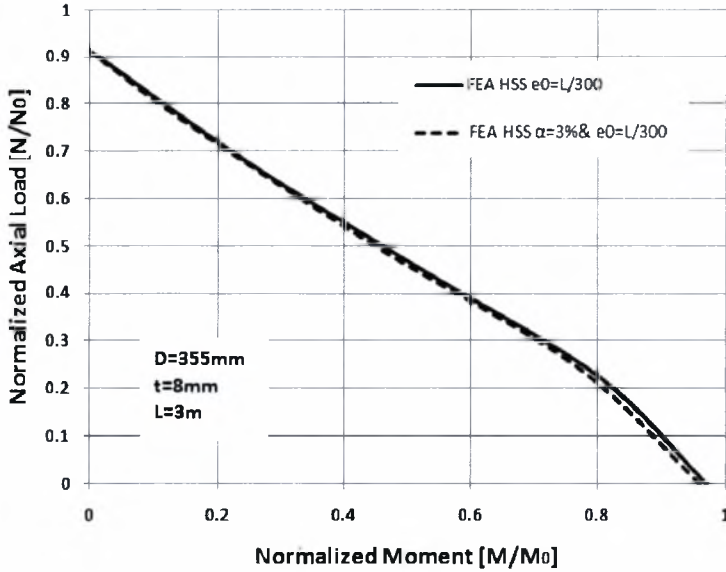


Figure 6.2.1 Comparison of interaction curves of the tube with $D=355\text{mm}$, $t=8\text{mm}$ and $L=3\text{m}$ with $e_0=L/300$ and the combination of $e_0=L/300$ and $\alpha=3\%$

As shown in Figure 6.2.1, additional out-of-roundness does not affect the structural behavior of the imperfect tubular member, so the models with the combination of the out-of-straightness and out-of-roundness exhibit similar behavior with the ones imposed with the out-of-straightness under combined loading.

As indicated in Chapter 5, even large values of out-of-roundness ($\alpha=10\%$ chosen for the development of stability curves Chapter 5), does not significantly affect the buckling response of the high strength steel tubular members, so the models with the combination of the out-of-straightness and out-of-roundness exhibit almost similar behavior under axial compression with the ones with the out-of-straightness.

6.3. Initial wrinkling

Initial wrinkling was imposed to the tube model with $D=323.9\text{mm}$, $t=10\text{mm}$, $L=3\text{m}$ and then subjected to combined axial compression and bending. More specifically, a linear elastic buckling analysis was conducted in order to obtain the buckling mode of the simply supported perfect tube model ($D=323.9\text{mm}$, $t=10\text{mm}$, $L=3\text{m}$) under pure bending. The buckling mode under bending consists of non-axisymmetric wrinkle development with the maximum wrinkle amplitude placed at the mid span of the tube at the upper compression fiber of the tube. The displacements obtained from the elastic buckling analysis were multiplied by a factor in order to obtain the maximum wrinkle amplitude up to 0.25 or 0.5 of the tube thickness. The wrinkled geometry was inserted as the initial stress-free tube geometry in order to conduct a non-linear finite element analysis under axial compression. The material characteristics, the boundary conditions and the loading sequence are described in Chapters 3, 4 and 6, respectively. It should be clarified that the amplitudes of initial wrinkling of $0.25t$ and $0.5t$ are considered rather high but are chosen in order to investigate the sensitivity of finite element results in the presence of initial wrinkling in theoretical basis. The wrinkled model ($w_0=0.5t$) and the loading conditions are shown in Figure 6.3.1. The interaction diagram for $w_0=0.5t$ in comparison with a perfect tubular is shown in Figures 6.3.2. The compression and bending values included in the interaction curves are normalized with $N_0 = \pi D_m t \sigma_y$ and $M_0 = D_m^2 t \sigma_y$, respectively.

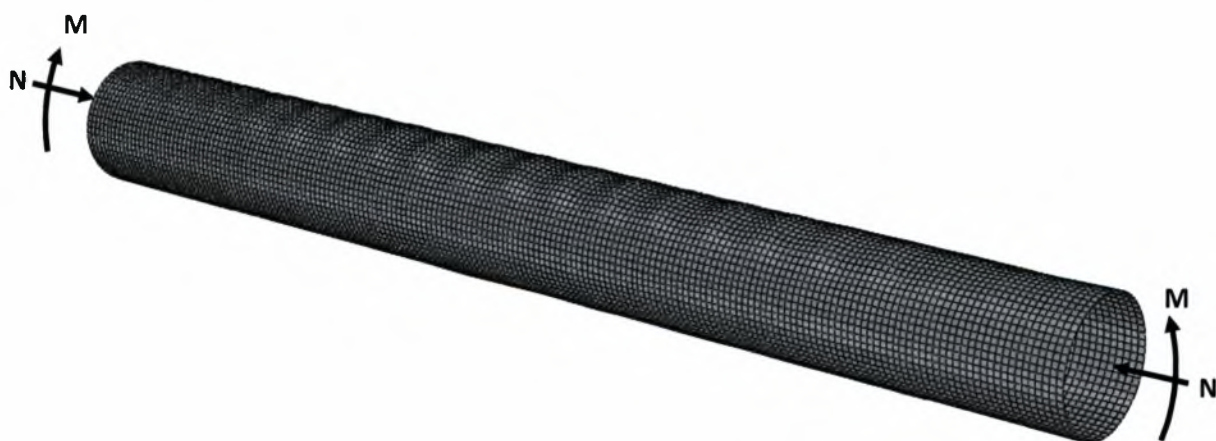


Figure 6.3.1 Loading and model configuration of the imperfect tubular member with $D=323.9\text{mm}$, $t=10\text{mm}$ and $L=3\text{m}$ ($w_0=0.5t$)

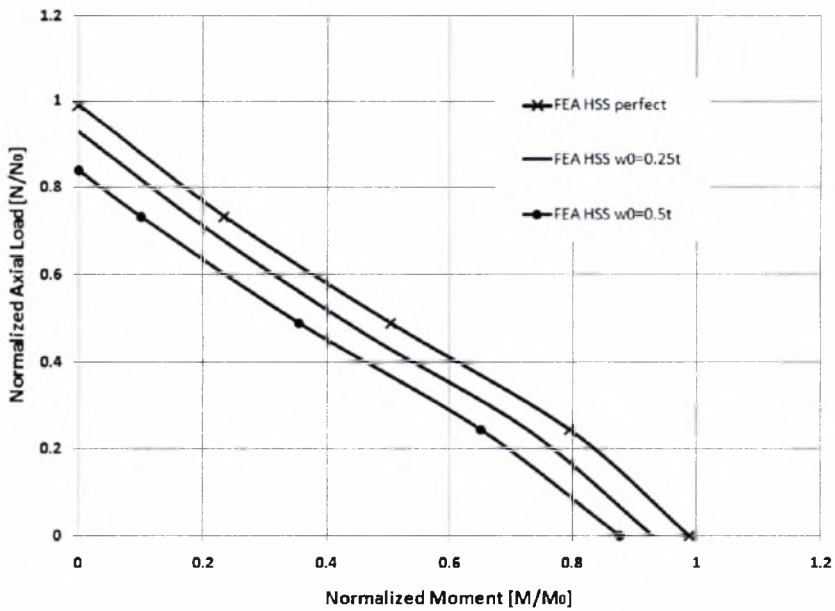


Figure 6.3.2 Comparison of interaction curves of the tube with $D=323.9\text{mm}$, $t=10\text{mm}$ and $L=3\text{m}$ between the perfect and wrinkled geometry with $w_0=0.25t$ and $0.5t$

It is obvious that, the structural strength, especially the buckling strength is highly affected by the increase of the wrinkling maximum amplitude, and the structural capacity is reduced in the presence of initial wrinkling. More specifically, for constant value of initially subjected axial compression, the bending capacity is reduced for 15% and the buckling strength is decreased for 20% when pure compression is considered. The failure modes for the tube with $D=323.9\text{mm}$, $t=10\text{mm}$, $L=3\text{m}$ with wrinkling amplitude of $w_0=0.5t$ are shown in the following Figures 6.3.3.



Figure 6.3.3a Deformed geometry of the tube model with $D=323.9\text{mm}$, $t=10\text{mm}$ and $L=3\text{m}$ ($w_0=0.5t$) under axial compression up to $0.25N_a$ and bending.



Figure 6.3.3b Deformed geometry of the tube model with $D=323.9\text{mm}$, $t=10\text{mm}$ and $L=3\text{m}$ ($w_0=0.5t$) under axial compression up to $0.5N_a$ and bending.



Figure 6.3.3c Deformed geometry of the tube model with $D=323.9\text{mm}$, $t=10\text{mm}$ and $L=3\text{m}$ ($w_0=0.5t$) under pure bending

It is observed that under combined loading of axial and bending with initial wrinkling a single “foot” buckle is developed on the tube wall. The local buckle is formed while bending is subjected, beyond the maximum bending moment where excessive rotation and deformation are already reached. It is noted, though, that the local buckle is not developed at the mid span of the tube length as expected amplitude of wrinkle.

Moment-rotation curves were developed for the model of $D=323.9\text{mm}$ and $t=10\text{mm}$ with maximum wrinkling amplitudes equal to $w_0/t=0.25$ and 0.5 so that the sensitivity of the results will be identified and the influence of the wrinkling in the bending capacity under combined loadings will be indicated. The wrinkled model (of both values of initial wrinkling) was first subjected to monotonic axial load up to $0.25N_a$ and then to monotonic bending load. The moment rotation curves are traced and compared for this type of imperfection. The comparison of moment rotation curves is shown in Figure 6.3.4. It is obvious that the moment capacity is reduced as the initial imperfection is increased. Herein, the maximum bending strength and the rotation capacity (when the axial load subjected is equal to $0.25N_a$) are reduced for 10% and 7% respectively in the case of $w_0/t=0.5$ compared with the case of

$w_0/t=0.25$. When $w_0/t=0.5$ imperfection is considered, the initial concentrated deformation imposed is larger than the amplitude of $w_0/t=0.25$. As a result, the buckle development for the case of the large value of initial wrinkling, tend to initiate at lower values of deformation and the maximum buckling load achieved is lower, as shown in Figure 6.3.4.

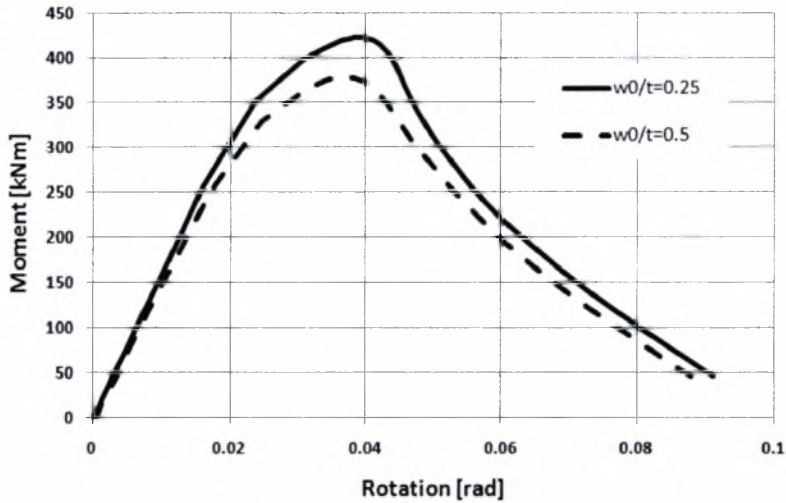


Figure 6.3.4 Moment-rotation curves of the tube with $D=323.9\text{mm}$, $t=10\text{mm}$ and $L=3\text{m}$ for the cases of $w_0=0.25t$ and $0.5t$ under combined loading with constant axial compression equal to $0.25N_a$

The deformed geometry for wrinkle amplitude $w_0=0.5t$ and $N=0.25N_a$ is shown in Figure 6.3.5. It is noted that in the present study, the case of $w_0=0.5t$, is investigated on a theoretical basis, since the specific value can be considered rather high and not encountered for industrial applications. As shown in the figure, strain localization is developed in a region not exactly in the middle length of the specimen.



Figure 6.3.6 Failure geometry for the model with $D=323.9\text{mm}$, $t=10\text{mm}$, $L=3\text{m}$ with $w_0=0.5t$ and constant axial compression equal to $0.25N_p$

Finally, the finite element results referring to a perfect and a wrinkled HSS tubular member with $D=323.9\text{mm}$, $t=10\text{mm}$ and $L=3\text{m}$ (classified as class 3 by European standards) were compared with the interaction diagrams proposed by the current standards and provisions available, as shown in Figure 4.3.7.

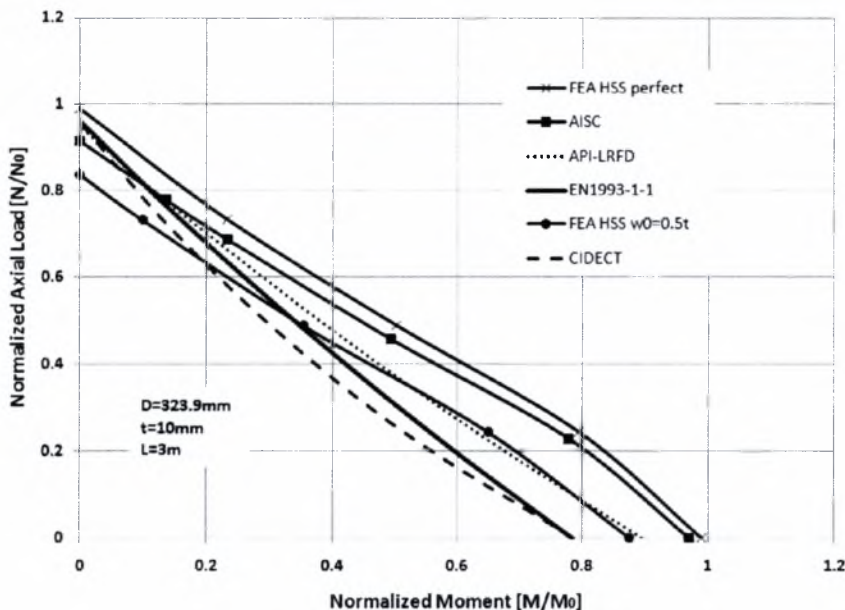


Figure 6.3.7 Interaction curves of a perfect and a wrinkled ($w_0=0.5t$) tubular member with $D=323.9\text{mm}$, $t=10\text{mm}$, $L=3\text{m}$ in comparison with the ones proposed by the current standards.

As shown in Figure 6.3.7, the strength values proposed by the current standards are conservative compared to the finite element results referring to the perfect tube. AISC-LRFD curve is the most correlative to the curve of the perfect tube, especially as pure bending is prevailing. API appears to be conservative in comparison with the perfect tube results but for $N < 0.3N_0$ API appears to be in convergence with the case of $w_0/t=0.5$. Moreover, European standards significantly underestimate the strength under combined loading compared to the perfect tube case. Additionally, compared to the case of $w_0/t=0.5$, the European standards are penalizing for axial load values $N < 0.5N_0$ but overestimating for $N > 0.3N_0$ where pure compression prevails.

7. Conclusions

In the present study, stability curves and interaction diagrams are developed for HSS tubular members with cross sections classified as class 3 and class 4 by European standards. Various types and amplitudes of initial imperfections were imposed such as: out-of-straightness, combination of out-of-straightness and out-of roundness and initial wrinkling of the tube wall. It is demonstrated that the larger the amplitude of the imposed imperfection, the lower the buckling and bending capacity becomes. Furthermore it was proved that out-of-roundness imperfection, despite the large amplitude chosen, does not affect the structural response of the HSS tubular member under axial compression, bending moment or combined loadings.

The finite element results for both stability curves and interaction diagrams are compared with the values proposed by the current European and American standards reported in Annex B. The AISC-LRFD provision appears to correlate better with the finite element results for both stability and interaction curves. API and European standards are not in good agreement with the finite analysis results, since their predictions overestimate the buckling strength, and sometimes underestimate significantly the bending strength, for the initial imperfections chosen in the present analysis.

References

- American Institute of Steel Construction, "Load Resistance Factor Design Specification for steel hollow structural sections", November 2000
- American Institute of Steel Construction, 2005, "Steel Construction Manual," 13th Edition, AISC 325-05
- American Petroleum Institute, "Recommended Practice, Designing and Constructing Fixed Offshore Platforms-Load and Resistance Factor Design", recommended practice 2A-LRFD, 1st Edition, July 1993
- Ballio, G., Finzi, L., Urbano, C. and Zandonini, P., Buckling of tubes in Niguage steel – experimental study and theoretical considerations, Construction Métallique, 1975.
- Beer, H. and Schulz, G., he European column curves, IABSE Int. Coll. On Column Strength, Paris Nov. 1972.
- Beg, Hladnik "Slenderness limit of Class 3 I cross-sections made of high strength steel", Journal of Constructional Steel Research, Volume 38, Number 3, July 1996 , pp. 201-217
- Bernt Johansson, Peter Collin, "Eurocode for high strength steel and applications in construction," Lulea University of Technology, Sweden
- CEN EN 1993-1-1, "Eurocode 3: Design of steel structures. Part 1-1: General rules and rules for buildings." European Committee for Standardization, May 1, 2005.
- CEN EN 1993-1-6, "Eurocode 3: Design of steel structures. Part 1-6: Strength and Stability of Shell Structures." European Committee for Standardization, January, 2007
- Corona E. and Kyriakides S., "On the Collapse of Inelastic Tubes Under Combined Bending and Pressure," International Journal of Solids and Structures, vol. 24 No 5, pp. 505-535, 1988
- Elchalakani, Zhao, Grzebieta "Bending tests to determine slenderness limits for cold-formed circular hollow sections", Journal of Constructional Steel Research, Volume 58, Number 11, November 2002, pp. 1407-1430
- European Convention for Constructional Steelwork (ECCS-EKS): Buckling of Steel shells, European Recommendations, 4th Edition, 1988

F.A.N. Al-Shawi "On the rotation capacity of structural steel circular hollow sections in plastic analysis", Journal of Constructional Steel Research, Volume 57, Number 1, January 2001, pp. 29-43.

International Committee for the Development and Study of Tubular Structures (CIDECT), "Structural stability of hollow sections", 1992

Jacquet, J. Essais de flambement et exploitation statistique (Buckling tests and their statistical analysis), Construction Métallique No 3, Sept. 1970.

Jiao H., Zhao X.-L., "Imperfection, residual stress and yield slenderness limit of very high strength (VHS) circular steel tubes", Journal of Constructional Steel Research, Volume 59, Number 2, February 2003 , pp. 233-249

Karamanos S. A., "Bending Instabilities of Elastic Tubes," International Journal of Solids and Structures, vol. 39, pp. 2059-2085, 2002

Massonnet, Ch. And Janss, J., Buckling tests on round and square tubes in high yield strength steel carried out for C.R.I.F. in the laboratories of the University of Liège, C.R.I.F. – Internal report (undated, Liège).

Rasmussen, Hancock "Test of High Strength Steel Columns" J. Construct Steel Research 34 (1995), 27-52.

Richter, Hanus, Wolf "Structural Steels of 690 MPa Yield Strength – a State of Art", 2nd International Symposium on High Strength Steel, Stiklestad, Verdal 23-24 April, 2002.

Sfintesco, D. European Steel Column Research, ASCE Struct. Engg. Conf. (Preprints 502), Seattle Washington, May 1967.

Sfintesco, D. Fondement expérimental des courbes européennes de flambement (Experimental basis of the European column curves), Construction Métallique No 3, Sept. 1970.

Sivakumaran K.S.; Bing Y. "Slenderness limit and ductility of high strength steel sections", Journal of Constructional Steel Research, Volume 46, Number 1, April 1998 , pp. 149-151

Tebedge, N. et al. Experimental studies on column strength of European heavy shapes, Proc. Internat. Colloquium on Column Strength, Paris 1972 (Published by IABSE)

Tebedge, N. et al. Méthod d'essai de flambement des barres à forte section (Testing methods for heavy columns), Construction Métallique No 4, Dec. 1971.

ANNEX A-Benchmark problems

The following 5 problems nonlinear finite element analysis of tubular members and the results may be used for calibrating and optimizing the simulation procedure of tube models. Parametric study is conducted in order to define the sensitivity of results under axial compression or combined loadings. The results were used for the simulation of the model tubes in order to define stability curves and interaction diagrams shown in Chapter 5 and 6. The results considering the optimization of the modeling procedure were also used for the simulation of the experiments to be conducted by CSM laboratory, described in ANNEX C.

A.1. Cross sectional ovalization instability of elastic tubes under bending-Problem#1

Finite element analysis was conducted in order to investigate the cross-section instability and compare the results to the ones calculated in [Karamanos (2002)], which corresponds to [1] in the following Figures. It is reminded that the results in [Karamanos 2002] have been obtained with an in house semi-analytical methodology. A circumferential strip of a pipe was modeled, corresponding to an elastic tube ($E=210\text{GPa}$ and $\nu=0.3$) with $D=323.9\text{mm}$ and $t=10\text{ mm}$, using shell and solid elements (S4R, S4, S8R and C3D8R), imposing the appropriate boundary and symmetry conditions. To exclude bifurcation phenomena from this analysis, the strip width should be as small as possible. Herein the width L is considered equal to the tube thickness and the material has been considered elastic to compare with the results in [Karamanos (2001)]. The boundary conditions chosen refer to a circumferential strip of infinitely long tube, where ovalization is developed on the tube cross section independently of boundary conditions.

The strip model is assumed to be within two plates at $z=0$ and $z=L$ as shown in Figure A.1.1. The first plate remains fixed and the second plate rotates. Moreover the strip nodes on the two plates are free to slide along the plate planes allowing the development of cross section ovalization

The moment- curvature curves obtained were normalized with the values of the elastic critical moment and curvature calculated at the bifurcation point according to the elastic "cross-section instability" theory. The values of the elastic moment and curvature for normalization are defined as follows [Karamanos (2002)]:

$$M_{BR} = \frac{Ert^2}{\sqrt{1-\nu^2}} \quad (\text{A.1})$$

$$K_{BR} = \frac{t}{r^2\sqrt{1-\nu^2}} \quad (\text{A.2})$$

The ovalization amplitude is defined as follows [Karamanos (2002)]:

$$\alpha = \frac{D_{\max} - D_{\min}}{2D_{\text{nom}}} \quad (\text{A.3})$$

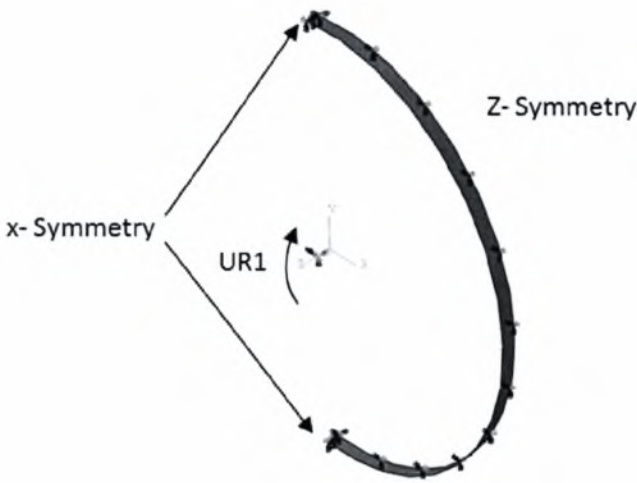


Figure A.1.1 Strip model geometry loading and boundary conditions

Parametric study on the elastic range considering S4R, S4, S8R shell elements with dense and coarse mesh is shown in the following figures. It is obvious that the results with the dense mesh are equivalent to those obtained using a coarse mesh. Furthermore, it is noted that the M-k curve presented in Figure A.1.2 & A.1.3 using shell elements, is in good correlation with the finite element analysis M-k curve presented in Figure7 (a) reported in [Karamanos (2002)].

The meshes used are described below:

S4R1004: 100 reduced integration 4-noded shell elements (S4R) along the circumference, 4 in the longitudinal direction.

S4R502: 50 reduced integration 4-noded shell elements (S4R) along the circumference, 2 in the longitudinal direction.

S4R302: 30 reduced integration 4-noded shell elements (S4R) along the circumference, 2 in the longitudinal direction.

S4302: 30 4-noded shell elements (S4) along the circumference, 2 in the longitudinal direction

S8R302: 30 8-noded (non-linear) reduced integration shell elements (S8R) along the circumference, 2 in the longitudinal direction.

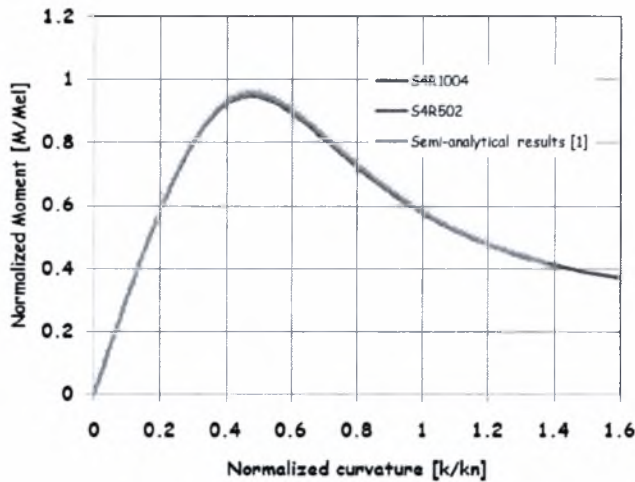


Figure A.1.2 Moment-curvature curves for the elastic tube strip using dense (S4R1004) and coarse (S4R502) mesh in comparison with the semi-analytical results obtained from [Karamanos (2002)]

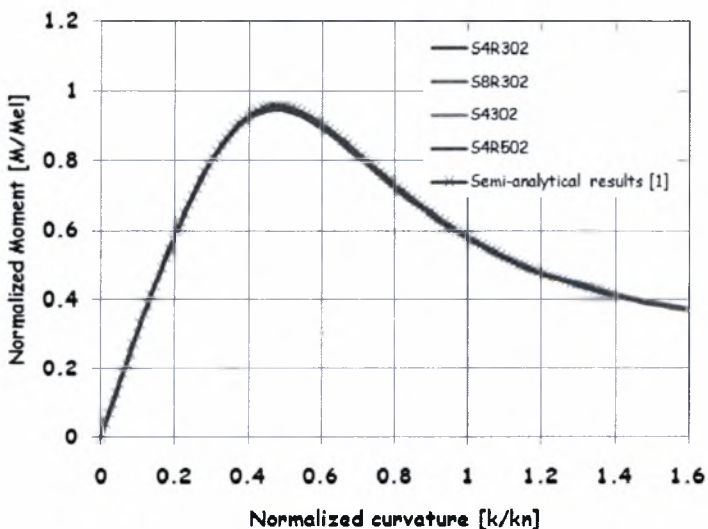


Figure A.1.3 Moment-curvature curves for the elastic tube strip using S4, S4R and S8R shell elements with relatively coarse mesh in comparison with the semi-analytical results obtained from [Karamanos (2002)]

The elastic α - k (ovalization-curvature) curve is defined for the model strip as shown in Figure A.1.4. It is noted that the curves obtained in the present study using S4R and S4 are in good correlation with the finite element analysis curve of Figure7 (b) reported in [Karamanos (2002)].

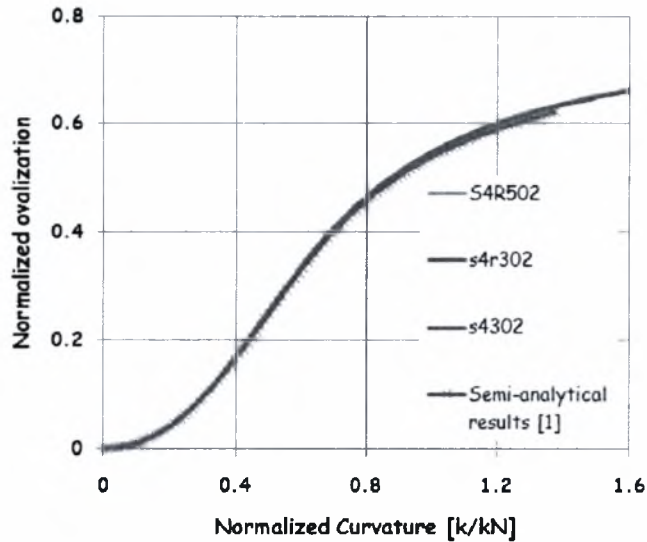


Figure A.1.4 Ovalization-curvature curves for the elastic strip using the S4R and S4 elements with relatively coarse mesh in comparison with the semi-analytical results obtained from [Karamanos (2002)].

Consequently, as shown in the above comparison curves, when shell elements are to be employed, the model “S4R302” can be chosen in order to optimize the computational time. The failure mode and cross section ovalization of the strip with S4R302 type mesh are shown in the following figure (Figure A.1.5).



Figure A.1.5. Large deformations due to cross-section ovalization for large value of curvature for the elastic strip using shell elements with S4R302 mesh type

A similar parametric study for tubes in the elastic range considering solid elements with dense (C3D8R10044) and coarse (C3D8R7022& C3D8R5022) mesh configuration has also been conducted. As shown in Figure A.1.6 and Figure A.1.7, M-k and α -k curves defined for the model with "C3D8R10044" mesh type (100 elements in the circumferential direction, 4 elements through thickness and 4 elements along the longitudinal direction) correlate quite well with the results presented in Figures 7(a) & (b) reported in [Karamanos (2002)].

The meshes used are described below:

C3D8R10044: 100 8-node linear reduced integration brick elements in the circumferential direction, 4 elements through thickness and 4 elements along the longitudinal direction

C3D8R7022: 70 8-node linear reduced integration brick elements in the circumferential direction, 2 elements through thickness and 2 elements along the longitudinal direction

C3D8R5022: 50 8-node linear reduced integration brick elements in the circumferential direction, 2 elements through thickness and 2 elements along the longitudinal direction

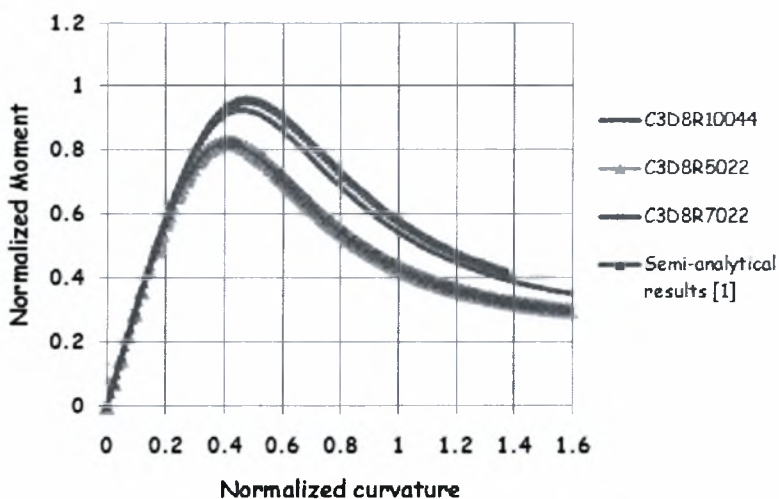


Figure A.1.6. Moment-curvature curves for the elastic tube strip using solid elements with dense and coarse mesh in comparison with the semi-analytical results obtained from [Karamanos (2002)].

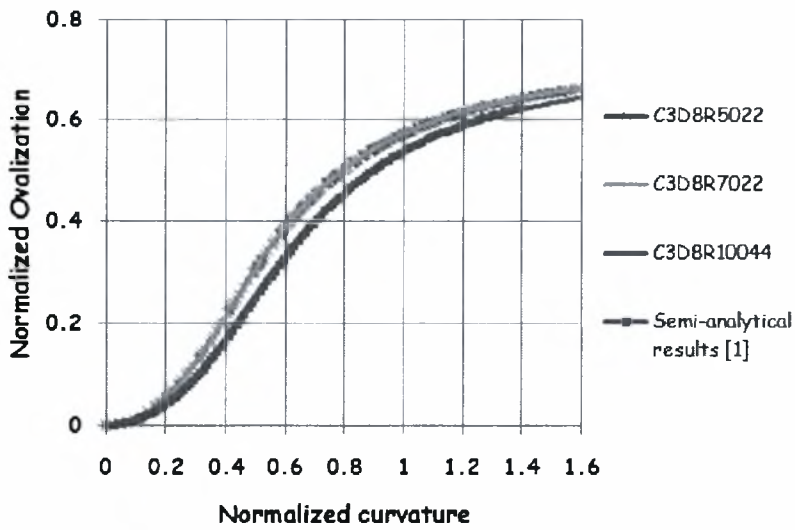


Figure A.1.7 Ovalization-curvature curves for the elastic strip solid elements with relatively coarse mesh in comparison with the semi-analytical results obtained from [Karamanos (2002)].

An indicative failure mode and cross-section ovalization of the elastic strip using solid elements with dense mesh (C3D8R10044) is shown in the Figure A.1.8 and Figure A.1.9.

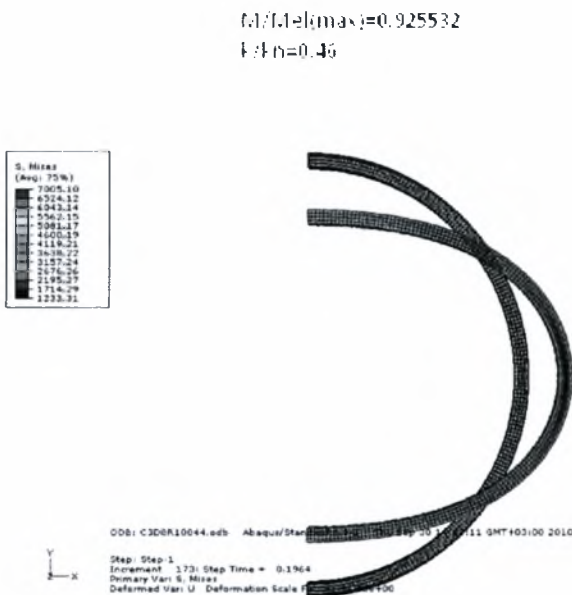


Figure A.1.8 Cross-section ovalization at point of the maximum moment ($k/k_n=0.46$) for the elastic strip using solid elements with dense meshing

M/Mel-0 339581
k/kn=1.3942

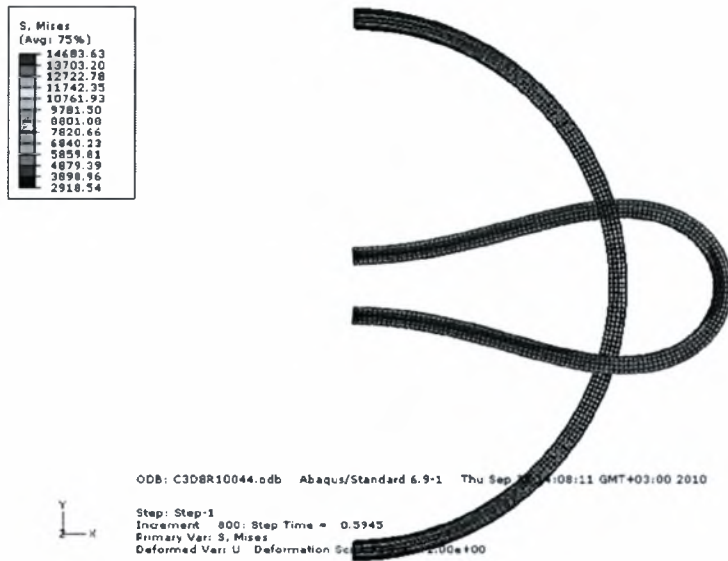


Figure A.1.9 Large deformations due to cross-section ovalization for $k/kn=1.39$ (large value of curvature) for the elastic strip using solid elements with dense mesh

Comparison between semi-analytical solution, solid elements and shell elements

The total comparison shown in Figure A.1.10 and Figure A.1.11 indicates that S4R302 offers practically, the same results with S4R502, S4R1004, C3D8R10044 and S8R302. Consequently, since the computational time using S4R302 is the lowest, among all the above cases chosen through this parametric study, the proposed type element to be implemented for the scheduled test simulations is the S4R element.

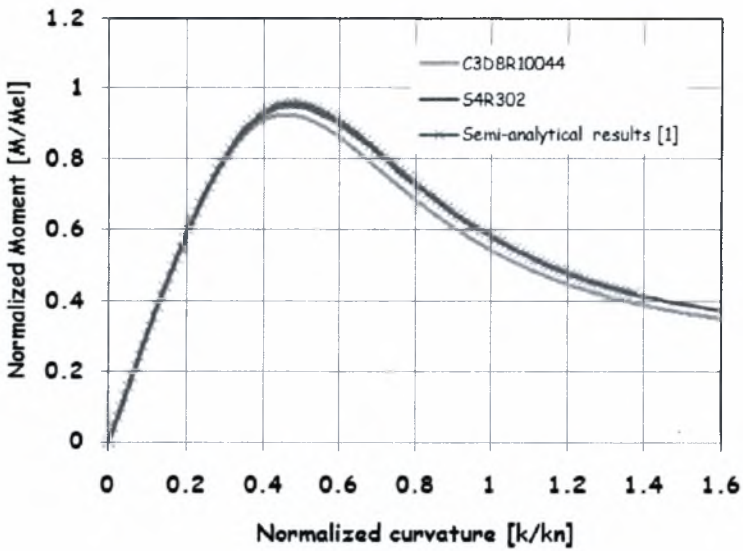


Figure A.1.10 Elastic moment-curvature curves using shell and solid elements in comparison with the semi analytical results obtained from [Karamanos (2002)].

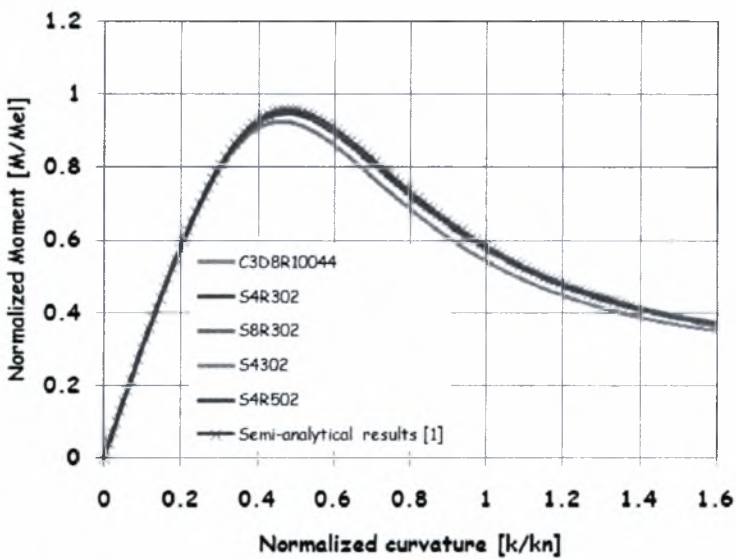


Figure A.1.11 Total comparison of elastic $M-k$ curves using shell and solid elements with the semi analytical results obtained from [Karamanos (2002)]

The conclusive results for the elastic strip model are shown in the following table (table A.1.1). The amplitudes of the maximum moment and the corresponding curvature and ovalization obtained for various types of elements are summarized below in table A.1.1.

Table A.1.1

type	M_{\max}	$\frac{M_{\max}}{M_{\max\text{-ref}}}$	k_m	$\frac{k_m}{k_{m\text{-ref}}}$	α_m	$\frac{\alpha_m}{\alpha_{m\text{-ref}}}$
S4R1004	3299.26	0.9975	0.0002	1.01368474	0.225356	1.03612
S4R502	3274.14	0.9895	0.0002	1.01368474	0.2291	1.053333
S4R302	3282.98	0.993	0.0002	1.01368474	0.227067	1.043986
S4302	3302.5	0.9985	0.0002	1.01368474	0.224476	1.032074
C3D8R10044	3197.8	0.967	0.000196	0.99341105	0.221756	1.019568
C3D8R7022	2840.3	0.8587	0.000173	0.8768373	0.221943	1.020428
C3D8R5022	2843.52	0.8597	0.000175	0.88697415	0.223989	1.029834
Semi-analytical	3307.56	1	0.000197	1	0.2175	1

A.2 Elastic Tube under pure axial compression (parametric analysis)-Problem#2

The present finite element analysis covers a theoretical problem for an elastic tubular (imperfect) column under axial compression that fails under Euler buckling. More specifically, parametric finite element analysis has been conducted for a tube with $D=323,9\text{mm}$, $t=10\text{mm}$ and 3m long, subjected to axial compression. Shell elements are used in a mesh sensitivity correspondence to the finite element analysis of the elastic strip. The set of nodes, applied on the tube wall, is related to the ones finally chosen for the strip model (Benchmark#1- Section A.1), 60 nodes along the circumference for the entire model and element size in the longitudinal direction equal to half thickness at the critical region at the mid span of the tube (500mm long).

The material used is elastic with $E=210000\text{ MPa}$ and $\nu=0.3$. It is noted that the model is simply supported with capped ends (RP1 and RP2) which are both free to rotate at the in-plane direction. Reference nodes (RP1 and RP2) are located at the centroids of the end sections, each one kinematically coupled with the corresponding end section shell nodes. RP1 is a hinge while RP2 allows to motion in the longitudinal direction of the tube, so that RP2 can be considered as a roller.

Two types of mesh were imposed on the model for element type S4R (chosen before):

- a) The first one includes 50 nodes in the longitudinal direction at section (AB) and at section (CD) and 100 nodes at the critical section (BC). Along the circumference 60 nodes were considered, constantly from A to D as shown in Figure 9.2.1(a). The buckling and post buckling behavior is shown at Figure A.2.2. The deformed geometry and wrinkling development are shown in Figures A.2.3 & 9.2.4.

In order to reach on the Euler global buckling state and not the local buckling mode as shown in Figure, an out-of-straightness imperfection was imposed with an amplitude of $L/1000$ in the mid length of the model.

The compressive axial load was normalized with the analytical elastic global buckling load (Euler), defined as follows, for simply supported member:

$$P_{cr,Euler} = \pi^2 \frac{EI}{(kL)^2} \text{ [N]} \quad (\text{A.2.1})$$

where

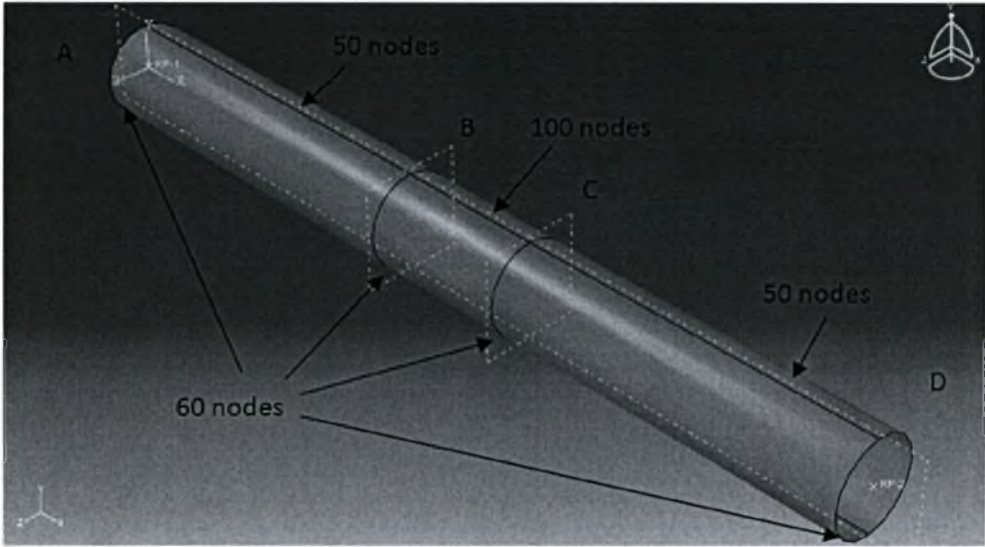
$$E=210000 \text{ [MPa]}$$

$$I = \frac{\pi}{4} (R_{in}^4 - R_{ex}^4) \text{ for tubular members [mm}^4\text{]} \quad (\text{A.2.2})$$

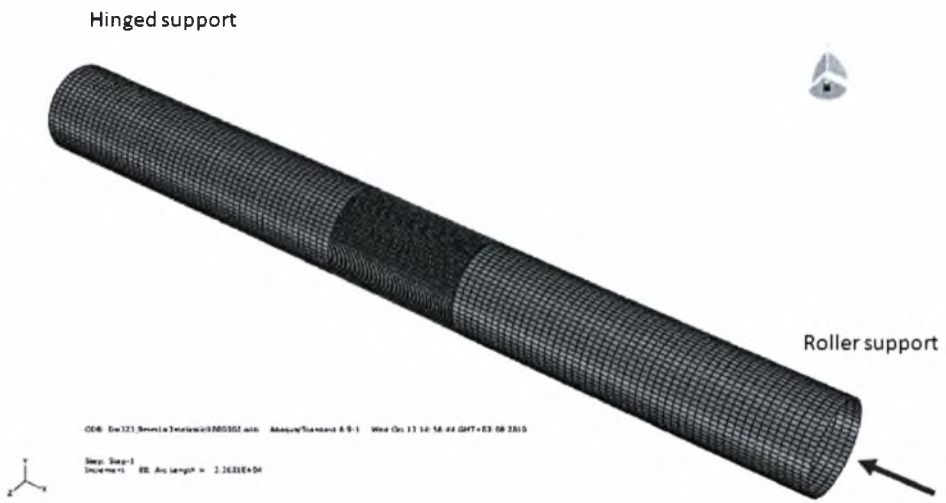
R_{in} and R_{ex} are the interior and exterior radius of the cross-section, respectively [mm^2]

K is the effective length factor, $K=1$ for simply supported beam-columns

L is the length of the tube [mm]



(a)



(b)

Figure A.2.1 Mesh configuration-type1 (a) and axial compression (b)

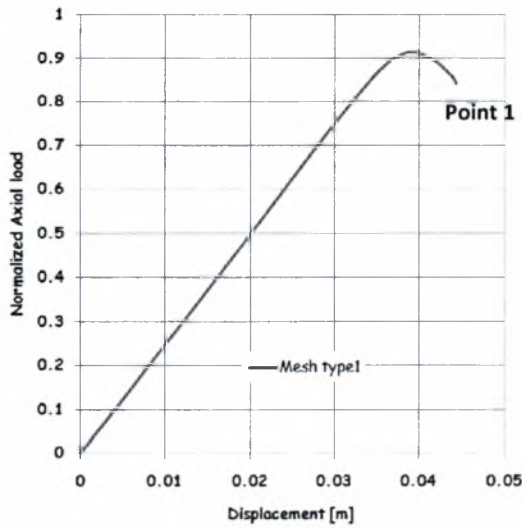


Figure A.2.2 Buckling and post buckling curves for normalized values of axial compressive load for mesh type-1



Figure A.2.3 Post buckling behavior where local buckling occurs wrinkling development, point

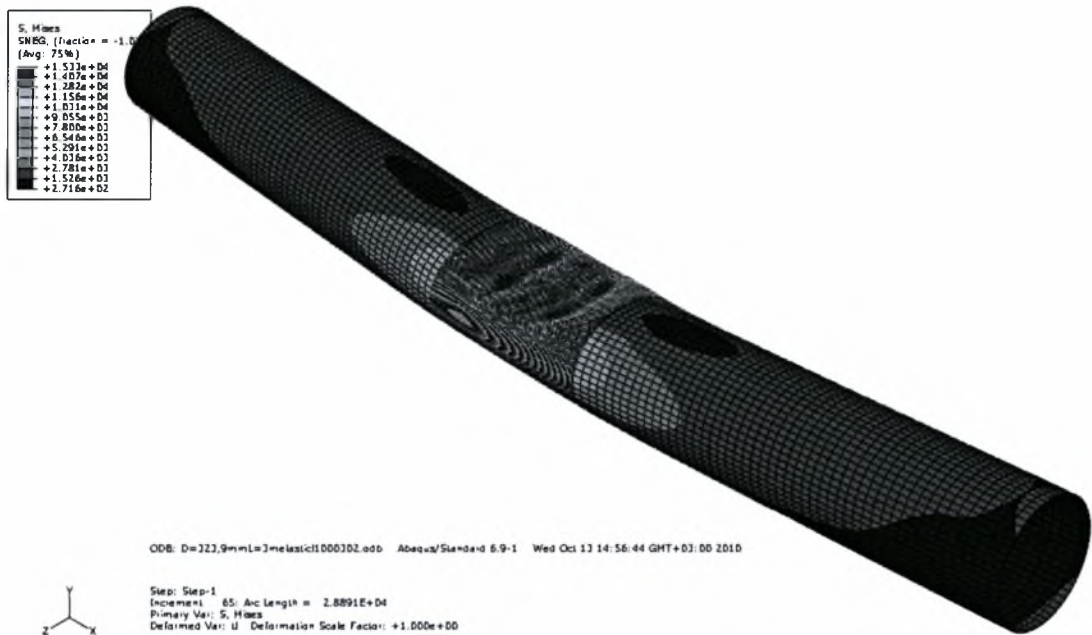
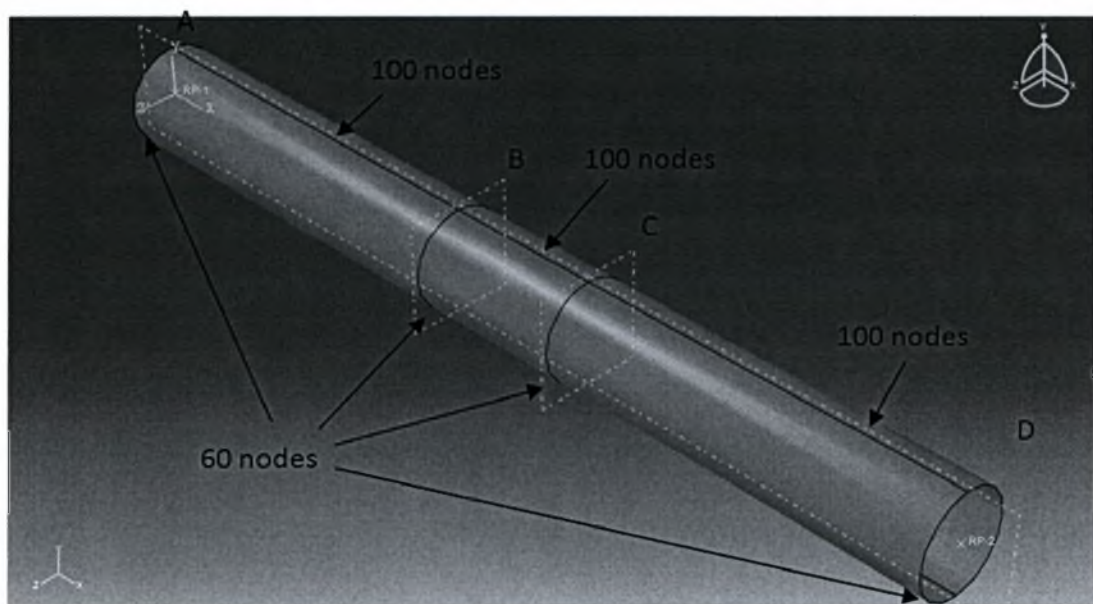


Figure A.2.4 Failure mode far beyond the critical buckling point

b) The second one (Type-2) includes 100 nodes in longitudinal direction at both sections (AB) and (CD) and 100 nodes at the critical section (BC). Along the cross section perimeter 60 nodes were inserted, constantly from A to D as shown in Figure A.2.5. The buckling and post buckling behavior is shown at Figure A.2.6. The deformed geometry and wrinkling development are shown in Figures A.2.7 & A.2.8.



(a)

Hinged support



(b)

Figure A.2.5 Mesh configuration of type-2 (a) and (b)

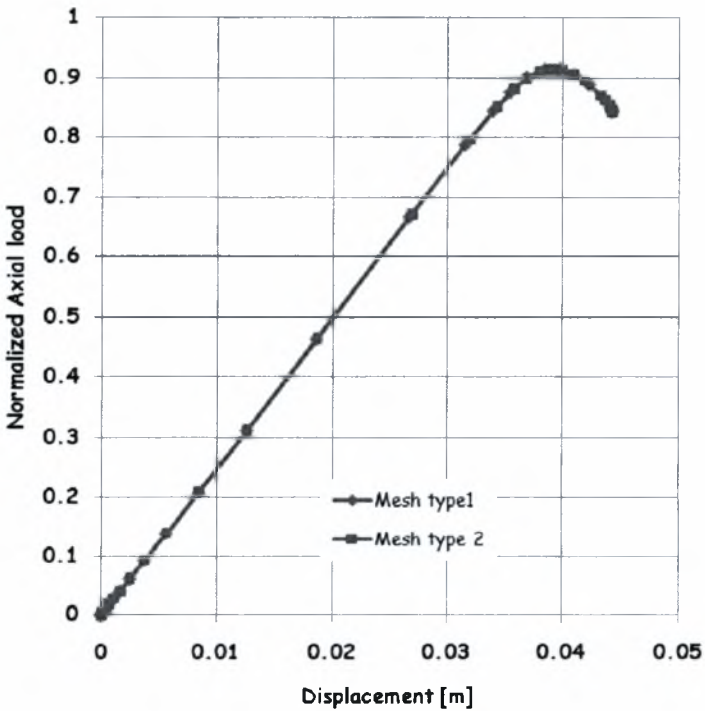


Figure A.2.6 Buckling and post buckling curves for normalized values of axial compressive load for mesh type1 and 2.

As shown in the above figures, global (Euler) buckling occurs first, as the vertical displacement at the middle of the tube increases. In sequence, two local buckles are gradually developed in the mid span of the model and local buckling occurs where the load

displacement curve presents a sharp point, after the maximum buckling load and the slope decrease. The mesh configuration (dense or sparse), out of the critical region does not affect the maximum buckling strength and the load displacement curves for the different mesh configurations are identical.



Figure A.2.7 Post buckling behavior where local buckling occurs and wrinkling development for mesh type 2, point 1

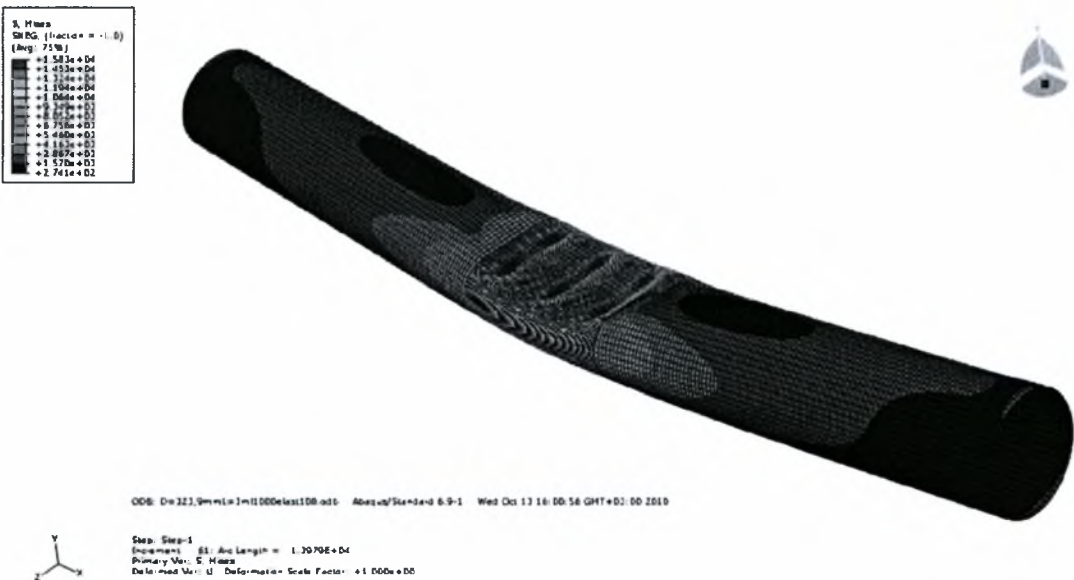


Figure A.2.8 Failure mode far beyond the critical buckling point for mesh type 2.

Furthermore, equilibrium paths were obtained for various amplitudes of out-of-straightness initial imperfection imposed to the tube with $D=323.9$ mm in order to reach the Euler buckling

load in the case of an almost straight tube. The finite element analysis was conducted on the entire elastic tube model with type2 mesh and S4R element type. As it is depicted in the following figure, when the value of $L/10000$ is imposed the analytical Euler buckling load is well reached, showing that the S4R element type is appropriate enough for this buckling analysis.

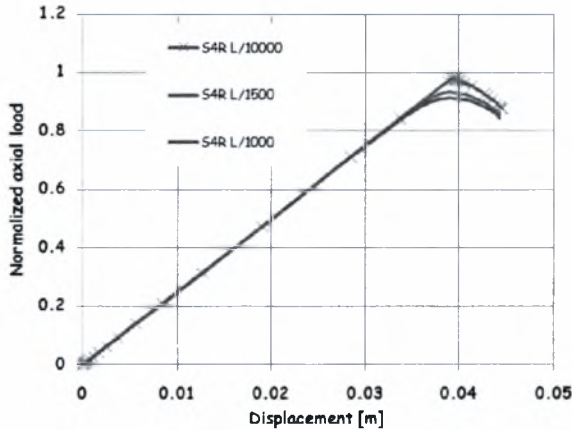


Figure A.2.9 Load displacement curves with different values of initial imperfection for the elastic tube with $D=323.9$ mm, $t=10$ mm, $L=3$ m and mesh type 2.

The following table (Table A.2.1) summarizes the critical buckling loads for different amplitudes of initial out-of-straightness, with respect to the Euler's elastic critical load N_{cr} .

Table A.2.1

Amplitude (e_0)	N/N_{cr}
L/1000	0.9151
L/1500	0.93364
L/2000	0.9438
L/10000	0.9775

A.3. Inelastic strip ovalization and inelastic tube failure under bending in comparison-Problem#3

Parametric finite element analysis has been conducted for elastic-plastic strip and tube model. The results were compared to the ones obtained from a series of small scale tests on stainless steel SS304 tubes reported in [Corona & Kyriakides (1988)].

As described in this experimental-analytical research, the material stress strain curves measured experimentally were represented by the three parameter Ramberg-Osgood fit shown in Figure A.3.1 and given by:

$$\epsilon = \frac{\sigma}{E} \left[1 + \frac{3}{7} \left(\frac{\sigma}{\sigma_y} \right)^{n-1} \right] \quad (\text{A.3.1})$$

where

$E = 186 \text{ GPa}$

$\sigma_y = 224 \text{ MPa}$

$n = 9.67$

Yield stress at residual strain of 0.2 is equal to 259 MPa. This value is considered as the yield stress σ_0 .

The present FEA simulation, both the strip and the tube model, corresponded to a steel tube specimen with nominal diameter-to-thickness ratio $D_0/t=34.7$, (outer diameter $D_0=31.4729\text{mm}$, thickness $t=0.907\text{mm}$) and length $L=570,6\text{mm}$. Furthermore, the specific specimen was subjected to pure bending (no external pressure) and the material anisotropy was small and therefore it was neglected.

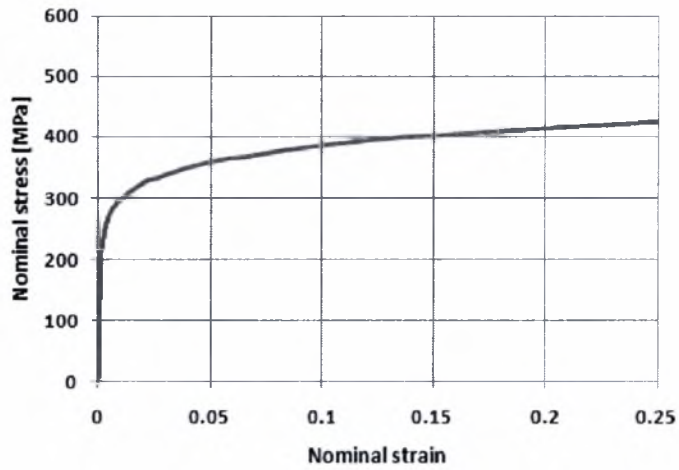


Figure A.3.1 Material stress strain curve of the steel 304 tubes specimens

The following figure shows the true stress and logarithmic plastic strain curve inserted as material data in the simulation procedure considering isotropic hardening.

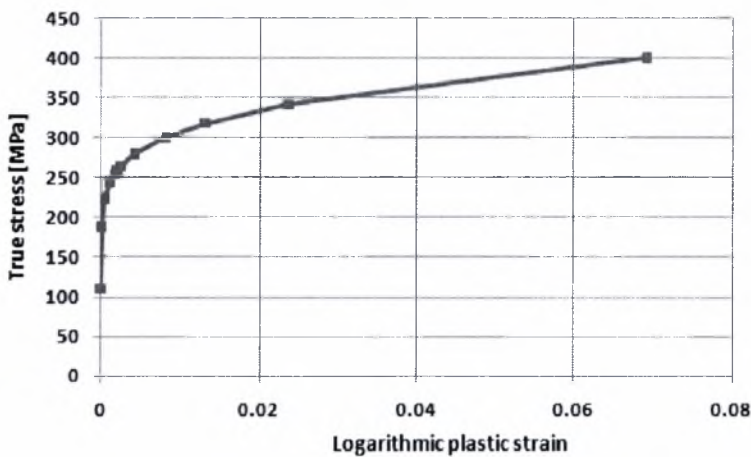


Figure A.3.2 Material $\sigma_{true}-\epsilon^{p ln}$ curve considered in Abaqus material data.

The strip elastic –plastic model correlated well with the three-dimensional elastic-plastic tube model. S4R shell elements were implemented for the strip model with 30 elements around half circumference, since the strip is modeled considering symmetry in x-y plane, and 2 elements along the width. The elastic-plastic strip model is simulated with the optimum mesh configuration derived from the parametric study of the elastic strip model (Benchmark#1- Section A.1).The normalized M-k curve of the elastic plastic strip is shown in Figures A.3.3 &A.3.4.

Moment-curvature curves were defined through a parametric study for the full scale tube model with different type and number of elements. S4, S4R, S8R elements were implemented and the results are shown in Figures A.3.3 & A.3.4 in comparison to the inelastic strip. As

shown the S4R60, S4R40 and S440 give identical results that are fairly well correlated with the experimental results. Although S8R elements give even better correlation in comparison with the S4 and S4R elements, the computational time increases. Consequently, the preferable shell elements for the three-dimensional finite element tube model are the S4R60 or S4R40.

The meshes are described below:

S4R60: 60 4-noded linear reduced integration shell elements (S4R) along the tube circumference

S4R40: 40 4-noded linear reduced integration shell elements (S4R) along the tube circumference

S440: 40 4-noded linear shell elements (S4) along the tube circumference

S8R20: 20 8-noded non-linear shell elements (S8R) along the tube circumference

The moment and curvature values shown in Figures 9.3.3 and 9.3.4 are normalized with M_0 and k_1 , respectively, calculated as follows:

$$M_0 = \sigma_0 D_0^2 t \quad (\text{A.3.2})$$

and

$$k_1 = t/D_0^2 \quad (\text{A.3.3})$$

where

D_0 is the mean tube diameter

t is the tube thickness

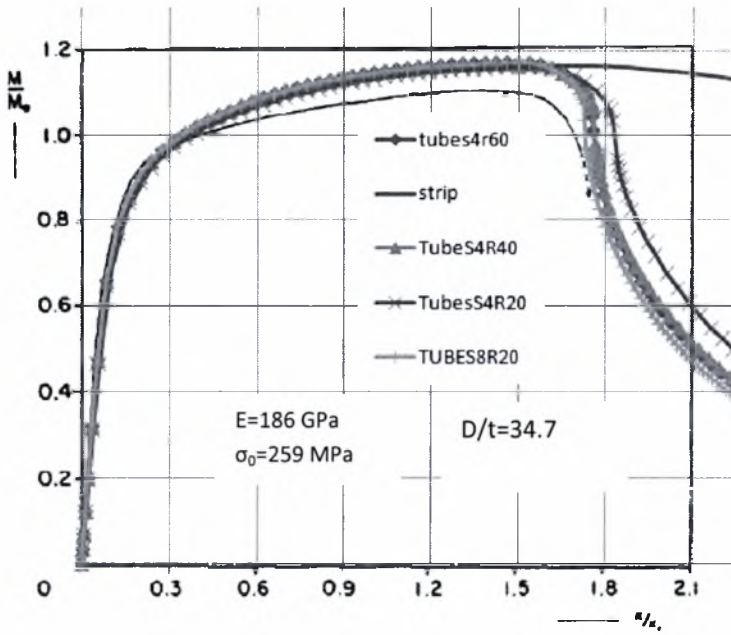


Figure A.3.3 Normalized $M-k$ curves for strip and steel 304 tube model with S4R and S8R shell elements in comparison with the experimental results in [Corona & Kyriakides (1988)]

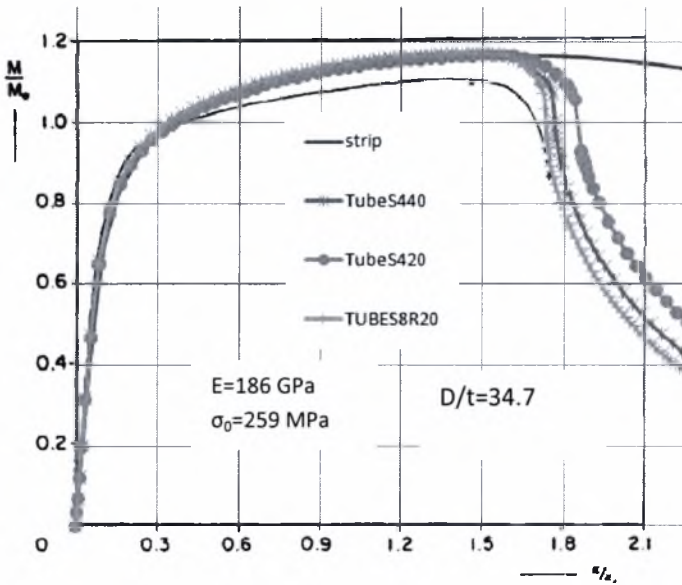


Figure A.3.4 Normalized $M-k$ curves for strip and steel 304 tube model with S4 and S8R shell elements in comparison with the experimental results in [Corona & Kyriakides (1988)]

The deformed shape of the finite element model with shell elements S4R60 is shown in the Figure A.3.5.

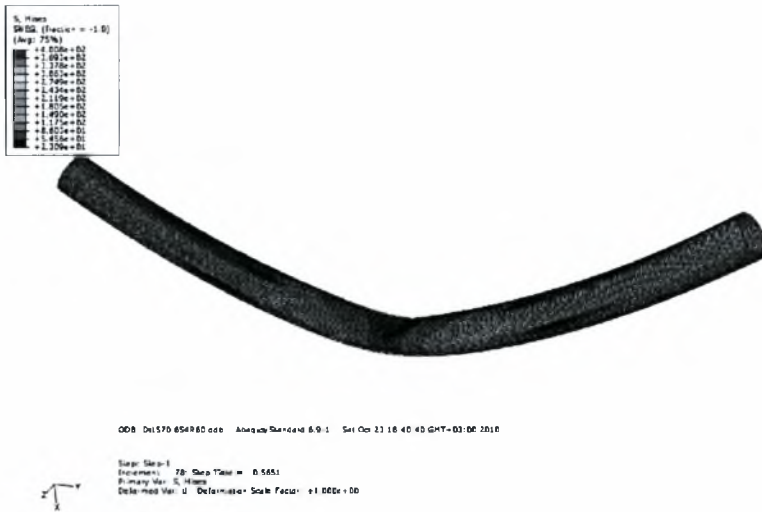


Figure A.3.5 Deformed shape of the model tube under pure bending

ANNEX B- Current provisions

B.1. Recommended practice for Planning, Designing and Constructing Fixed Offshore Platforms- Load and Resistance Factor design [American Petroleum Institute-API, 1993]

B.1.1 Axial Compression

The recommendations given in this section are applicable to stiffened and unstiffened cylinders having a thickness $t \geq 6\text{mm}$, diameter-to-thickness ratio $D/t < 300$ and having yield strengths less than 414 MPa (60 ksi).

B.1.1.1 Column Buckling

The nominal axial compressive strength for tubular members subjected to column buckling should be determined from the yield stress according to the following equations:

$$F_{cn} = [1.0 - 0.25\lambda^2] F_y \quad \text{for} \quad \lambda < \sqrt{2} \quad (\text{B.1.1.1-a})[(\text{D.2.2-2a})]^*$$

$$F_{cn} = \frac{1}{\lambda^2} F_y \quad \text{for} \quad \lambda \geq \sqrt{2} \quad (\text{B.1.1.1-b}) [(\text{D.2.2-2b})]$$

where

λ = column slenderness parameter defined as follows:

$$\lambda = \frac{KL}{\pi r} \left[\frac{F_y}{E} \right]^{0.5} \quad (\text{B.1.1.1-c}) [(\text{D.2.2-2c})]$$

where

F_{cn} = nominal axial compressive strength, in stress units

E = Young's modulus of elasticity

K = effective length factor

L = unbraced length

r = radius of gyration

* The second number refers to the Eq. number of the corresponding current provision described in each chapter.

B.1.1.2 Local Buckling

The possibility of local buckling of the tubular members should be examined calculating the elastic and inelastic local buckling stresses as follows:

a) Elastic Local Buckling

The nominal elastic local buckling strength should be determined from:

$$F_{xe} = 2C_x E (t/D) \quad (B.1.2-1)[(D.2.2-3)]$$

Where

F_{xe} = nominal elastic local buckling strength, in stress value

C_x = critical elastic buckling coefficient

D= outside diameter

t= wall thickness

x= subscript for the member longitudinal axis

The theoretical value of C_x is 0.6. However, a reduced value of $C_x = 0.3$ is recommended for use in the above equation to account the effect of initial imperfections.

b) Inelastic Buckling

The nominal inelastic local buckling strength should be determined from:

$$F_{xc} = F_y \quad \text{for} \quad \frac{D}{t} \leq 60 \quad (B.1.2-2)[(D.2.2-4a)]$$

$$F_{xc} = \left[1.64 - 0.23(D/t)^{1/4} \right] F_y \quad \text{for} \quad \frac{D}{t} > 60 \quad (B.1.2-3)[(D.2.2-4b)]$$

Where

F_{xc} = nominal inelastic local buckling strength, in stress units

In case that $F_{xc} < F_y$, or $F_{xe} < F_y$ a cylindrical member in compression is possible to fail due to local buckling. In order to calculate global (column) buckling, the nominal yield strength (F_y) in

Eqs (B.1.1.a) & (B.1.1.b) is replaced by the minimum value between the nominal inelastic local buckling strength (F_{xc}) and the nominal elastic local buckling strength (F_{xe}).

B.1.2. Bending

The nominal bending strength (in stress units) for tubular members should be determined from the following equations in terms of the yield stress F_y and the diameter-to-thickness ratio:

$$F_{bn} = \left(\frac{W_{pl}}{W_{el}} \right) F_y \quad (\text{B.1.2-a}) \quad [(\text{D.2.3-2a})]$$

For $D/t \leq 10340/F_y$ (F_y in MPa)

For $D/t \leq 1500/F_y$ (F_y in ksi)

$$F_{bn} = \left[1.13 - 2.58 \left(\frac{F_y D}{Et} \right) \right] \left(\frac{W_{pl}}{W_{el}} \right) F_y \quad (\text{B.1.2-b}) \quad [(\text{D.2.3-2b})]$$

For $10340/F_y \leq D/t \leq 20680/F_y$ (F_y in MPa)

For $1500/F_y < D/t \leq 3000/F_y$ (F_y in ksi)

$$F_{bn} = \left[0.94 - 0.76 \left(\frac{F_y D}{Et} \right) \right] \left(\frac{W_{pl}}{W_{el}} \right) F_y \quad (\text{B.1.2-c}) \quad [(\text{D.2.3-2c})]$$

For $20680/F_y \leq D/t \leq 300$ (F_y in MPa)

For $3000/F_y < D/t \leq 300$ (F_y in ksi)

Where

F_{bn} nominal bending strength, in stress units

W_{el} elastic section modulus $W_{el} = \pi R_m^2 t$

W_{pl} plastic section modulus $W_{pl} = 4R_m^2 t$

B.1.3 Combined Axial Compression and Bending

Cylindrical members under combined axial compressive and bending loads should be designed to satisfy the minimum of the following conditions:

$$\frac{f_c}{F_{cn}} + \frac{1}{F_{bn}} \left(\frac{f_{by}}{1 - \frac{f_c}{F_{ey}}} \right) \leq 1.0 \quad (\text{B.1.3-1}) \text{ [(D.3.2-1)]}$$

And

$$1 - \cos \left[\frac{\pi}{2} \frac{f_c}{F_{xc}} \right] + \left(\frac{f_{by}}{F_{bn}} \right) \leq 1.0 \quad (\text{B.1.3-2}) \text{ [(D.3.2-2)]}$$

where

f_c is the compressive stress due to factor loads ($f_c < \phi_c F_{cn}$)

f_b is the bending stress due to factor loads ($f_b < \phi_b F_{bn}$)

F_{cn} is the nominal axial compressive strength calculated in Eqs B.1.1.1 [D.2.2], in stress units

F_{bn} is the nominal bending strength calculated in Eqs B.1.2 or [D.2.3], in stress units

$\phi_c=1$, the resistance factor for axial compressive strength

$\phi_b=1$, the resistance factor for bending strength

C_{my} reduction factor corresponding to the member y axis defined equal to 1 from the table D.3-1.

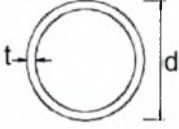
F_{ey} Euler buckling strength corresponding to the member y axis, in stress units

$$F_{ey} = \frac{F_y}{\lambda_y^2}$$

λ_y column slenderness parameter defined by Equation (B.1.1.1-c) [(D.2.2-2c)], where the parameters K, L and r are chosen to correspond to the bending about the y direction.

B.2. Eurocode3: Design of steel structures

In order to calculate the buckling stress of a tubular member, the classification of the tubular cross section should be determined in accordance to Table 5.2

Tubular sections						
						
Class	Section in bending and/or compression					
1	$d/t \leq 50\epsilon^2$					
2	$d/t \leq 70\epsilon^2$					
3	$d/t \leq 90\epsilon^2$					
NOTE For $d/t > 90\epsilon^2$ see EN 1993-1-6.						
$\epsilon = \sqrt{235/f_y}$	f_y	235	275	355	420	460
	ϵ	1.00	0.92	0.81	0.75	0.71
	ϵ^2	1.00	0.85	0.66	0.56	0.51

B.2.1. Buckling strength in axial compression for tubular sections

When the tubular cross section is identified as class 1, 2 & 3 then following procedure is followed according to EN-1993(part 1-1)[2], otherwise, when class 4 is considered EN-1993-1-6 [EN-1993-1-6, 2007] should be followed:

B.2.1.1 Buckling strength in axial compression Class 1, 2 & 3 [EN-1993-1-1, 2005]

The buckling strength under axial compression for a tubular member is defined as follows

$$N_{b,Rd} = \chi A f_y \quad \text{for class 1, 2 and 3} \quad (\text{B.2.1.1-1})[(6.47)]$$

where

$N_{b,Rd}$: buckling strength under axial compression

χ : reduction factor for the corresponding buckling mode

A : area of the tubular cross section

For members subjected to axial compression, χ value is defined in terms of member slenderness as follows:

$$\chi = \frac{1}{\Phi + \sqrt{\Phi^2 - \lambda^2}} \quad (\text{B.2.1.1-2})[(6.49)]$$

where:

$$\Phi = 0.5 \left[1 + \alpha(\lambda - 0.2) + \lambda^2 \right]$$

$$\lambda = \sqrt{\frac{Af_y}{N_{cr}}} = \frac{L_{cr}}{i} \frac{1}{\lambda_1} \quad \text{for class 1, 2 and 3} \quad (\text{B.2.1.1-3}) \quad [(6.50)]$$

where

L_{cr} : the effective buckling length

i : radius of gyration

$$\lambda_1 = \pi \sqrt{\frac{E}{f_y}} = 93.9\epsilon$$

$$\epsilon = \sqrt{\frac{235}{f_y}} \quad (f_y \text{ in N/mm}^2)$$

α : imperfection factor is defined in Table B.2.1(section 6.1) based on the buckling curve
Table 6.2

Table 2.1[6.1]

Buckling curve	a0	a	b	c	d
α	0.13	0.21	0.34	0.49	0.76

The buckling curve for hot-formed steel tubular members should be obtained from Table 6.2. For S235/ 275/ 355/ 420, "a" buckling curve is obtained and for S460 the "a0".

When the tubular cross section is identified as class 4, the procedure below is followed according to EN-1993(part 1-6)[EN -1993-1-1, 2007]:

B.2.1.2 Buckling Strength Class4

a) Method1

For class 4 sections, the buckling curve consists of two “branches”. The global relative member slenderness is obtained from B.2.1.1-3 or 6.50 and the buckling resistance factor χ from B.2.1.1-2 or 6.49. For small amplitudes of member slenderness, shell buckling prevails so the compression design load is reduced by a factor χ_x which is calculated according to EN-1993-1-6 for class 4 sections. For intermediate and large values of member slenderness the procedure proposed by 1993-1-1 is followed where the compressive strength is reduced by the factor χ obtained from Eqs B.2.1.1-2 and global buckling behavior is considered according to class 3 sections. An indicative buckling curve described above is schematically shown in Figure B.2.1.2-1.

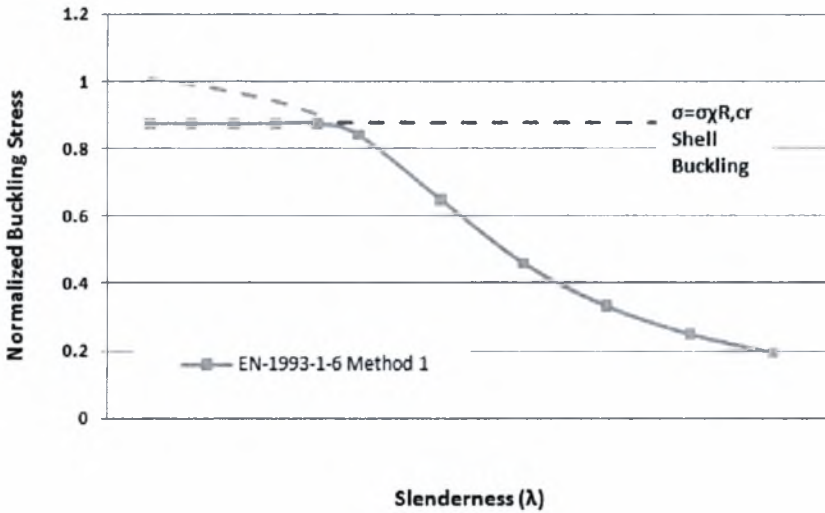


Figure B.2.1.2-1 Buckling curve for class 4 cross-sections described in Method 1

b) Method2 [EN-1993-1-6, 2007]

Alternatively, in order to define the buckling curve for class 4 sections, the compressive strength is reduced by the χ_x factor for every value of member slenderness. The procedure followed is described as follows:

For class 4 cross sections the global relative member slenderness should be obtained from:

$$\lambda = \sqrt{\frac{N_{x,Rd}}{N_{Rcr}}} \quad (B.2.1.2-1)$$

The global buckling reduction factor χ is defined according to EN-1993-1-1[2]:

$$\chi = \frac{1}{\Phi + \sqrt{\Phi^2 - \lambda^2}}$$

where

$$\Phi = 0.5 \left[1 + \alpha(\lambda - 0.2) + \lambda^2 \right]$$

The critical meridional buckling load is given as:

$$N_{x,Rd} = \sigma_{x,Rd} A \quad (\text{B.2.1.2-2})$$

And

The Eulerian elastic critical axial load:

$$N_{Rcr} = \pi^2 \frac{EI}{(kL)^2} \quad (\text{B.2.1.2-3})$$

where

$\sigma_{x,Rd}$ is the elastic meridional stress defined according to the provisions of Annex D of EN-1993-1-6 calculated in section 2.1.2.1

A is the cross section area.

E is the elastic Young modulus

I is the inertia of the cross section

k is the effective buckling length factor based on the boundary conditions

B.2.1.2.1 Local buckling stress design

(1) The buckling resistance should be represented by the buckling stresses as defined in 1.3.6. The design buckling stresses should be obtained from:

$$\sigma_{x,Rd} = \sigma_{x,Rk} / \gamma_{M1} \quad (\text{B.2.1.2.1-1})[(8.11)]$$

(2) The characteristic buckling stresses should be obtained by multiplying the characteristic yield strength by the buckling reduction factor χ :

$$\sigma_{x,Rk} = \chi_x f_{yk} \quad (\text{B.2.1.2.1-2})[(8.12)]$$

(3) The buckling reduction factor χ_x should be determined as a function of the relative slenderness of the shell λ from:

$$\chi = 1 \quad \text{when } \lambda_x \leq \lambda_0 \quad (\text{B.2.1.2.1-3a}) \quad [(8.13)]$$

$$\chi = 1 - \beta \left(\frac{\lambda_x - \lambda_0}{\lambda_p - \lambda_0} \right)^\eta \quad \text{when } \lambda_0 < \lambda_x < \lambda_p \quad (\text{B.2.1.2-3b}) \quad [(8.14)]$$

$$\chi = \frac{\alpha}{\lambda_x^2} \quad \text{when } \lambda_p \leq \lambda_x \quad (\text{B.2.1.2.1-3c}) \quad [(8.15)]$$

Where

α is the elastic imperfection reduction factor

β is the plastic range factor

η is the interaction component

λ_0 is the squash limit relative slenderness

The values of the above parameters (α , β , η , λ_0) should be taken from Annex D described below in section 2.1.2.2.2.

The value of the plastic limit relative slenderness λ_p should be determined from:

$$\lambda_p = \sqrt{\frac{\alpha}{1 - \beta}} \quad (\text{B.2.1.2.1-4}) \quad [(8.16)]$$

The relative shell slenderness parameter should be determined from:

$$\lambda_x = \sqrt{\frac{f_{yk}}{\sigma_{x,Rcr}}} \quad (\text{B.2.1.2.1-5}) \quad [(8.17)]$$

B.2.1.2.2 ANNEX D

Expressions for buckling limit state evaluation using stress design are calculated as described below:

B.2.1.2.2.1 Elastic critical meridional buckling stress

(1)The following expressions may only be used for shells with boundary conditions BC1 or BC2 defined in Table 5.1 section 5 of EN-1993-1-6.

(2)The length of the shell segment is characterized in terms of the dimensionless length parameter ω :

$$\omega = \frac{l}{r} \sqrt{\frac{r}{t}} \quad (\text{B.2.1.2.2-1})[(\text{D.1})]$$

Where

l: cylinder length between defined boundaries

r: radius of cylinder middle surface

t: thickness of shell

(3) The elastic critical meridional buckling stress, using a value of C_x from (11), (13) or (15), should be obtained from:

$$\sigma_{x,Rcr} = 0.605 E C_x \frac{t}{r} \quad (\text{B.2.1.2.2-2})[(\text{D.2})]$$

where C_x depends on the value of ω .

(4)For medium-length cylinders, which are defined by:

$$1.7 \leq \omega \leq 0.5 r/t \quad (\text{B.2.1.2.2-3})[(\text{D.3})]$$

The factor C_x should be taken as:

$$C_x = 1.0 \quad (\text{B.2.1.2.2-4})[(\text{D.4})]$$

(5)For short cylinders, which are defined by:

$$\omega \leq 1.7 \quad (\text{B.2.1.2.2-5})[(\text{D.5})]$$

The factor C_x should be taken as:

$$C_x = 1.36 - \frac{1.83}{\omega} + \frac{2.07}{\omega^2} \quad (\text{B.2.1.2.2-6})[(\text{D.6})]$$

(6) For long cylinders, which are defined by:

$$\omega > 0.5 r/t \quad (\text{B.2.1.2.2-7})[(\text{D.7})]$$

The factor C_x should be taken as:

$$C_x = C_{x,N} \quad (\text{B.2.1.2.2-8})[(\text{D.8})]$$

In which $C_{x,N}$ is the greater of:

$$C_{x,N} = 1 + \frac{0.2}{C_{xb}} \left[1 - 2\omega \frac{t}{r} \right] \quad (\text{B.2.1.2.2-9}) [(\text{D.9})]$$

And

$$C_{x,N} = 0.60 \quad (\text{B.2.1.2.2-10}) [(\text{D.10})]$$

where C_{xb} is a parameter depending on the boundary conditions and being taken from table D.1

(7) For long cylinders as defined in (6) that satisfy the additional condition:

$$\frac{r}{t} \leq 150 \text{ and } \omega \leq 6 \left(\frac{r}{t} \right) \text{ and } 500 \leq \frac{E}{f_{y,k}} \leq 1000 \quad (\text{B.2.1.2.2-11}) [(\text{D.11})]$$

The factor C_x may alternatively be obtained from

$$C_x = C_{x,N} \left(\frac{\sigma_{xE,N}}{\sigma_{xE}} \right) + \left(\frac{\sigma_{xE,M}}{\sigma_{xE}} \right) \quad (\text{B.2.1.2.2-12})[(\text{D.12})]$$

where

σ_{xE} is the design value of meridional stress $\sigma_{xE,d}$

$\sigma_{xE,N}$ is the component of $\sigma_{xE,d}$ that derives from axial compression (circumferentially uniform component)

$\sigma_{xE,M}$ is the component of $\sigma_{xE,d}$ that derives from tubular global bending (peak value of the circumferential varying component)

The following simpler expression may also be used in place of expression (B.2.1.2.2-12)[(D.12)]

$$C_x = 0.6 + 0.4 \left(\frac{\sigma_{xE,M}}{\sigma_{xE}} \right) \quad (\text{B.2.1.2.2-13})[(\text{D.13})]$$

B.2.1.2.2.2 Meridional buckling parameters

(1)The meridional elastic imperfection reduction factor α_x should be obtained from:

$$\alpha = \frac{0.62}{1 + 1.91(\Delta w_k/t)^{1.44}} \quad (\text{B.2.1.2.2-14})[(\text{D.14})]$$

where Δw_k is the characteristic imperfection amplitude:

$$\Delta w_k = \frac{1}{Q} \sqrt{\frac{r}{t}} \quad (\text{B.2.1.2.2-15})[(\text{D.15})]$$

(2) where Q is the meridional compression fabrication quality parameter which should be taken from the table D.2 for the specified fabrication tolerance quality class

(3)The meridional squash limit slenderness λ_0 , the plastic range factor β , and the interaction exponent η should be taken as:

$$\lambda_0=0.20 \quad \beta=0.60 \quad \eta=1.0 \quad (\text{B.2.1.2.2-16})[(\text{D.16})]$$

(4)For long cylinders that satisfy the special conditions of D1.2.1 (7), the meridional squash limit slenderness λ_0 may be obtained from:

$$\lambda_0 = 0.20 + 0.10 \left(\frac{\sigma_{xE,M}}{\sigma_{xE}} \right) \quad (\text{B.2.1.2.2-17})[(\text{D.17})]$$

where

σ_{xE} is the design value of the meridional stress $\sigma_{xE,d}$

$\sigma_{xE,M}$ is the component of $\sigma_{xE,d}$ that comes from tubular global bending (peak value of the circumferential varying component)

(5)Cylinders need not be checked against meridional shell buckling if they satisfy:

$$\frac{r}{t} \leq 0.03 \frac{E}{f_{yk}} \quad (\text{B.2.1.2.2-18})[(\text{D.18})]$$

B.2.2 Bending

The classification of the cross section should be defined from Table 5.2 of Eurocode 3 (EN-1993-1-1): Design of steel structures.

B.2.2.1 Bending Class 1, 2 & 3 [EN-1993-1-1, 2005]

(1)The tubular members under bending loads should be designed to satisfy:

$$\frac{M_{Ed}}{M_{c,Rd}} \leq 1.0 \quad (\text{B.2.2.1-1})[(6.12)]$$

(2)The design value of bending moment is defined as follows:

$$M_{c,Rd} = M_{pl,Rd} = W_{pl} f_y \quad \text{class 1 or 2} \quad (\text{B.2.2.1-2a})[(6.13)]$$

$$M_{c,Rd} = M_{el,Rd} = W_{el,min} f_y \quad \text{class 3} \quad (\text{B.2.2.1-2b})[(6.14)]$$

where

W_{pl} is the plastic section modulus

W_{el} is the elastic section modulus

B.2.2.2 Bending Class 4 [EN-1993-1-6, 2007]

The design bending strength is defined as follows:

$$M_{x,Rd} = W_{el} \sigma_{x,Rd} \quad (\text{B.2.2.2-1})$$

where

$\sigma_{x,Rd}$ should be obtained from the equation (2.1.2-2) or (8.12) of EN1993-1-6 and C_x may be obtained by equation (2.1.2-19) or (2.1.2-20),[(D.12 or D.13)] considering $\frac{\sigma_{xE,M}}{\sigma_{xE}} = 1.0$ and

$$\frac{\sigma_{xE,N}}{\sigma_{xE}} = 0, \text{ for pure bending.}$$

B.2.3 Combined loads

B.2.3.1 Class 1, 2 & 3 [EN-1993-1-1, 2005]

Classification of cross section, Table 5.1

The stability of members with constant cross section not susceptible to torsional displacements (i.e. tubular members) should satisfy the following equations:

$$\frac{N_{Ed}}{\chi N_{Rd}} + k_{yy} \frac{M_{Ed}}{M_{Rd}} \leq 1.0 \quad [\text{B.2.3.1-1}] \quad [(6.61)]$$

Where

N_{Ed} , $M_{y,Ed}$ are the design values of the axial compression and bending strength

χ reduction factor due to flexural buckling

k_{yy} interaction factor obtained from Annex A(Method1)

For the interaction equation [B.2.3.1-1] or (6.61) simply supported members are considered with or without lateral supports subjected to axial compression and bending moments or lateral loads.

B.2.3.2 Class 4 [EN-1993-1-6, 2007]

The methodology proposed is described as followed and the interaction curve is defined similar to section 2.3.1, Eq 2.3.1-1:

$$\frac{N_{Ed}}{N_{x,Rd}} + k_{yy} \frac{M_{Ed}}{M_{x,Rd}} \leq 1.0 \quad (\text{B.2.3.2-1})$$

where

$N_{x,Rd}$ is the axial load calculated in Eq.2.1.2-2 considering pure compression for class 4 cross sections according to EN-1993-1-6

$M_{x,Rd}$ is the moment strength calculated in Eq 2.2.2-1 considering pure bending for class 4 cross sections according to EN-1993-1-6

K_{yy} is interaction factor obtained from Annex A(Method1) similar to section according to EN-1993-1-1

B.3 Structural stability of hollow sections [CIDECT1992]

The classification of the tubular cross sections is defined from Table 4 (page 14) the same as EN1993-1-1[2].

B.3.1 Tubular Members in axial compression for class 1, 2 & 3

The design buckling load of a compression member is given by the condition:

$$N_d \leq N_{b,Rd}$$

Where

N_d is the working load

$N_{b,Rd}$ is the design buckling resistance capacity of the member

$$N_{b,Rd} = \chi A f_y \quad \text{for class 1, 2 and 3} \quad (B.3.1-1)[(3.1)]$$

where

$N_{b,Rd}$: buckling strength under axial compression

χ : reduction factor for the relative buckling curve (Figure 3, Table 11 through 14) dependent on the non-dimensional slenderness λ of a column.

A : area of the tubular cross section

The buckling curves can be described analytically by the equation:

$$\chi = \frac{1}{\Phi + \sqrt{\Phi^2 - \lambda^2}} \quad \text{but} \quad \chi \leq 1.0 \quad (B.3.1-2)[(3.3)]$$

With

$$\Phi = 0.5 \left[1 + \alpha (\lambda - 0.2) + \lambda^2 \right] \quad (B.3.1-3)[(3.4)]$$

and

$$\lambda = \sqrt{\frac{Af_y}{N_{cr}}} = \frac{L_{cr}}{i} \frac{1}{\lambda_1} \quad \text{for class 1, 2 and 3}$$

Where

L_{cr} : the effective buckling length

i : radius of gyration

$$\lambda_1 = \pi \sqrt{\frac{E}{f_y}} = 93.9\varepsilon$$

$$\varepsilon = \sqrt{\frac{235}{f_y}} \quad (f_y \text{ in N/mm}^2)$$

α : imperfection factor is defined in the following Table

Buckling curve	a_0	a	b	c
α	0.13	0.21	0.34	0.49

The buckling curve for hot-formed high strength steel should be obtained from Table 10b (CIDECT1992) or Table 6.2 (EN1993-1-1).

For S235/ 275/ 355/ 420, "a" buckling curve is obtained and for S460 the "a0".

B.3.2 Tubular members in bending for class 1, 2 & 3

The tubular members under bending loads should be designed to satisfy:

$$\frac{M_{Ed}}{M_{Rd}} \leq 1.0 \quad (\text{B.3.2-1})$$

The design value of bending moment is defined as follows:

$$M_{Rd} = M_{pl,Rd} = W_{pl} f_y \quad \text{class 1 or 2} \quad (\text{B.3.2-2a})$$

$$M_{Rd} = M_{el,Rd} = W_{el,min} f_y \quad \text{class 3} \quad (\text{B.3.2-2b})$$

where

W_{pl} is the plastic section modulus

W_{el} is the elastic section modulus

B.3.3 Members in combined compression and bending class 1, 2 & 3

The relation of compression and bending strength is based on the following linear interaction formulae:

$$\frac{N_{Sd}}{N_{b,Rd}} + K_y \frac{M_{Sd}}{M_{Rd}} \leq 1 \quad (\text{B.3.3-1})[(5.1)]$$

Where

N_{Sd} = Design value of axial compression

$$N_{b,Rd} = \chi N_{pl} = \chi A f_y \quad (\text{B.3.3-2})[(5.2)]$$

χ = reduction factor defined in section 3.1

A = cross sectional area

f_y = yield strength

M_{Sd} = Maximum absolute design value of the bending moment about y-y axis according to the first order theory.

$M_{Rd} = M_{el,Rd} = W_{el} f_y$ by elastic utilization of a cross section (class 3) defined in Section B.3.2

$$(\text{B3.3-3})[(5.3)]$$

$M_{Rd} = M_{pl,Rd} = W_{pl} f_y$ by plastic utilization of a cross section (class 1 and 2) defined in section B.3.2

$$K_y = 1 - \frac{N_{sd}}{\chi N_{pl}} \mu_y, \text{ however } K_y \leq 1.5 \quad (\text{B.3.3-4})[(5.4)]$$

$$\mu_y = \lambda_y (2\beta_{M,y} - 4) + \left(\frac{W_{pl}}{W_{el}} - 1 \right), \text{ however } \mu_y < 0.9 \quad (\text{B.3.3-5})[(5.5)]$$

$\beta_{M,y}$ is the equivalent uniform moment factors according to Table 16, column 2, in order to determine the form of the bending moment distribution M_y .

B.3.4 Members in axial compression, bending and combined loads- class 4 [ECCS 1988]

In cases, where thin-walled circular hollow sections are applied, the procedure of substituting the yield strength f_y in the already mentioned formulae by the real buckling stresses can be used.

The buckling stresses can be calculated by the procedure described in [ESSC, 1988].

B.3.4.1 Buckling Stress σ_u

σ_u is given by:

$$\sigma_u = \frac{\alpha \sigma_{cr}}{\gamma} \quad \text{with } \gamma = 4/3 \quad \text{when} \quad \alpha \sigma_{cr} \leq \frac{1}{2} f_y \quad (\text{B.3.4.1-1a})[(2)]$$

$$\sigma_u = f_y \left[1 - 0.4123 \left(\frac{f_y}{\alpha \sigma_{cr}} \right)^{0.6} \right] \quad \text{when} \quad \alpha \sigma_{cr} \geq \frac{1}{2} f_y \quad (\text{B.3.4.1-1b})[(3)]$$

In these equations f_y is the yield stress, α is a reduction factor given by R1.5.1-1.5.4 and

$$\sigma_{cr} = \frac{E}{\sqrt{3(1-\nu^2)}} \frac{t}{r} = 0.605E \frac{t}{r} \quad (\text{B.3.4.1-2a})[(4)]$$

Is the critical compressive stress for an axially loaded, perfect elastic cylinder in which a pure state of uniform membrane stresses exists before buckling and whose edges are immovable in both the radial and circumferential directions during buckling.

With the shell slenderness parameter λ_x defined by $\lambda_x = \sqrt{\frac{f_y}{\alpha \sigma_{cr}}}$ (B.3.4.1-2b)

the Eqs (3.4.1-1a) and (3.4.1b) or [(2)] and [(3)] may be written respectively:

$$\frac{\sigma_u}{f_y} = \frac{0.75}{\lambda_x^2} \quad \text{when } \lambda_x \geq \sqrt{2}$$

$$\frac{\sigma_u}{f_y} = 1 - 0.4123\lambda_x^{1.2} \quad \text{when } \lambda_x \leq \sqrt{2}$$

The additional factor γ is not necessary for a very thick and short cylinder which does not fail by buckling, but by yielding. If one omits the additional safety factor $\gamma=4/3$ entirely, the above Eqs are developed as follows:

$$\frac{\sigma_u}{f_y} = 1 - 0.25\lambda_x^2 \quad \text{when } \lambda_x \leq \sqrt{2} \text{ (elastic-plastic region) (B.3.4.1-3a)[(5)]}$$

$$\frac{\sigma_u}{f_y} = \frac{1}{\lambda_x^2} \quad \text{when } \lambda_x \geq \sqrt{2} \quad \text{(B.3.4.1-3b)[(6)]}$$

These two equations also give identical ordinates and slopes at $\lambda_x = \sqrt{2}$.

B.3.4.2 Pure axial compressive load for class4

The reduction factor $\alpha=\alpha_0$ is defined as follows considering pure axial compression:

$$\alpha_0 = \frac{0.83}{\sqrt{1+0.01r/t}} \quad \text{for } r/t < 212 \quad \text{(B.3.4.2-1a)}$$

[(13)]

$$\alpha_n = \frac{0.70}{\sqrt{0.1+0.01r/t}} \quad \text{for } r/t > 212 \quad \text{(B.3.4.2-1b)}$$

The shell slenderness parameter λ_x is calculated by (3.4.1-2b) and the local buckling stress σ_u by either (B.3.4.1-3a)[(5)] or (B.3.4.1-3b)[(6)]. The compressive buckling load is calculated by Eq (B.2.1.2-2), where $\sigma_{x,Rd}$ corresponds to σ_u . The global member slenderness and the buckling reduction factor are defined by Eq. (B.2.1.2-1) of EN-1993-1-1 [EN-1993-1-1, 2005].

B.3.4.3 Pure bending of the cylinder for class4

The reduction factor $\alpha = \alpha_b$ is defined as follows considering pure bending:

$$\alpha_b = 0.1887 + 0.8113\alpha_0 \quad (\text{B.3.4.2.2-1})[(14)]$$

where α_0 is given by Eqs. B.3.4.2.1-1a&b or (13) and Eqs (14) has been experimentally verified for $r/t < 1500$

The shell slenderness parameter λ_x is calculated by (B.3.4.1-2b) and the local buckling stress σ_u by either (B.3.4.1-3a)[(5)] or (B.3.4.1-3b)[(6)]. The bending moment is calculated by Eq (B.2.2.2-1), where $\sigma_{x,Rd}$ corresponds to σ_u .

B.3.4.4 Combined loading for class 4

The interactive equation for class 4 proposed, is similar to Eq (B.3.3-1) or [5.1] for class 3 (CIDECT, Section 5), where the compressive ($N_{b,Rd}$) and bending values (M_{Rd}) are calculated by Sections B.3.4.2 and B.3.4.4, respectively, while the k_y factor is calculated according to:

$$K_y = 1 - \frac{N_{Sd}}{N_{b,Rd}} \mu_y$$

where

$N_{b,Rd}$ is calculated according to Section B.3.4.2 for pure compression of class4 cross section and μ_y is defined by Section B.3.3

B.4 AISC-Load and Resistance Factor Design Specification for Steel Hollow Structural Sections [AISC 2000]

B.4.1. Design Requirements

B.4.1.1 Classification of Steel Sections

HSS are classified for local buckling of the wall in compression as compact, noncompact, or slender-element cross-sections according to the limiting wall slenderness ratios λ_p and λ_r in Table 2.2-1. For an HSS to qualify as compact, the wall slenderness ratio λ must be less than or equal to λ_p . If λ exceeds λ_p but is less than or equal to λ_r , the HSS is noncompact. If λ exceeds λ_r , the HSS is a slender-element cross-section. The wall slenderness ratio λ shall be calculated as follows:

- (a) For round HSS, $\lambda = D/t$, where D is the outside diameter and t is the wall thickness. This Specification is applicable only to round HSS with λ less than or equal to $0.448E/F_y$, where E is the modulus of elasticity and F_y is the specified minimum yield stress.

B.4.1.2 Design by Plastic Analysis

Design by plastic analysis is permitted when λ is less than or equal to λ_p for plastic analysis in Table 2.2-1, where $\lambda = D/t$.

Element	Wall Slenderness Ratio, λ	Limiting Wall Slenderness	
		λ_p (compact)	λ_r (noncompact)
Round HSS for axial compression for flexure for plastic analysis	D/t [a]	n.a. $0.0714E/F_y$ $0.0448E/F_y$	$0.114E/F_y$ $0.309E/F_y$ n.a.

[a] D/t must be less than or equal to $0.448E/F_y$

B.4.2 Tubular Compression Members

The design strength for flexural buckling of compression members is P_n :

$$P_n = F_{cr} A_g \quad (\text{B.4.2-1})[(4.2-1)]$$

F_{cr} shall be determined as follows:

a) For $\lambda_c \sqrt{Q} \leq 1.5$

$$F_{cr} = Q \left(0.658^{Q\lambda_c^2} \right) F_y \quad (\text{B.4.2-2}) [(4.2-2)]$$

b) For $\lambda_c \sqrt{Q} > 1.5$

$$F_{cr} = \left(\frac{0.877}{\lambda_c^2} \right) F_y \quad (4.2-3) [(4.2-3)]$$

where

$$\lambda_c = \frac{KI}{r\pi} \sqrt{\frac{F_y}{E}} \quad (\text{B.4.2-4}) [(4.2-4)]$$

Q shall be determined as follows:

(a) For $\lambda \leq \lambda_r$ in Section B.4.1.1 or (2.2), $Q = 1$

(b) For $\lambda > \lambda_r$ in Section B.4.1.1. or(2.2),

For round HSS with $\lambda < 0.448E/F_y$,

$$Q = \frac{0.0379E}{F_y (D/t)} + \frac{2}{3} \quad (\text{B.4.2-5})[(4.2-5)]$$

B.4.3. Beams and other Flexural Members

For round HSS, for $\lambda \leq \lambda_p$ in Section B.4.1.1 or (2.2),

$$M_n = M_p = F_y Z \quad (\text{B.4.3-1})[(5.1-1)]$$

(i) For $\lambda_p < \lambda \leq \lambda_r$,

$$M_n = \left(\frac{0.0207 E}{D/t} \frac{E}{F_y} + 1 \right) F_y S \quad (\text{B.4.3-2a})[(5.1-2)]$$

(ii) For $\lambda_r < \lambda \leq 0.448E/F_y$,

$$M_n = \frac{0.330E}{D/t} S \quad (\text{B.4.3-2b})[(5.1-3)]$$

where S is the elastic section modulus

Z is the plastic section modulus

B.4.4 Members under Combined Forces

The interaction of flexure and axial force shall be limited by Equations B.4.4-1a and B.4.4.1b or (7.1-1) and (7.1-2).

(a) For $P_u/\phi_c P_n \geq 0.2$,

$$\frac{P_u}{\phi_c P_n} + \frac{8}{9} \left(\frac{M_{ux}}{\phi_b M_{nx}} \right) \leq 1.0 \quad (\text{B.4.4-1a})[(7.1-1)]$$

(a) For $P_u/\phi_c P_n < 0.2$,

$$\frac{P_u}{2\phi_c P_n} + \left(\frac{M_{ux}}{\phi_b M_{nx}} \right) \leq 1.0 \quad (\text{B.4.4-1b}) [(7.1-2)]$$

P_u = required axial compressive strength, kips (N)

P_n = nominal compressive strength determined in accordance with Sections B.4.2 or (3.1), kips (N)

M_u = required flexural strength determined in accordance with LRFD Specification Section C1 [API-LRFD, 2000] described below, kip-in. (N-mm)

M_n = nominal flexural strength determined in accordance with Section B.4.3 or (5.1), kip-in.(N-mm)

x = subscript relating symbol to strong-axis bending

$\phi = 1$ for compression

$\phi_b = 1$ for bending

The calculation of the flexural strength M_u is described in Section C1 of the LRFD-AISC [AISC –LRFD 2000] including second order effects and is depicted below:

On the basis of elastic analysis, M_u for beam-columns shall be determined from a second-order elastic analysis or from the following approximate second-order analysis procedure:

$$M_u = B_1 M_{nt} + B_2 M_{lt} \quad (\text{B.4.4-2})[(\text{C1-1})]$$

where

M_{nt} = required flexural strength in member assuming there is no lateral translation of the frame, kip-in.

M_{lt} = required flexural strength in member as a result of lateral translation of the frame only, kip-in.

$$B_1 = \frac{C_m}{1 - P_u/P_{el}} \geq 1 \quad (\text{B.4.4-3})[(\text{C1-2})]$$

$P_{el} = A_g F_y / \lambda_c^2$ where λ_c is the slenderness parameter

$$\lambda_c = \frac{l}{r\pi} \sqrt{\frac{F_y}{E}}$$

P_u = required axial compressive strength for the tubular member

$C_m = 1$ a coefficient based on elastic first-order analysis assuming no lateral translation whose value shall be taken as follows:

- (a) For compression members not subjected to transverse loading between their supports in the plane of bending,

$$C_m = 0.6 - 0.4(M_1/M_2) \quad (\text{B.4.4-4})[(\text{C1-3})]$$

where M_1/M_2 is the ratio of the smaller to larger moments at the ends of the unbraced member in the plane of bending under consideration. M_1/M_2 is positive when the member is bent in reverse curvature, negative when bent in single curvature.

(b) For compression members subjected to transverse loading between their supports, the value of C_m shall be determined either by rational analysis or by use of the following values:

For members whose ends are restrained $C_m=0.85$

For members whose ends are unrestrained $C_m=1.00$

$$B_2 = \frac{1}{1 - \Sigma P_u \left(\frac{\Delta_{oh}}{\Sigma HL} \right)} \quad \text{(B.4.4-5a)[(C1-4)]}$$

or

$$B_2 = \frac{1}{1 - \frac{\Sigma P_u}{\Sigma P_{e2}}} \quad \text{(B.4.4-5b)[(C1-5)]}$$

ΣP_u = required axial strength of all columns in a story, kips

Δ_{oh} = lateral inter-story deflection, in

L = story height, in

$P_{e2} = A_g F_y / \lambda_c^2$, kips, where λ_c is the slenderness parameter.

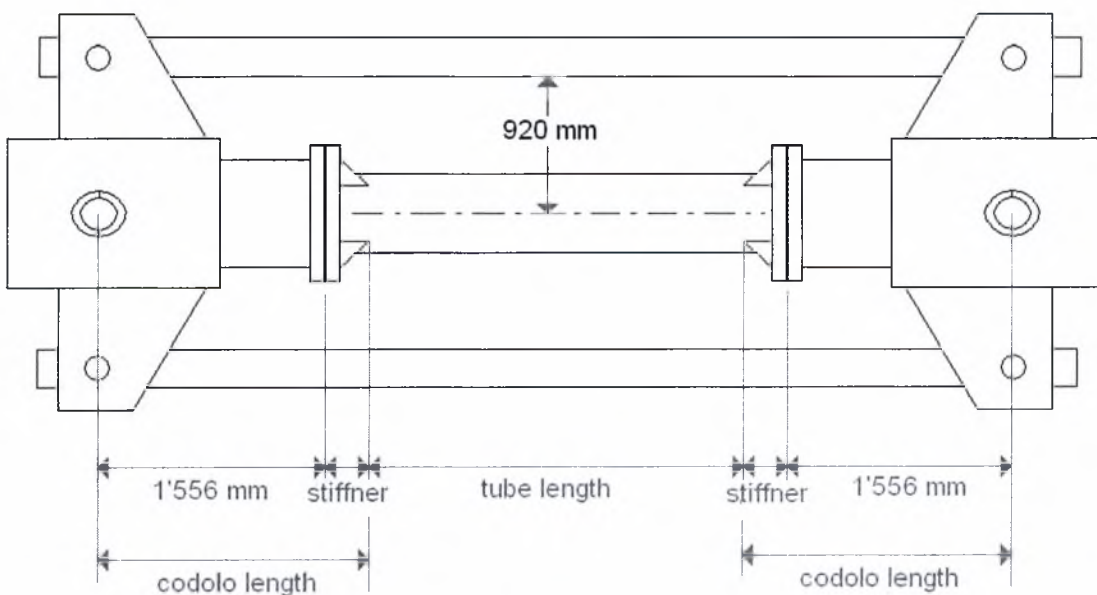
For compression beam column members investigated in the present study are not included in a frame structure, so the second term of the equation (B.4.4.-2) referring to the B_2 parameter is omitted and M_1/M_2 ratio is considered equal to unity.

ANNEX C-Simulation of CSM experiments

In this Chapter a case study is described related to the present investigation in order to simulate the monotonic beam-column experiments to be carried out by CSM (Centro Sviluppo Materiali, Rome, Italy), in the course of ATTEL European project. The aim of the present analysis is to estimate, except from the buckling strength, the residual moment capacity when combined compression and bending are subjected to imperfect tubular members. It is noted that the present analysis is conducted before the experiments are conducted and before initial imperfections are measured. The results will be updated after experimental testing is completed.

C.1 HSS tubular members with initial out-of straightness under combined loadings

The test configuration and the geometrical characteristics of the tubular columns, provided by CSM laboratory are shown in Figures C.1.1 and Table C.1. Further details for the simulation procedure are given below.



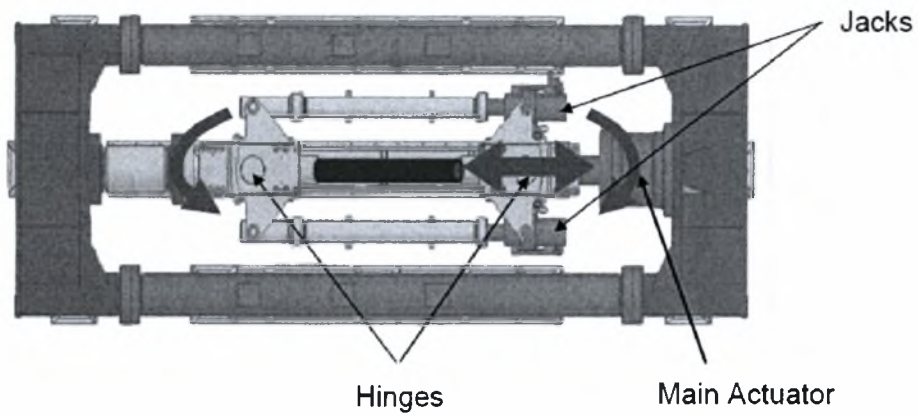


Figure C.1.1 Test configuration by CSM

Table C.1 Geometrical characteristics

Cross section	Tube length [mm]		Stiffener length [mm]	Codolo length [mm]
	short	long		
A (355 x 12)	1490	4490	180	1736
B (323.9 x 10)	1490	4490	180	1736

C.1.1 Model Simulations

Tube specimens of both types A & B and 4490 mm long have been simulated. As measurements of initial geometrical imperfections have not yet been available, an indicative out-of-straightness imperfection was imposed with an amplitude of $L/1000$ in the mid span of the tubular specimen. The geometry, the load and boundary conditions, the mesh configuration, the failure mode and buckle development are briefly shown for tube type B in the following Figure C.1.2. The same configuration is used for tube type A.

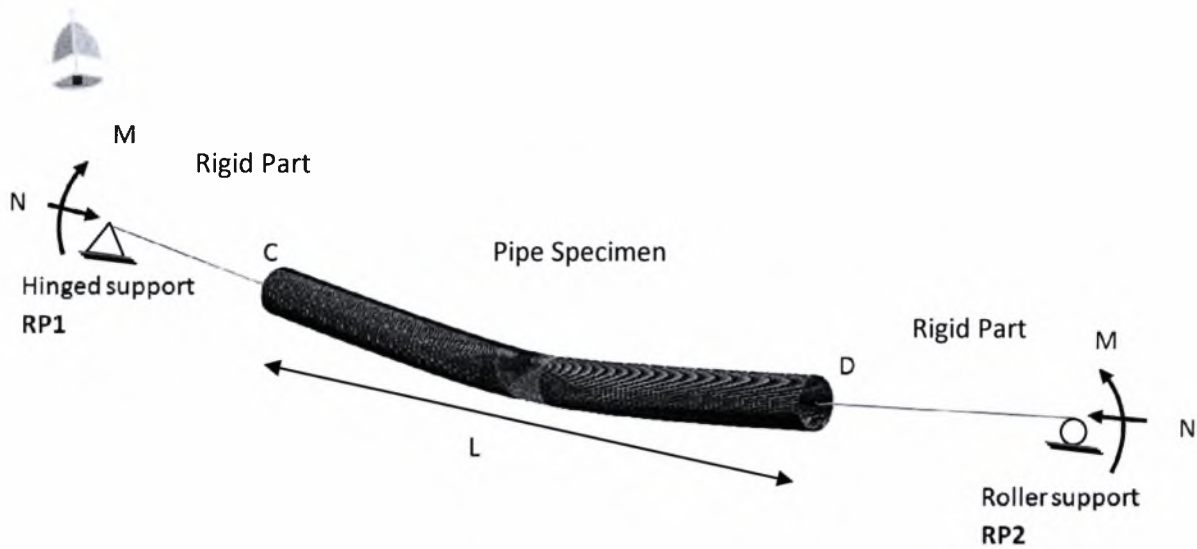


Figure C.1.2 The geometry, the load, the boundary conditions and the failure mode of the tube specimen B with $L=4490\text{mm}$ and out-of-straightness $L/1000$

C.1.2 Geometry

The tube part, $L=4490$ mm long, is defined as a deformable shell structure with an initial stress-free out-of-straightness single-bow deflection of amplitude 4.49 mm ($L/1000$) at mid span.

The “codolos”, 1736mm long, are considered as beam sections of a very large sectional area and inertia, approximating a stiff compact section.

C.1.3 Material Properties

Material data for the characterization of the tubular part, is derived from the inelastic material data of specimen 4B derived from coupon tests conducted by CSM laboratory. The values inserted are the true stress and the logarithmic plastic strain. The elastic Young’s modulus and the Poisson’s ratio are 200000 MPa and 0.3, respectively. For the inelastic region, the values considered for the true stress and the logarithmic plastic strain given in table C.2 and Figure C.1.3:

Table C.2

σ_{true}	ϵ_{In}^p
380.688	0.
582.55	0.000233447
698.975	0.000675541
733.409	0.00157872
738.19	0.00248678
744.152	0.00455555
748.715	0.00652363
752.517	0.00848349
756.839	0.0104449
761.666	0.0123645
766.92	0.014239
772.725	0.0163347
825.17	0.0361025
860.754	0.0560061
879.123	0.0758552

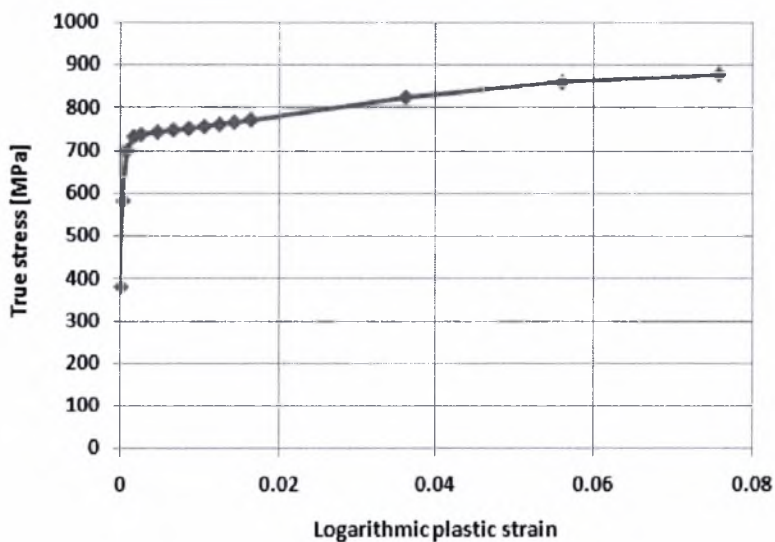


Figure C.1.3 True stress- logarithmic plastic strain curve for both types of tubular members

The “codolos” are considered to have elastic behavior with a very large value of elastic Young’s modulus $E=10^7$ MPa (Poisson’s ratio $\nu=0.3$), approaching the behavior of a rigid member.

C.1.4 Boundary conditions

The model is simply supported with capped ends (RP1 and RP2), at the “codolo” free edges, which are both free to rotate at the in-plane direction. RP1 is a hinge while RP2 allows to motion in the longitudinal direction of the tube, so that RP2 can be considered as a roller.

C.1.5 Load Conditions (Combined loading)

Finite element analysis was conducted for the tube models under monotonic axial compression in order to estimate the maximum buckling load. The maximum load for tube type A, is estimated equal to $N_{u,A}=5358$ kN and for tube type B $N_{u,B}=3613.67$ kN. Similarly, pure bending was subjected to the models in order to estimate the maximum bending moment, which is equal to $M_{max}=1028.89$ kNm, for tube type A, and $M_{max}=713.438$ kNm for tube type B.

Under combined loading conditions a “N→M” loading sequence is followed. More specifically, at first, axial compressive load is subjected at the two free edges of the “codolos”, at the direction of the tube axis. The values of the axial load subjected are 0.25, 0.5 and 0.75 of the maximum buckling strength obtained from the finite element analysis considering pure axial compression (N_u). Secondly, keeping the axial force constant, (second step) bending load is subjected at the in-plane direction until an ultimate bending moment is reached. The relevant interaction diagrams for both types of geometry are shown in Figures C.1.4 and C.1.5.

C.1.6 Interactions

The tube nodes located at cross sections C and D are coupled with the end nodes of the “codolos” through the “tie” function.

C.1.7 Finite Element Mesh

The critical buckling area is considered at the mid span of the tube, equal to 490 mm. Reduced integration 4-noded shell elements, S4R, were employed with 60 nodes around the circumference and 98 nodes in the longitudinal direction of the critical tube area. Additionally, 5 integration points are applied through thickness for the entire tube model. The mesh configuration of the critical area is chosen through parametric analysis reported in ANNEX A.

As expected, the mesh configuration of the remaining tube out of the critical area does not affect the finite element results.

Three dimensional linear beam elements (B31) were applied with 4 nodes along both codolos' longitudinal direction.

Interaction diagrams for tube types A & B are shown in Figures C.1.4 & C.1.5. The axial load and moment values obtained are normalized with the axial and bending loads N_0 and M_0 defined as follows:

$$N_0 = \pi D_m t \sigma_y \text{ and } M_0 = D_m^2 t \sigma_y$$

with $\sigma_y=735$ MPa as used in the finite element analysis.

C.1.8 Results

Interaction Curves

Comparison of interaction diagrams between tube A and B is shown in Figure C.1.6 where axial load and bending values were not normalized.

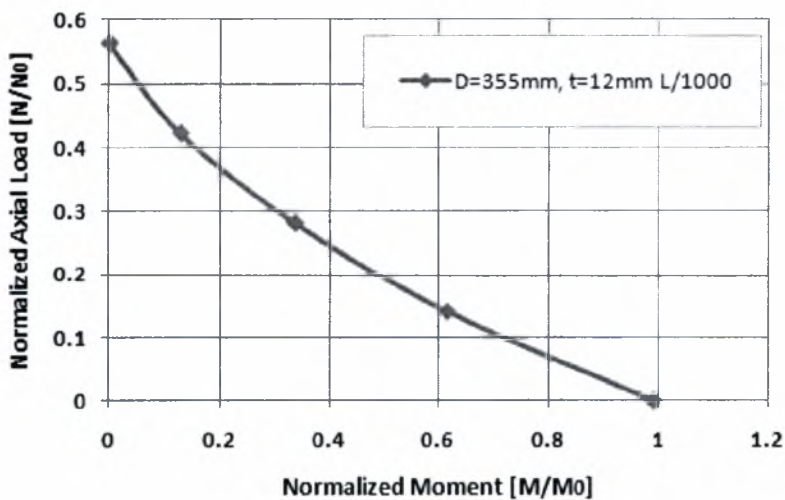


Figure C.1.4 Interaction diagram for the tube specimen A ($D=355\text{mm}$, $t=12\text{mm}$) with $L=4490$ mm and out-of-straightness $L/1000$

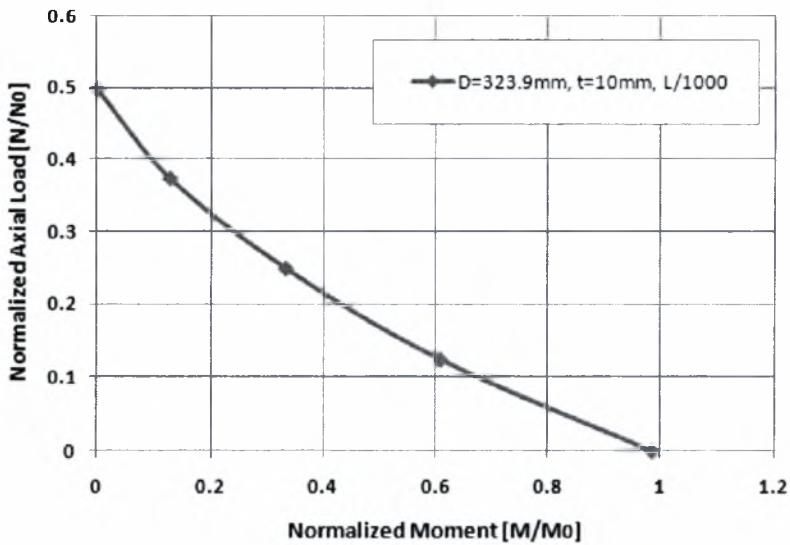


Figure C.1.5 Interaction diagram for the tube specimen B ($D=323.9\text{mm}$, $t=10\text{mm}$) with $L=4490$ mm and out-of-straightness $L/1000$

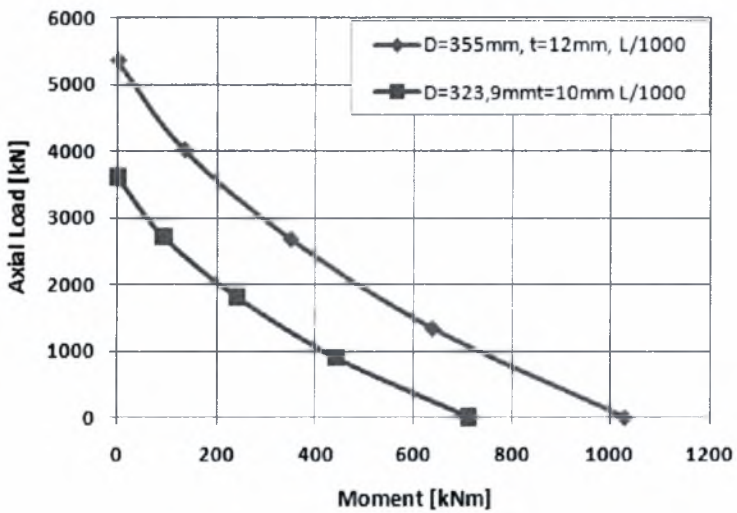


Figure C.1.6 Comparison of interaction diagrams for types A and B

The maximum values of axial load, bending moment, the corresponding vertical deflection and axial displacement for pure compression, pure bending and combined loading are summarized in Table C.3, for tube type A, and table 8.4 for tube type B.

Table C.3 Load and displacement values for tube type A

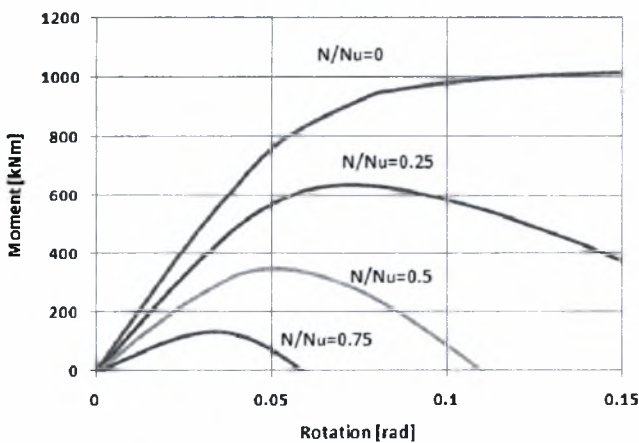
N (kN)	N/N ₀	M _{max}	M _{max} /M ₀	w (mm)	u (mm)
0	0	1028.89	0.99	678.2	135.86
1339.5	0.14	638.68	0.615	235.15	21.76
2679.0	0.28	349.24	0.34	159.5	14.46
4018.5	0.42	133.77	0.13	128.6	13.9
5358.0	0.56	0	0	51.2	10.73

Table C.4 Load and displacement values for tube type B

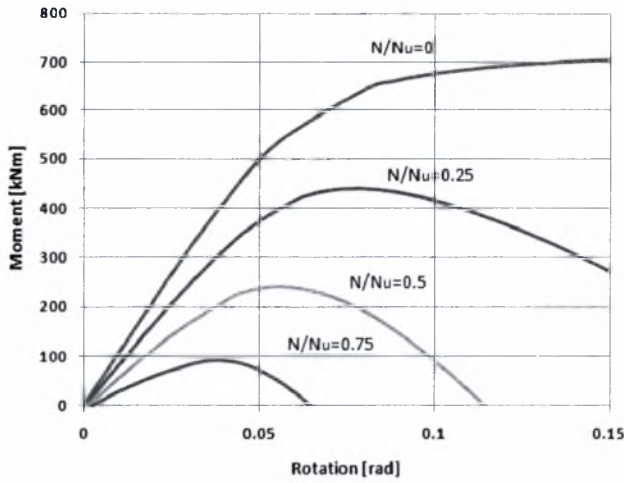
N (kN)	N/N ₀	M _{max}	M _{max} /M ₀	w (mm)	u (mm)
0	0	713.44	0.985	611.25	111.45
903.42	0.125	440.70	0.609	230.99	20.18
1806.84	0.25	240.97	0.333	156.81	12.95
2710.25	0.374	92.72	0.128	113.611	11.07
3613.67	0.5	0	0	55.37	9.60

Moment vs Rotation curves

The moment rotation curves are summarized in Figures C.1.7a & b, for tube type A and B respectively, where N₀ load is defined as the maximum load estimated considering pure compression through FE analysis. As mentioned above, for tube type A, N₀ is equal to 5358.01 kN and for type B equal to 3613.67 kN.



(a)

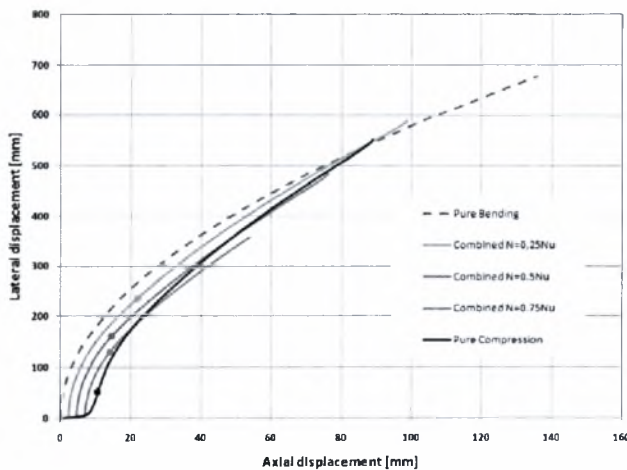


(b)

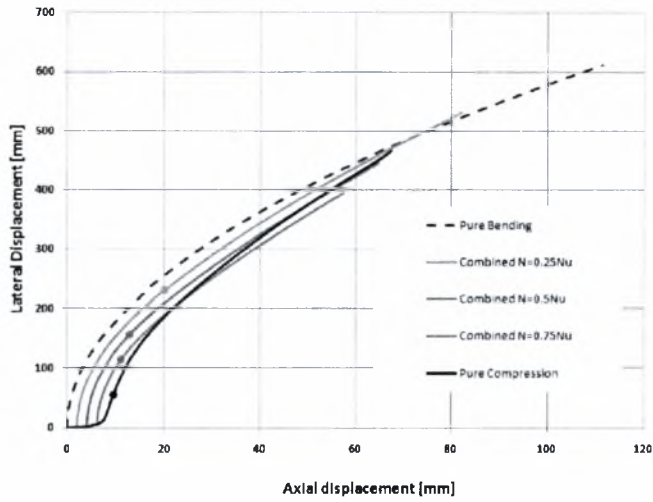
Figure C.1.7 Moment- rotation curves for tube type (a) A and (b) B for various amplitudes of initial subjected axial load, N_u is the estimated strength under pure axial compression through FE analysis

Lateral vs axial Displacement curves

The lateral deflection is caused by the combined loading conditions (axial force and the bending moment) subjected at the point of the roller support and is measured at the mid length of the tube along the compression fiber of the tube wall. The lateral deflection in terms of axial displacement of the “codolo” end(the roller support) is shown in the following figures for different amplitudes of axial load and for both tube types. As shown in Figures C.1.8a & b, the point where the maximum bending load is reached is highlighted for each loading condition and for each tube type, except from the pure bending.



(a)

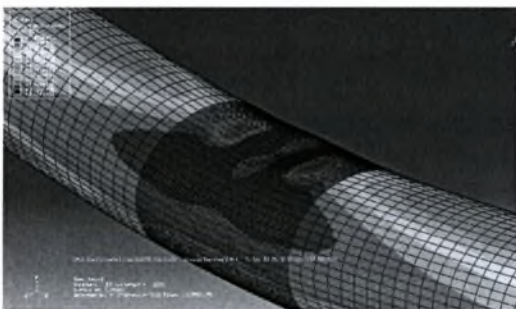


(b)

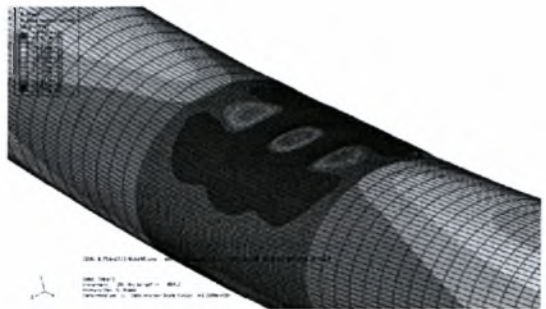
Figure C.1.8 Lateral deflection in terms of axial displacement for tube type (a) A and (b) B

Taking into account that the lateral deflection maximum spacing between tube center and bending arms is 920 mm, as defined in CSM test configuration, the maximum lateral deflection for tube type A is calculated equal to 742mm and for tube type B equal to 758mm, measured from the compression fiber of the tube wall. Herein, as it is shown in the above figures, the maximum bending moment is achieved at significantly lower levels of the calculated maximum lateral displacement for both tube types.

The buckle development for type A is illustrated when the subjected axial load is equal to $0.25N_u$ in Figure C.1.9a, while in Figure C.1.9b, the buckle development is shown for type B when axial load subjected is equal to $0.75N_u$.



(a)



(b)

Figure C.1.9 Buckle development at the mid span of the tube (a) for tube type A when $N=0.25N_u$ and (b) for tube type B when $N=0.75N_u$

C.2 Initially wrinkled steel tubular member under axial compression

Initial wrinkling was imposed to the tube model similar to the ones to be tested by CSM with $D=193.7\text{mm}$ and then subjected to axial compression. Linear elastic buckling analysis was conducted in order to obtain the buckling mode of the simply supported tube model ($D=193.7\text{mm}$, $t=10\text{mm}$, $L=4590\text{mm}$) under pure bending. The buckling mode under bending consists of non-axisymmetric wrinkle development with the maximum wrinkle amplitude placed at the mid span of the tube at the upper compression fiber of the tube. The displacements obtained from the elastic buckling analysis were multiplied by a factor in order to obtain the maximum wrinkle amplitude up to half of the tube thickness. The wrinkled geometry was inserted as the initial stress-free tube geometry in order to conduct a non-linear finite element analysis under axial compression. The material data is derived from tensile tests performed by CSM (specimen 4B-Table C.2). The equilibrium path and the failure mode are shown in Figure C.2.1 and Figure C.2.2, respectively. The compressive stresses obtained from the simulation procedure were normalized with the yield stress equal to 735 MPa.

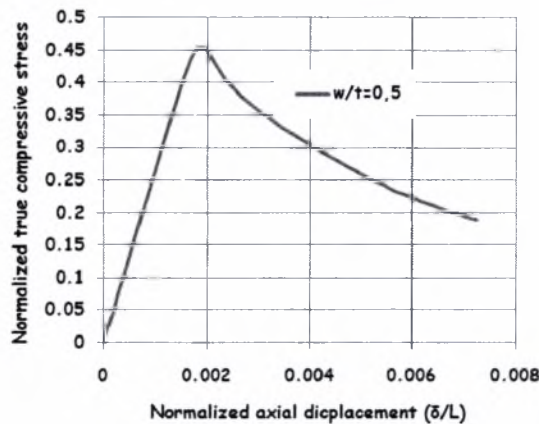


Figure C.2.1 Load displacement curve for the wrinkled tube with $w_0/t=0.5$

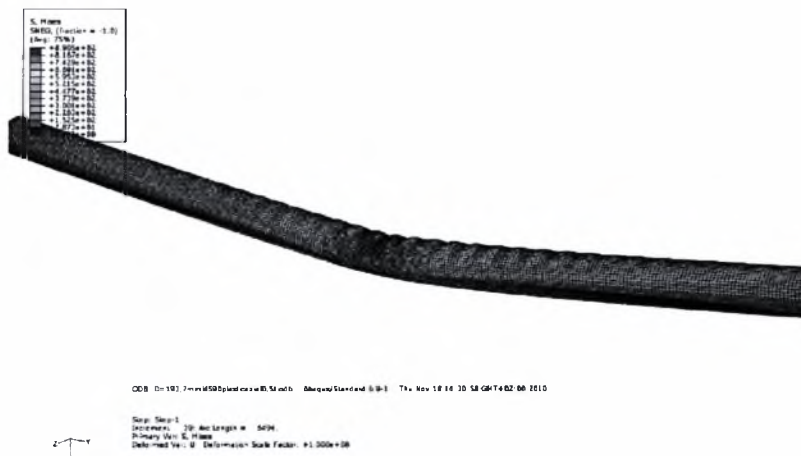


Figure C.2.2 Failure mode for the wrinkled tube with $w_0/t=0.5$



ΠΑΝΕΠΙΣΤΗΜΙΟ ΘΕΣΣΑΛΙΑΣ
ΒΙΒΛΙΟΘΗΚΗ



004000105772